Oxidative stress as a mechanism for silver particle toxicity

Pål Amdal Magnusson

Master Thesis in Toxicology

Department of Biosciences

Faculty of Mathematics and Natural Sciences

University of Oslo

December 2014

Acknowledgements

The work presented in this thesis was carried out at the Department of Chemicals and Radiation, Division of Environmental Medicine, at the Norwegian Institute of Public Health during the time period from January 2013 to December 2014 for the Master's Degree in Toxicology. Main supervisor was Dr Christine Instanes, and Dr Nur Duale and Dr Oddvar Myhre were co-supervisors, all from the NIPH. Professor Ketil Hylland was my internal supervisor at the University of Oslo.

Firstly, I want to thank my eminent supervisors at the NIPH, Christine, Nur and Oddvar for giving me this opportunity and for teaching me all the stuff I've learned the last couple of years. Thank you for always having time for my questions, for teaching me handy lab-tricks and for your great help in the writing process.

I want to thank my internal supervisor, Ketil Hylland at the University of Oslo for his inspiring lectures, giving me both interest and insight in the exciting field of toxicology.

My gratitude goes to Gunnar Brunborg, Department Director at MIKS, for giving me the opportunity to do my thesis at your lab and for allowing me to use your employees' valuable time for answering all my questions. Thank you also for giving me the opportunity to work at your lab (for real money!) when you needed an extra couple of hands for RNA-isolation. I want to thank everyone at MIKS for being so welcoming, enjoyable and helpful. Special thanks goes to Hildegunn for pedagogically teaching me all I know about handling cells and doing qPCR, to Nana for starting the project that I got to continue, and to my fellow master student, Trygve, for sharing my frustrations and for giving invaluable advice on both statistics and chess during these two years.

Thank you, all of my friends, for giving me laughs and a life outside the lab. Thank you, mamma, pappa and Ane for being so supportive of me, even when I babble on about microscopic things.

Last, but not least, thank you Kathy. I am deeply grateful for your patience, encouragement and ability to make me laugh during the work with this thesis. I couldn't have done it without you.

Oslo, December 2014

Pål Amdal Magnusson

Abstract

Nanoparticles are structures with at least one dimension smaller than 100 nm. Nanoparticles are already present in hundreds of commercially available products, and the use of nanotechnology is expected to continue to grow both in terms of areas of application and in volume. Because of their small size and special physiochemical properties, the toxic properties of nanoparticles may be different from the bulk chemical from which they are derived.

Silver nanoparticles are widely used because of their antibacterial properties, but have been shown to cause toxic effects both *in vitro* and *in vivo*. Generation of reactive oxygen species (ROS) and induction of oxidative stress is considered as the most plausible mechanism for silver particle toxicity, and the mitochondria have been suggested as a vulnerable target for silver particle induced ROS. Most available *in vivo* studies on silver particles have focused on the tissue distribution and toxicokinetics of the particles, and there are few *in vivo* studies addressing ROS as a possible mechanism for silver particle toxicity. In particular, there is a lack of data regarding the effects of silver particles on gene expression.

In this thesis, we investigated the effects of 20 nm (Ag20) and 200 nm (Ag200) silver particles on generation of ROS and on the mitochondrial membrane potential of mouse embryonic fibroblasts (MEFs) *in vitro*. We also investigated the effects of silver particle exposure on the expression of (22) genes related to inflammation, oxidative stress, antioxidant defence, intercellular signalling and DNA damage repair the in brains and testes of mice *in vivo* using qPCR assay. Mice and MEF cells of both $Ogg1^{+/+}$ (WT) and $Ogg1^{-/-}$ (KO) were used in all the experiments, as models for reduced repair capacity for oxidative DNA damage.

Our investigation showed that silver particles of both 20 and 200 nm size induced generation of ROS in KO MEF cells after 24 hours exposure, with effects at lower concentrations for the nanoparticles. Our investigation into the effects of silver particle exposure on mitochondrial membrane potential was inconclusive, possibly because of nanoparticle interference with the assay. Gene expression analysis of brain and testis of mice treated with a single intravenous dose of 5 mg/kg bw silver particles (Ag20 or Ag200) showed a small up-regulation of antioxidant defence genes in both genotypes, with the nanoparticles causing up-regulation at day 1 and the microparticles (>100 nm, <100 µm) causing up-regulation at day 7. Significant up-regulation of ROS producing NADPH oxidases in brain suggests that this pathway may be involved in the toxicity. The gene expression in testis did not change markedly following silver particle exposure, and this suggests that the testis may be less vulnerable to the toxic effects of silver particles.

Taken together, our results suggest that generation of ROS and induction of oxidative stress, possibly through the NADPH oxidase- or the *Cd47*-pathways, are responsible for the toxicity seen after exposure to nanoparticles both *in vitro* and *in vivo*.

Table of contents

Abbreviations

8-oxoG	7,8-dihydro-8-oxoguanine
Ag	Silver
AgMP	Silver microparticle (< 100 µm)
AgNP	Silver nanoparticle (< 100 nm)
BBB	Blood-brain barrier
BER	Base Excision Repair
BTB	Blood-testis barrier
cDNA	Complementary DNA
CNS	Central Nervous System
Cq	Quantification cycle
DCFH-DA	2,7-dichlorodihydrofluorescein
dH_2O	Distilled water
DNA	Deoxyribonucleic acid
H_2O_2	Hydrogen peroxide
I.v.	Intravenous
JC-1	5,5',6,6'-tetrachloro-1,1',3,3'-tetraethylbenzimidazolylcarbocyanine iodide
KO	Knock-out (*Ogg1*$^{-/-}$)
MEF	Mouse embryonic fibroblast
MP	Microparticle (0.1 – 100 µm diameter)
mRNA	Messenger RNA
NP	Nanoparticle (<100 nm diameter)
OD	Optical density (absorbance)
Ogg1	8-OxoGuanine DNA glycosylase 1
PBS	Phosphate-buffered saline
PCR	Polymerase chain reaction

RNA	Ribonucleic acid
RNase (enzyme)	Ribonuclease
ROS	Reactive oxygen species
RT (enzyme)	Reverse Transcriptase
RT-PCR	Reverse transcription PCR
SEM	Standard error of the mean
qPCR	Quantitative real-time PCR
WT	Wild type ($Ogg1^{+/+}$)

1 Introduction

1.1 General background

Nanoparticles (NPs) are structures with at least one dimension being less than 100 nanometres (nm). Although humans have been exposed to natural nanoparticles throughout their evolutionary history, such exposure has increased dramatically over the last century due to anthropogenic sources, and is likely to increase further as the possibility for engineering nanoparticles are being developed (Oberdorster *et al.*, 2005b).

Today NPs are present in hundreds of commercially available products and the number of applications for these particles is constantly growing. These product groups include cosmetics, sunscreens, paints and coatings, catalysts and lubricants, water treatments, textiles and sport items, medical and health care products, food products and packing (Surendiran *et al.*, 2009).

Due to physiochemical properties of NPs attributed to their small size, chemical composition, surface structure, solubility, shape, and aggregation, (Nel *et al.*, 2006) their toxic potential cannot be directly predicted by the properties of the corresponding bulk material (Oberdorster *et al.*, 2005a; Oberdorster, *et al.*, 2005b). Engineered NPs are manufactured from a diverse group of substances each with an array of unique physicochemical characteristics. Hence, NPs will differ in the levels of toxicity they induce and the mechanism by which they exert these effects.

The toxicity of different nanomaterials has been the focus of multiple recent studies, and a broad spectrum of potential hazards has been discovered. Several nanoparticles have been shown to be potentially neurotoxic (Sharma and Sharma, 2012), toxic to reproduction and development (Ema *et al.*, 2010; McAuliffe and Perry, 2007) and genotoxic (Rim *et al.*, 2013). In addition, inhaled nanomaterials, such as carbon nanotubes, may cause pulmonary inflammation similar to that of e.g. asbestos fibres (Oberdorster, *et al.*, 2005b).

As the use of NPs constantly increasing, interaction with the environment and human exposure is inevitable. The impact for human health is still not well known or characterized and a strategy for risk assessment of these compounds is highly needed.

1.1.1 Regulation of nanoparticles in the REACH-system.

The use of chemicals in Europe is regulated by the REACH-regulation. REACH is an acronym for Registration, Evaluation, Authorization and restriction of Chemicals, and the regulation is to apply to all chemicals produced in- or imported to the European Union. In the REACH system, producers and importers of chemicals have to register all chemicals which are produced or imported in quantities greater than 1 tonne per year with documentation on the properties, use and potential hazards and risks presented by the substance. The level of

documentation required is decided by the tonnage level of which the chemical is imported or produced. Further, an additional documentation is required once the chemicals are imported or produced in quantities greater than 10, 100 or 1000 tonnes/year. These documentation requirements also apply to nanoparticles as long as they meet the tonnage-requirement.

The REACH regulation was established at a time when nanomaterials were not of particular concern, and is designed to enable good risk assessment of bulk chemicals. Hence, there are few nano-specific documentation requirements, and properties that are of great importance to nanomaterial toxicity, such as surface chemistry, are not required for chemicals registered in REACH. The tonnage levels triggering the different documentation criteria is another problem, as most nanoparticles are used in large volumes, but low tonnage. Hence, few engineered nanoparticles meet the tonnage levels that trigger the higher documentation-requirements. In fact, of the approximately 12 000 registrations in REACH, only 13 are registrations of nanomaterials (S. Andersen, Norwegian Environment Agency, personal communication October 2014).

The European Commission, which is responsible for the REACH-regulation, is working on including more nano-specific documentation and test requirements in REACH. In the absence of proper nano-specific testing criteria that gives a good basis for risk assessment of nanomaterials within the REACH system, research on the toxicity of different NPs is crucial.

1.2 Silver nano- and microparticles

It is currently estimated that silver nanoparticles (AgNPs) are the nanoparticles with the highest degree of commercialization (Ahamed *et al.*, 2008; Rejeski and Lekas, 2008). Due to their antibacterial properties, they are widely used for medical applications such as coating of medical equipment (catheters, surgical equipment and prostheses), in wound dressings, and, of increasing importance, in drug delivery (Kumari and Yadav, 2011; Soumya and Hela, 2013).In addition to the medical applications, AgNPs are used in a number of household products where antibacterial properties are desired. AgNPs are used as detergents, in wall paints, textiles and cosmetics, as well as in the lining of washing machines, dishwashers and refrigerators (Edwards-Jones, 2009). This wide use of AgNPs in consumer and medical products may lead to possible exposure through the gastrointestinal tract, the respiratory system and directly through the bloodstream as for some of the medical applications.

AgNPs have been shown to be toxic to a number of animal species and cultured cells (Gaiser *et al.*, 2013; Johnston *et al.*, 2010). Ag-particle toxicity has often been associated with ion release, generation of reactive oxygen species and induction of oxidative stress (Johnston, *et al.*, 2010). Examples for both inflammatory (Nishanth *et al.*, 2011) and anti-inflammatory (Wong *et al.*, 2009) effects of AgNPs have been reported, and there are also conflicting results with regards to the ability of AgNPs to cause oxidative stress (Nishanth, *et al.*, 2011; Powers *et al.*, 2011). The physicochemical characteristics of the NPs, such as size, shape, and solubility, and also the choice of model, exposure times, and concentrations are maybe the reason for these conflicting results.

There is also an ongoing discussion on whether the toxic effects seen after exposure to AgNPs are due to the nanoparticles themselves, or the release of silver ions (Ag+) from the particles (Wijnhoven *et al.*, 2009), or both (Lubick, 2008). A recent study investigating the changes in gene expression levels in human lung epithelial cells after exposure to both AgNPs and Ag ions (in the form of silver nitrate, $AgNO_3$, which dissolves into Ag+ and NO_3- in solution), found a considerable difference in the response (Foldbjerg *et al.*, 2012). Foldbjerg *et al.* (2012) observed up-regulation of more than 1000 genes in cells treated with AgNPs compared with 133 genes in cells treated with Ag+ ions. This suggests that the Ag-particles themselves directly contribute to toxicity in a way that cannot solely be explained by the release of silver ions.

1.2.1 Toxicokinetics of silver particles

The risk of dermal, inhalation or ingestion exposure to silver nano- and microparticles (Ag-particles) are all relevant due to the commercial use of Ag-particles (Johnston, *et al.*, 2010). Direct exposure of organs to NPs through the bloodstream is likely for medical applications, and there is potential for NPs to reach the bloodstream through inhalation (Muhlfeld *et al.*, 2008), through the skin (Korani *et al.*, 2011), or via the gastrointestinal tract (Schleh *et al.*, 2013). A schematic overview of the fate of Ag-particles in the body is shown in figure 1.2.1.

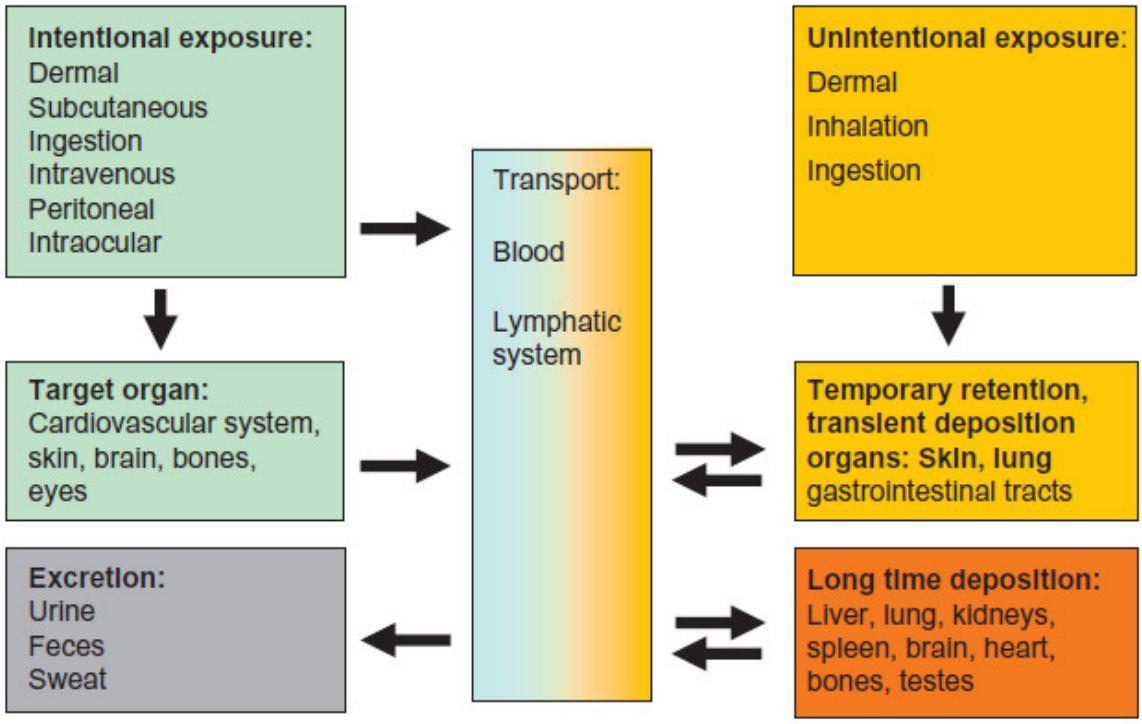

Figure 1.2.1: Toxicokinetics of silver nanoparticles. *A schematic representation of the fate of silver nanoparticles in the body. Adapted from Kruszewski et al. (2011).*

The liver appears to be the primary target organ of Ag-particles through all routes of exposure, but Ag-particles are also found in the spleen, lungs, skin, brain, testes, and kidneys (McAuliffe & Perry, 2007). A dose-dependent distribution of Ag-particles to different tissues is shown both after single dose (Dziendzikowska *et al.*, 2012) and repeated dose studies (Kim *et al.*, 2008; Park *et al.*, 2010). These studies show that Ag-particles are able to cross both the blood-brain barrier and the blood-testes barrier.

Cellular uptake of Ag nanoparticles occurs by pinocytosis, endocytosis dependent on caveolae and lipid raft composition, clathrin-dependent endocytosis and phagocytosis (AshaRani *et al.*, 2009). Intracellularly, Ag-particles appear to be uniformly distributed, and have been found in the cytosol, mitochondria and nucleus (AshaRani, Low Kah Mun, Hande, & Valiyaveettil, 2009). The uptake kinetics, intracellular localization and exocytosis are dependent on the size, surface characteristics (including coating type, if any), the ability of the nanoparticles to form aggregates, as is further discussed in section 1.5.1), as well as the cell type (Bartłomiejczyk, Lankoff, Kruszewski, & Szumiel, 2013).

Orally administered Ag-particles are mainly excreted through faeces, suggesting low bioavailability (Park, 2013), but also to some degree through urine (Dziendzikowska, *et al.*, 2012). Excretion through faeces is the main route of excretion of Ag-particles after intravenous exposure (Park *et al.*, 2011). Dziendzikowska, *et al.* (2012) observed that the excretion of Ag in urine and faeces was much lower in rats treated with 200nm Ag-particles than with 20nm Ag-particles, suggesting that larger particles are less available for excretion.

1.3 Oxidative stress, antioxidant defence and DNA damage-repair

1.3.1 Oxidative stress

Generation of ROS and the induction of oxidative stress are considered the most plausible mechanism of toxicity for Ag nanoparticles (Foldbjerg *et al.*, 2011). ROS are highly reactive compounds which may bind to biological molecules, thereby causing damage. Examples of ROS products are superoxide ($O_2^{\bullet-}$), hydroperoxyl radicals (HO_2^-), hydrogen peroxide (H_2O_2) and hydroxyl radicals ($^{\bullet}OH$). ROS are regularly generated at low levels as by-products of normal cellular processes, such as aerobic respiration and other O_2 consuming- or producing processes. ROS are also by-products of cytochrome P-450-mediated biotransformations, which are important detoxification pathways, and may be generated by specialized cells-types involved in the defence against invading microorganisms.

Neutrophils, eosinophils, monocytes, macrophages and brain microglia produce ROS through the NADPH oxidase enzyme (Babior, 2004; Bianca *et al.*, 1999; Sankarapandi *et al.*, 1998), and use this to combat invading microorganisms. NADPH oxidase is a complex enzyme consisting of five subunits (figure 1.3.1) that catalyses the production of superoxide from oxygen and NADPH. Activation of the enzyme involves in the phosphorylation of one of the cytosolic components. Proinflammatory cytokines such as TNFα and *Il-1*β have been reported to initiate NADPH oxidase activation in microglia of the brain (Mander *et al.*, 2006).

NADPH oxidase activity have been suggested as a possible mechanism for neurodegeneration in neuronal diseases such as Parkinson's disease (Myhre *et al.*, 2013), and as a possible mechanism for toxicity caused by nanoparticles (Mo *et al.*, 2009).

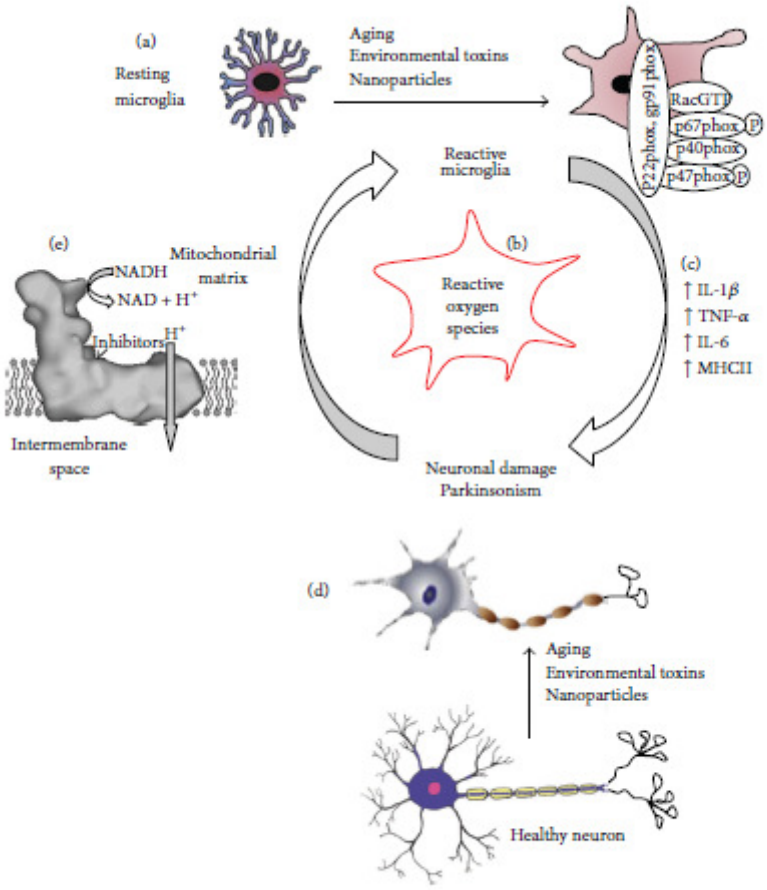

Figure 1.3.1: Nanoparticles, along with other chemical stress and aging may alter microglia reactivity and activation of the phagocytic NADPH oxidase complex. *(a) Stimulation of microglia induces the parallel activation of oxidase components within the cytoplasm. This activation causes the phosphorylation of the p47phox and p67phox subunits of the NADPH oxidase complex. These subunits then translocate to the membrane where they interact with the p22phox and gp91phox (NOX) subunits to initiate ROS production (b). Excessive or prolonged inflammation (e.g., IL-1β, IL-6, TNF-α) (c) and ROS resulting from increased microglial activation may contribute to neuronal damage (d). In addition, chemicals can damage complex I in mitochondria (e) and induce deleterious changes to neurons by ROS generation and ATP depletion. The figure is adapted from Myhre, et al. (2013)*

Due to this inherent ROS-generation, mammalian cells have a large number of antioxidant defences, both enzymatic and non-enzymatic, to counter the toxic ROS-molecules (see section 1.3.2). Oxidative stress is the state in which the activity of ROS overwhelms the cellular antioxidant mechanisms' capacity to prevent damage. Oxidative stress may be the result of either a decrease in the defensive mechanisms or an increase of intracellular ROS. In either way, the result is potential damage to biological molecules and activation of specific biological signaling pathways.

1.3.2 Antioxidant defence

Cells have a number of both enzymatic and non-enzymatic antioxidant mechanisms. The enzymatic defence includes superoxide dismutases (Sod) that converts $O_2^{-\bullet}$ to H_2O_2, catalases and peroxidases that detoxify peroxides such as H_2O_2 (shown in figure 1.3.2), and enzymes involved in the production and maintenance of reduced glutathione, an intracellular antioxidant.

In addition to the enzymatic defences, there are a number of antioxidants, some of the obtained via food, protect the cell by reacting with and detoxifying ROS.

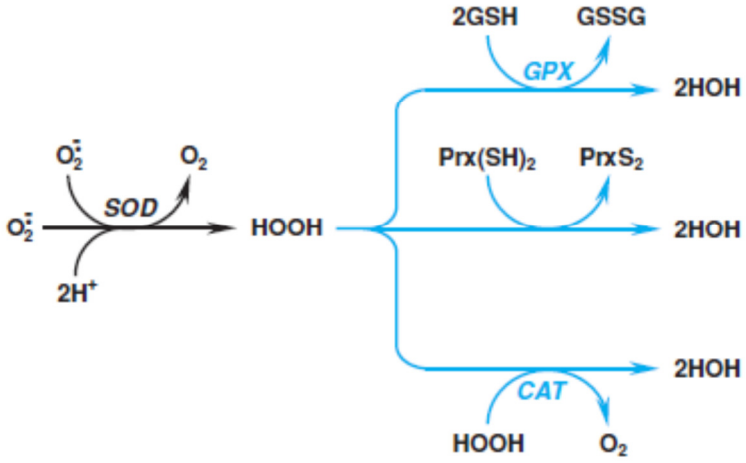

Figure 1.3.2: Antioxidant defence enzymes: *Detoxification of superoxide radical ($O_2^{-\bullet}$) by superoxide dismutase (SOD) and hydrogen peroxide (H_2O_2/HOOH) by glutathione peroxidase (GPX), peroxiredoxin (Prx(SH)$_2$) and catalase (CAT). Adapted from Casarett et al. (2008).*

1.3.3 DNA damage repair pathway

The main concern of oxidative stress is the attack of ROS on biological molecules. Proteins, lipids in the membrane and DNA are main targets. DNA damage caused by ROS includes a multitude of oxidized base lesions, abasic sites, single and double-strand breaks (Ahamed, *et al.*, 2008). Oxidation of guanine may generate 7,8-dihydro-8-oxoguanine (8-oxoG), which is highly mutagenic because it can pair with adenine as well as cytosine. A base-pair with adenine gives rise to a G:C to T:A transversions (Cheng *et al.*, 1992).

The most prevalent repair mechanism in which damaged bases are removed from the DNA is the base excision repair (BER) and the nucleotide excision repair (NER) pathways. In the BER pathway, only the damaged base is removed by lesion-specific enzymes called a glycosylases (Seeberg *et al.*, 1995). In NER pathways, a section of bases around the damaged base is removed. In both repair mechanisms, the strand opposing the damaged base serves as a template for DNA polymerase and DNA ligase enzymes to restore the intact DNA strand.

The main enzyme responsible for removing 8-OxoG lesions is the 8-OxoGuanine DNA glycosylase 1 (*Ogg1*) enzyme (Krokan *et al.*, 2000). The *Ogg1* enzyme removes the 8-OxoG base-paired with a C, and the DNA backbone is subsequently cleaved at the abasic site (AP site) by the human AP endonuclease 1 enzyme (encoded by the *Apex1* gene). Even though *Ogg1* is the main enzyme responsible for removal of 8-OxoG lesions, there are other glycosylases, such as Nei-like proteins (*Neil1*, *Neil2* and *Neil3*) which are capable of removing the 8-OxoG lesions, and these enzymes are therefore regarded as back-up systems (Katafuchi *et al.*, 2004).

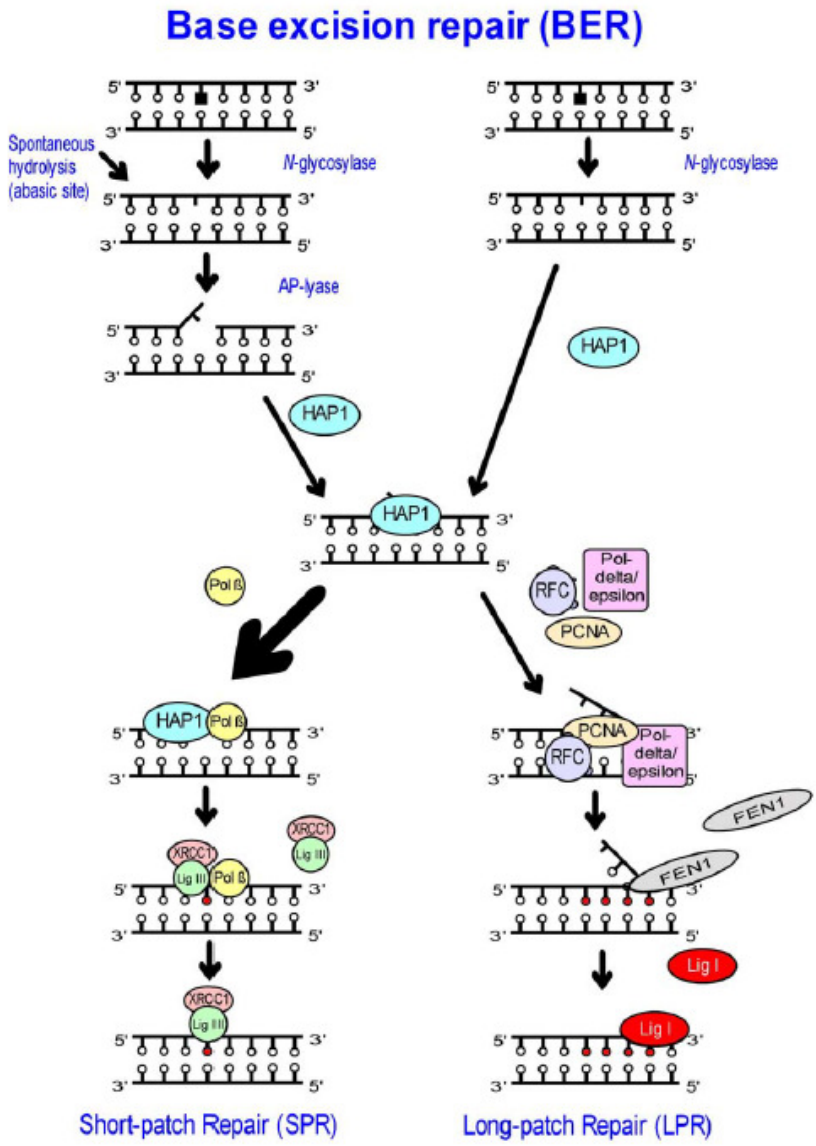

Figure 1.3.3: Schematic representation of the base excision repair (BER) mechanism. *An outline of the base excision repair (BER) pathway. N-glycosylases include Ogg1, Neil1, Neil2 and Neil3. Abbreviations in chronological order: HAP1, human AP endonuclease 1; Polh, DNA polymerase h; XRCC1, X-ray cross complementing protein 1; LigIII, DNA ligase III; PCNA, proliferating cell nuclear antigen; RFC, replication factor C; Poly –(, DNA polymerase y –(; FEN1, Flap endonuclease; Lig1, DNA ligase 1. Adapted from Olsen et al. (2005).*

1.4 Organs

Investigation of the effects of Ag-particles exposure on the gene expression level of some selected genes of brain, testis, liver and lung, from mice has been performed in this thesis. Due to limited time, it was not possible to analyse all these samples with quantitative real-time polymerase chain reaction (qPCR). We therefore chose to limit the analysis of gene expression levels to the samples from brain and testis tissues. Both the brain and testes are organs with important functions that are vulnerable to toxicants, and therefore, are protected by the blood-brain- and the blood-testis barrier, respectively. It has been reported that Ag-particles at the nanoscale are able to cross both these barriers (see section 1.2.1).

1.4.1 Brain

The brain serves as the centre of the nervous system, and is regarded as the most complex organ of the human body. The brain is particularly susceptible to oxidative damage, due to a number of reasons. The brain has a very high demand for oxygen and though it accounts for only a few percent of the body weight, it accounts for about 20 % of the total oxygen consumption of the body. The brain has reduced enzymatic defence against ROS compared with other tissues, with low catalase- and moderate glutathione peroxidase activity (Marklund *et al.*, 1982) and low levels of superoxide dismutase activity (Marklund, 1984).

Access of chemicals from blood to the brain is restricted by the blood-brain barrier (BBB). The BBB is a highly selective permeability barrier that separates the circulating blood from the brain tissue. The BBB is formed by the endothelial cells of blood capillaries in the brain. Tight junctions between the cells prevent diffusion of polar compounds through the intercellular space between the cells. Diffusion of lipophilic compounds is restricted by a large number of ATP binding cassette-transporters (ABC-transporters) present in the endothelial cell membranes pumping xenobiotics from the endothelial cells back into the blood.

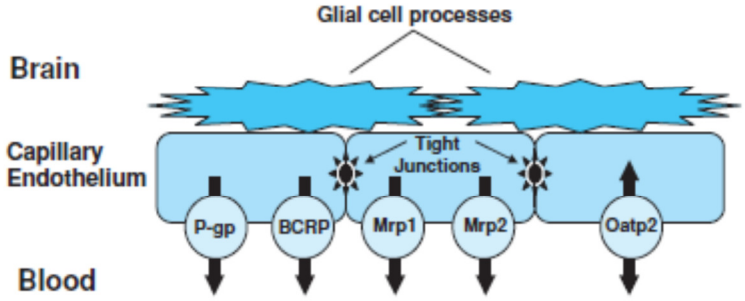

Figure 1.4.1: Schematic representation of the blood-brain barrier. *The figure shows the presence of tight junctions between the endothelial cells, as well as the ABC-transporters in the blood-facing membranes of the endothelial cells. The ABC-transporters listed in the figure are P-gp: P-glycoprotein, BCRP: Breast Cancer Resistant protein, Mrp1: Multidrug resistance protein 1, Mrp2: Multidrug resistance protein 2 and Oatp2: Organic-anion transporting peptide 2. Figure adapted from Casarett, et al. (2008)*

The BBB allows the passage of water, some gases, and lipid soluble molecules by passive diffusion, as well as the selective transport of necessary molecules such as glucose and amino acids. Several studies have shown that Ag-particles are able to cross the BBB (Sharma *et al.*, 2010) and Dziendzikowska *et al.* (2012) showed that Ag-particles of 20 nm and 200 nm accumulated in the brains of rats exposed to a single i.v. (intravenous) dose of 5 mg/kg bw, reaching maximal values 28 days post exposure.

In addition to systemic distribution of Ag-particles through the circulatory system, it has been shown that inhaled nanoparticles can be deposited in the nasopharyngeal region of the respiratory tract and from there may translocate to the brain through the olfactory nerve in rats (Oberdorster *et al.*, 2004). This creates an additional way of direct exposure of nanoparticles to the brain, although, as is pointed out by the authors, the relevancy for human exposure must be treated with caution, as there are major physiological differences between the upper respiratory systems of humans and rats. E.g. that only 5% of the human nasal mucosa is olfactory epithelium as opposed to 50% in rats, and the fact that rats are obligatory nose breathers, whereas humans are mixed oro-nasal/nasal breathers (Oberdorster, *et al.*, 2004). It has been showed that Ag-particles may cause inflammation and disruption of the BBB and thereby increase its permeability *in vitro* (Trickler *et al.*, 2010). Sharma, *et al.* (2010) showed that exposure to 50-60 nm AgNPs caused disruption of the BBB, and hence may induce brain oedema, *in vivo*,

Concern have been voiced over the potential of Ag-particles to reach the hippocampal area of the brain which is central for processes linked to memory formation and learning (Myhre *et al.*, 2013). Liu *et al.* (2012) observed increased concentrations of ROS in hippocampal homogenate from male Wistar rats treated with Ag particle suspension nasal drops every two days for 14 consecutive days in both the low dose (3 mg/kg bw) and high dose (30 mg/kg bw) groups. They also observed histopathological changes in the hippocampus, along with reduced performance in the Morris water maze test for spatial cognition. In contrast, Liu *et al.* (2013) observed no impact on the spatial cognition of rats given daily intraperitoneal administration of Ag-particles every day for 7 days.

1.4.2 Testis

Negative effects on male reproductive health have been observed in western countries in the last decades, as revealed by the increased incidence of testicular cancer, genital abnormalities, poor sperm quality and reduced fertility. These male reproductive disorders are believed to be caused by a combination of lifestyle and environmental factors (Boisen *et al.*, 2001).

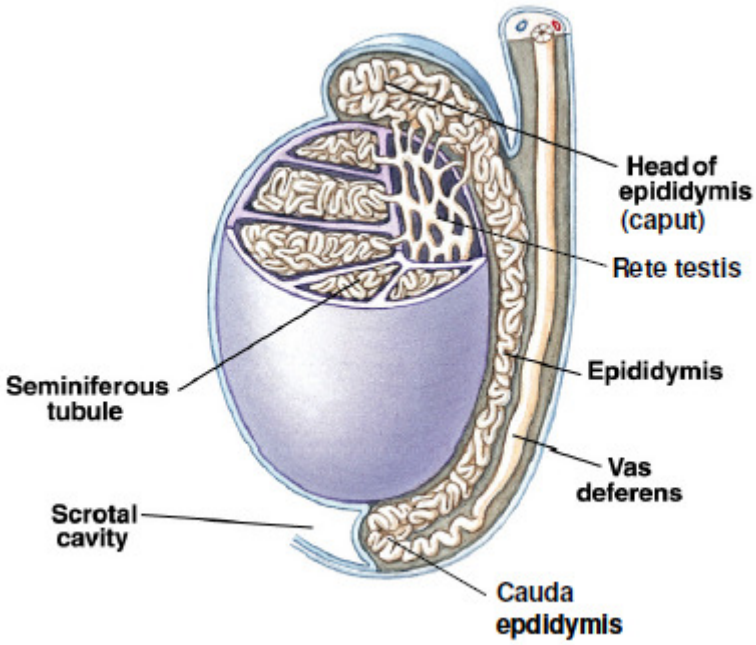

Figure 1.4.2 Anatomy of the testis. *The seminiferous tubules are coiled loops connected to the rete testis, which leads to the epididymis. The epididymis consists of the caput and cauda epididymis that leads to the vas deferens. Adapted from (Silverthorn et al., 2009).*

The testicle is a vital part of the male reproductive organ, and is responsible for the production of produce sperm cells and steroid hormones, such as testosterone. The testis is physically enclosed by a capsule (*tunica albuginea*), and further subdivided into the intertubular-/interstitial compartment and the seminiferous tubule compartment (figure 1.4.2). The interstitial compartment contains Leydig cells, responsible for production of steroid hormones, mast cells, macrophages and the blood- and lymphatic-vessels. The seminiferous tubule compartment contains the germ cells and the Sertoli cells, and it is where the production of sperm cells, the spermatogenesis, takes place. The Sertoli cells protect the maturing germ cells from harmful influences via the blood-testis barrier (BTB) (Bart *et al.*, 2002). This barrier consists of tight junctions between the Sertoli cells and efflux transporters pumping xenobiotics out of the Sertoli cells (figure 1.4.2). The BTB is generated as the first rounds of spermatogenesis are initiated at puberty.

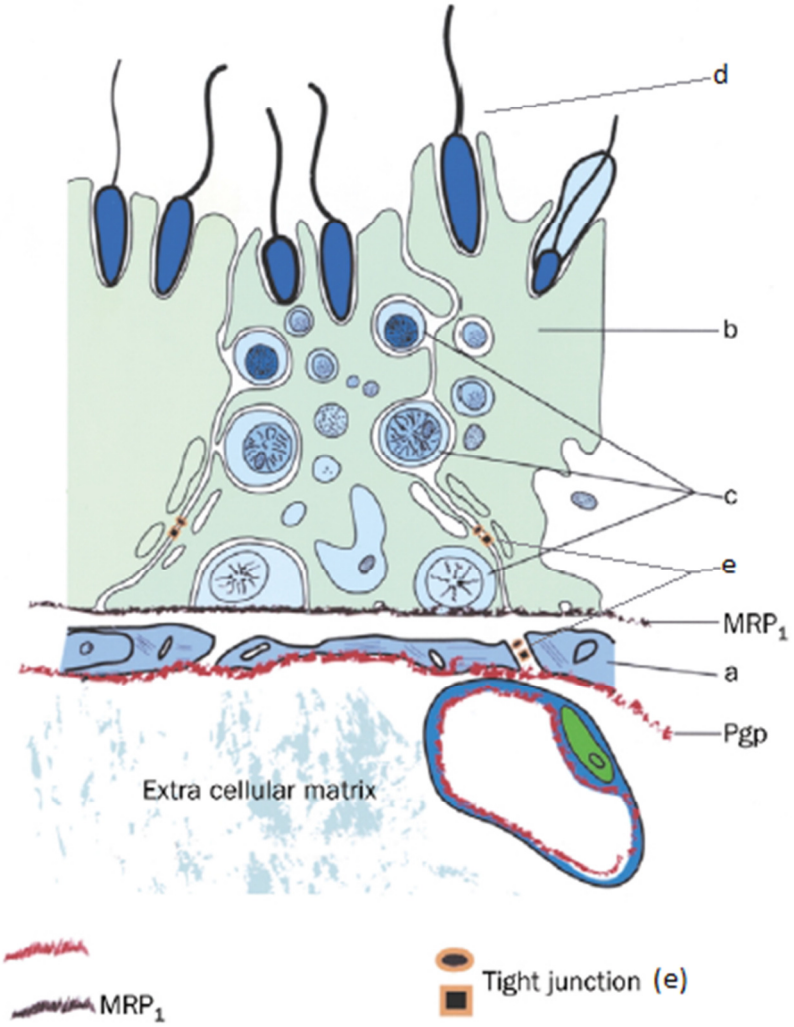

Figure 1.4.2: Schematic overview of tight junctions (e), P-glycoprotein (Pgp), and Multidrug resistance protein 1 (MRP1) in relation to their function in the blood–testis barrier. *a=myoid-cell layer; b=Sertoli cell; c=maturing germ cells; d=mature germ cell; e=tight junction. The figure is adapted with modifications from Bart, et al. (2002).*

Several studies have reported that nanoparticles are capable of crossing the BTB (De Jong *et al.*, 2008; Lankveld *et al.*, 2010), and Ag-particles may contribute to the overall environmental stress which the testicle cells are subjected to (Ema, *et al.*, 2010). It has previously been found that Ag-particles cause cytotoxicity in testicular cells *in vitro* (Asare *et al.*, 2012), and DNA strand breaks (Asare *et al.*, 2014) as well as possible altering of Leydig cell function (Garcia-Reyero *et al.*, 2014) *in vivo*.

1.5 Methodological considerations

1.5.1 Choice of silver particles and exposure doses

The same Ag-particles were used both in the *in vitro* cell culture study and in the *in vivo* animal study. The size of the Ag-particles used in the studies were ~20 nm (hereafter referred

to as Ag20), and ~200 nm (hereafter referred to as Ag200), and both Ag-particle types were purchased from Plasmachem GmbH, Germany, and they have spherical in shape.

These Ag-particles were selected based on literature search (e.g. Asare *et al.*, 2012; Dziendzikowska, *et al.*, 2012; Gromadzka-Ostrowska *et al.*, 2012), and both Ag-particles have been extensively characterized (Lankoff *et al.*, 2012).

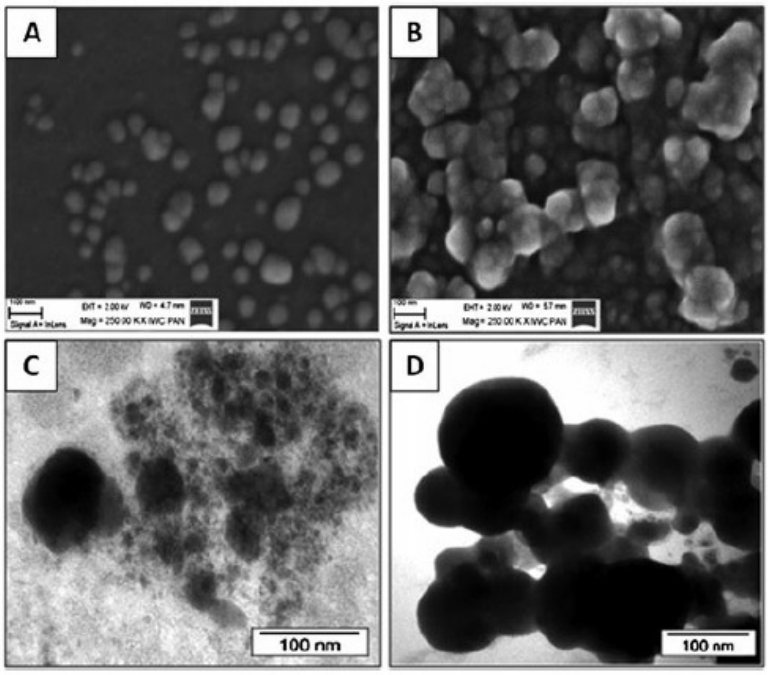

Figure 1.5.1: Scanning- (SEM) and transmission electron microscope (TEM) images of Ag20- and Ag200-particles. *(A) SEM image of Ag20-particles, (B) SEM image of Ag200-particles, (C) TEM image of Ag20-particles, (D) TEM image of Ag200-particles.*

In the *in vitro* cell culture studies, different concentrations of both Ag20 and Ag200-particles were used and their effects were compared. The concentration range between 10 µg/mL and 200 µg/mL was selected based on literature (Asare, *et al.*, 2012; Lee *et al.*, 2014).

The single i.v. injection dose of 5 mg/kg body weight (bw) was selected based on previous studies (Dziendzikowska, *et al.*, 2012), and may be regarded as a relatively moderate dose compared with the results of other studies (Kim *et al.*, 2010; Tiwari *et al.*, 2011). A NOAEL (no observable adverse effect level) of 30 mg/kg bw and a LOAEL (lowest observable adverse effect level) of 125 mg/kg bw has been suggested after a subchronic oral toxicity study (Kim *et al.*, 2010). The gastrointestinal uptake of Ag-particles has been estimated to be between 1.2 – 4.2 % in oral toxicity studies using doses of 1 - 10 mg/kq bw with greater uptake with the highest dose (Lin *et al.*, 2014). Our i.v. dose of 5 mg/kg bw should therefore be slightly lower than the effective dose of the LOAEL suggested byKim, *et al.* (2010), and may therefore be regarded as moderate. Intravenous exposure was also regarded as a relevant route of exposure for the Ag-particles used in medical applications. A study investigating the blood silver levels of burn patients treated with containing wound dressings showed that the blood levels were increased in the course of the treatment, but that these increases were not

associated with signs of toxicity (Vlachou *et al.*, 2007). In addition, Ag-particles have also been shown to reach the circulatory system via other exposure routes (Johnston, *et al.*, 2010).

Fresh preparation of Ag-particles before each exposure is important, as Ag-particles tend to agglomerate in suspension (Bihari *et al.*, 2008). A detailed description of particle preparation is presented in section 2.1.2.

1.5.2. Mouse embryonic fibroblasts (MEFs) and the *Ogg1* knock-out mouse model

In vitro toxicity testing can give important mechanistic information about substances. As an *in vitro* testing is relatively cheap, and several studies can be done in parallel, it is an important supplement to the *in vivo* toxicity testing. Mouse embryonic fibroblasts (MEF) cells are isolated from mid-gestation mouse embryos and can either be cryopreserved until use as primary cells, or immortalized to a cell line. As the isolation of MEFs are relatively easy to perform, and as the cells can be isolated from mice with different genetic alterations, MEF cells are ideal for studying the effects of specific genetic mutations (Xu, 2005).

Previous studies have showed that human male germ cells have a low capacity to repair certain types of oxidative DNA damage, in contrast to the highly efficient repair in rodents (Olsen *et al.*, 2001; Olsen *et al.*, 2003). To mimic the reduced repair-capacity of human germ cells, mice and MEF cells with a knock out (KO) mutation at the 8-oxoguanine DNA glycosylase-gene (*Ogg1*$^{-/-}$), were used along with mice and cells with the wild type (WT) genotype (*Ogg1*$^{+/+}$). The mice were a generous gift from Klungland and co-workers at the Oslo University Hospital (Klungland *et al.*, 1999), and the MEF cell cultures were kindly given to us by Professor Lars Eide and co-workers at the Oslo University Hospital.

In addition to being a good model for the reduced repair capacity of human germ cells, the *Ogg1* model is also relevant in the studies of other types of oxidative damage. For example, the *Ogg1* KO mice have been used as a model for mild Parkinsonism (Cardozo-Pelaez *et al.*, 2012).

1.5.3 Reactive oxygen species (ROS) measurement

2,7-dichlorodihydrofluorescein (DCFH-DA) is a stable dye which diffuses passively through the cellular membrane. Intracellular esterase activity results in the formation of DCFH, a non-fluorescent compound that is trapped in the cells. DCFH is oxidized by hydrogen peroxide (H_2O_2) and other low molecular weight peroxides, to the highly fluorescent compound DCF. Thus, the fluorescence intensity is proportional to the amount of H_2O_2 produced by the cells, and may be measured to establish the level of ROS in the cells (Myhre *et al.*, 2003). The DCFH-DA assay has been used in several previous studies of ROS generation caused by Ag-particles (e.g. Hussain *et al.*, 2005; Lee, *et al.*, 2014; Piao *et al.*, 2011).

1.5.4 Mitochondrial membrane potential assay

The mitochondrial membrane potential (ΔΨm) is an important parameter for mitochondrial function and it can be used as a marker of early signs of apoptosis (Green and Reed, 1998; Petit *et al.*, 1995). In order to investigate the connection between ROS generation and apoptosis, the JC-1 mitochondrial membrane potential assay was performed after 24-hour exposure to Ag20- and Ag200-particles as described in section 2.1.2. The 24 hour exposure time to Ag-particles was chosen based on our ROS-measurements, described in section 3.1.1.

5,5',6,6'-tetrachloro-1,1',3,3'-tetraethylbenzimidazolylcarbocyanine iodide (JC-1) is a fluorescent dye that selectively enters mitochondria and reversibly changes colour from green to red depending on the mitochondrial membrane potential. In healthy cells with high mitochondrial membrane potential, the JC-1 dye forms complexes known as J-aggregates that emit a red fluorescence, whereas in unhealthy cells with low ΔΨm, the dye remains in its monomeric form, emitting green fluorescence. The ratio between the fluorescence intensity of the J-aggregates (red) to that of the JC-1 monomers (green) is used as an indicator of cell health according to the manufacturer's protocol, i.e., the lower the ratio, the more cells with a low ΔΨm, indicating compromised cell health.

1.5.5 Gene expression analysis

The flow of information from DNA to gene product is the fundamental principle of molecular biology. The genetic information contained by DNA is transcribed to mRNA molecules, which are then translated to proteins within the individual cells. Proteins, in turn, are directly responsible for cell organization and function, and may also regulate the synthesis of other molecules.

When a cell is exposed to a toxic agent, it may respond by changing its normal processes, and this can be reflected as qualitative or quantitative changes in gene expression levels. A change in gene expression levels will lead to downstream changes in protein production encoded by these genes, and further downstream metabolic changes because of these proteins. In this thesis, the effects of exposure to Ag-particles on gene expression levels in WT and KO mice were investigated.

For gene expression analysis to give a correct image of the RNA population in the samples examined, it is of high importance that the RNA extracted from the samples is of high quality. Low-quality RNA can seriously compromise downstream analysis (such as qPCR and microarray) and may lead to incorrect interpretations of the data. It is therefore essential that an extensive RNA quality control is performed. RNA quality encompasses both RNA purity (absence of contaminants such as DNA, protein, carbohydrates and lipids) and RNA integrity.

Compared with DNA, RNA is relatively unstable molecules which are prone to enzymatic, chemical or physical degradation. RNA molecules are readily degraded by Ribonuclease enzymes (RNases), and these enzymes present in the environment. Bacteria and moulds are common in both dust particles and on human skin, and they are the most common sources of RNases. It is therefore essential to provide an RNase-free environment throughout the RNA-isolation procedure and in any subsequent handling of RNA-samples, and this may be done by spraying all equipment, as well as gloves with RNase inhibitors. In addition to RNases from the environment, many tissues, e.g. liver, contain a large amount of RNases, which are activated upon thawing. Storing the RNA at very low temperatures (-80 °C), and keeping the samples on ice during processing, may help in preventing the RNA from being degraded. In addition, lysis solutions supplied with commercial RNA isolation kits usually contains RNase inhibitors such as guanidine thiocyanate.

Quick and efficient tissue homogenization is an important factor which may influence the RNA quality and yield. To establish a quick and robust homogenization protocol, we compared two homogenization methods: Ultra-Turrax (IKA-Werke, Germany) and Precellys (Bertin Technologies, France) in a pilot study. The results from this study are presented in section 3.2.1.

RNA cannot serve as templates in the qPCR assay. Therefore, the isolated RNA has to be copied into complementary DNA (cDNA) by a reverse transcription (RT) reaction. The RT reaction should result in a cDNA population that is representative for the original mRNA population of the sample. The RT reaction is still not completely understood, and is considered to represent the uncertain step in gene expression analysis (Malboeuf *et al.*, 2001; Zhang *et al.*, 2001).

The actual quantitative real-time PCR (qPCR) is the real time quantification of the cDNA created in the RT-reaction, and amplified by PCR. The polymerase chain reaction (PCR) was invented in 1987 (Mullis; *et al.*, 1987) to amplify fragments of DNA. The PCR reaction relies on the ability of heat-stable DNA polymerase enzymes, such as Taq-polymerase, to extend short single-stranded synthetic oligonucleotides (primers) during repeated cycles heating and cooling of the reaction for DNA melting and enzymatic replication of the DNA, a process known as thermal cycling. The primers are designed to specifically bind to the DNA fragment to be amplified, and the DNA polymerase uses these primers as templates for DNA extension. As the PCR reaction progresses, the DNA fragments that are generated are themselves used as templates for further replication, thus leading to an exponential increase in DNA fragments. Each cycle doubles the amount of target DNA, proceeding until one of the reaction ingredients becomes limiting, upon which the reaction reaches a plateau.

The qPCR was developed by Higuchi *et al.* (1992) and measures, as suggested by the method name, the quantitative increase in PCR products in a real time. A master mix, containing a fluorescent probe marker, such as SYBR Green, a heat stable polymerase, deoxyribonucleotides (dNTPs), and magnesium salt is mixed with diluted sample cDNA, and during the repeated heating and cooling of the qPCR reaction, the fluorescent probe binds to

the double stranded helix of produced DNA and the fluorescence is measured after each cycle. The quantification cycle (Cq) is the fractional cycle number at which the fluorescence exceeds a fixed threshold, and how quickly a sample reaches this threshold depends on the amount of cDNA for the specific gene sequence in the original sample. The Cq value is therefore an estimate of the amount of RNA in the cells or tissue. The gene expression analysis is therefore a good way to estimate the toxic response of cells at a molecular level (Stevens *et al.*, 2000). Though the results from gene expression analysis should be extrapolated with caution, gene expression analysis may be a useful biomarker for the early stages of toxicity, and also may be of great use in investigating mechanism of toxicity.

1.6 Aims

The uses of nanotechnology are expanding, and as a result humans are exposed to increasing number of different nanomaterials. The potential human health hazards are not well characterized. Therefore, more knowledge about the potential health hazards by nanoparticles is needed. Investigating the mechanism of toxicity is a first step in understanding how these particles affect humans and the environment. The aim of this thesis was to evaluate oxidative stress as a possible mechanism of Ag-particle toxicity. More specifically, we wanted to get answers to the following questions:

- Does exposure to Ag-particles contribute to ROS generation *in vitro*?

- Does exposure to Ag-particles affect the mitochondrial integrity *in vitro*?

- Does exposure to Ag-particles modulate the expression of genes involved in oxidative stress, inflammation and DNA damage repair pathways in mice?

2 Materials and methods

2.1 Cell cultures

Mouse embryonic fibroblasts (MEFs) cell lines established from mid-gestation mouse embryos from wild-type (*Ogg1*$^{+/+}$) and genetically modified knockout (*Ogg1*$^{-/-}$) mice were employed for the *in vitro* experiments. The *Ogg1* gene codes for the 8-OxoGuanine DNA glycosylase 1 enzyme, which as described in the introduction section 1.5.2, is responsible for the excision of 8-oxoguanine, a mutagenic base that occurs as a result of exposure to reactive oxygen. The MEF cells were cryopreserved in liquid nitrogen and thawed at passage nr. 5 for the KO cells and nr. 8 for the WT cells.

2.1.1 Culturing conditions

The cell cultures were routinely maintained in Dulbecco's Modified Eagle's Medium (DMEM) containing 4.5 g/L Glucose, 10 % Foetal Calf Serum (FCS), 1 % 200 mM L-Glutamine (final concentration 16.6 mM) and 1 % penicillin/streptomycin (P/S). The cells were grown in 75 cm^2- or 175 cm^2 Costar cell culture flasks (Corning Inc.) at 37 °C with 5 % CO2 and saturated humidity in a cell cultivator.

MEF cells are prone to differentiate if grown at very high or very low densities. It was therefore important to split the cells before they exceeded 75% confluence. The cells were passaged when they reached ~75% confluence, using Trypsin-EDTA and counted as described in detail in appendix A.1.1. – A.1.3.

2.1.2 Preparation of silver particles

Ag-particles (Ag20 and Ag200) were weighed and dissolved with sterile distilled water, to achieve a stock solution with a concentration of 5 mg/mL. Then, the stock solution was sonicated on ice for 3 minutes, after which the Ag-particle solution was mixed with 10X bovine serum albumin (BSA) and 10X phosphate buffered saline (PBS) in a 8:1:1 ratio to achieve a final concentration of 2 mg Ag-particles/mL, and a final BSA concentration of 150 mg/mL (Bihari *et al.*, 2008). The Ag-particle solutions were further diluted in cell culture media to the experimental concentrations.

2.1.3 Reactive oxygen species (ROS) measurement

A main objective of this thesis was to evaluate whether the toxic effects of Ag-particles may be linked to the generation of reactive oxygen species (ROS). To investigate the generation of ROS in WT and KO MEF cells after exposure to Ag-particles *in vitro*, the dye

2,7-dichlorodihydrofluorescein (DCFH-DA) assay was employed, which is described in section 1.5.4.

MEF cells were seeded in black walled 96-well plates 24 hours before exposure. Both WT and KO cells were seeded in 45 wells each in a 100 µL growth medium/well. The remaining six wells were used as blanks. Cells were treated with five different doses of Ag20- or Ag200 particles: 10 µg/mL, 20 µg/mL, 50 µg/mL, 100 µg/mL and 200 µg/mL. The experiment was performed four times with three technical replicates in each. H_2O_2 (1mM and 100 µM) were used as positive controls; while vehicle treated cells were used as negative controls.

After 3, 6 or 24 hour exposure, the exposure medium was removed and the cells were washed with 100 µL preheated PBS. Medium containing 20 µM of the dye DCFH-DA was then added to the cells, and further incubated at 37 °C for 20 min. Then, the medium was removed and the cells were washed with 100 µL PBS and another 100 µL of PBS was added. Fluorescence intensity was measured by the ClarioSTAR plate reader at wavelengths between 488 and 526 nm.

The protocol described above is as a result of many different method optimizations. We tried a different approach wherein the cells were grown in 12-well plates, and cells were harvested by gentle scraping. There were no visible ROS-measurement trends in the data when cells were scraped.

2.1.4 Mitochondrial membrane potential assay

Apoptosis is a cellular process involving a genetically programmed series of events leading to cell death. A distinctive feature of the early stages of this programmed cell death is the disruption of active mitochondria. This mitochondrial disruption includes changes in the membrane potential and alterations to the oxidation–reduction potential of the mitochondria. The JC-1 dye is, as described in section 1.5.5, sensitive to differences in mitochondrial membrane potential ($\Delta\Psi m$). In healthy cells with high $\Delta\Psi m$, JC-1 forms aggregates that emit a red fluorescence, whereas in unhealthy cells with low $\Delta\Psi m$ JC-1 will remain in the monomeric form and emit green fluorescence.

MEF cells were seeded in 96-well plates 24 hours before exposure. Both WT and KO cells were seeded in 45 wells each in a 100 µL growth medium/well. The remaining six wells were used as blanks. MEF cells were treated with three different doses of Ag20- or Ag200 particles: 10 µg/mL, 50 µg/mL and 200 µg/mL. The experiment was performed five times with three technical replicates in each. A H_2O_2 concentration of 100 µM was used as positive control, as this was suggested by the manufacturer, and two triplicates of untreated cells for each genotype were used as negative controls.

The JC-1 staining solution was prepared according to the manufacturer's instruction by diluting room temperated JC-1 reagent in pre-heated cell culture medium. The manufacturer advised 1:10 dilution, but noted that dilutions of 1:20 may be used if the staining after 1:10

dilution is too strong. We diluted the JC-1 reagent 1:13,2 as this allowed us to thaw one aliquot of 50 µL/JC-1 reagent per independent experiment.

After 24 hour exposure, the 10 µL of prepared JC-1 staining solution was added to each well. Cells were incubated with JC-1 at at 37 °C for 20 minutes. After incubation, the plate was centrifuged for five minutes at room temperature and 400g. After centrifugation, the supernatant was carefully removed, and 200 µL of assay buffer was added to each well. The plate was then centrifuged for another five minutes at room temperature and 400g. This step was repeated one more time, after which the supernatant was removed and 100 µL assay buffer was added to each well. Fluorescence intensity was measured by the ClarioSTAR plate reader at wavelengths 560/595 nm and 485/535 nm.

2.2 Animals

To get more insight into the mechanisms of toxicity of Ag-particles, the gene expression in the brains and testis of WT and KO mice exposed to Ag-particles at 1 and 7 days was analysed. As we wanted to investigate the role of the 8-oxoguanine DNA glycosylase (*Ogg1*) gene in oxidative damage repair following Ag-particle exposure, mice with of both WT and KO for this gene were used in the study.

2.2.1 Animal models

Animals were 8 to 12 week old and both have C57BL/6 background. The $Ogg1^{-/-}$ mouse was derived from the C57BL/6 mice and 129SV, crossed with Big Blue® C57BL/6 mice (Stratagene, La Jolla, CA,USA) to achieve $Ogg1^{-/-}$ Big Blue® mice, obtained as a generous gift from Klungland and co-workers at the Oslo University Hospital.

Breeding and care were performed in-house at the Norwegian Institute of Public Health, Oslo, Norway, and details are presented in appendix A.1 Isogenic $Ogg1^{+/+}$ (WT) and $Ogg1^{-/-}$ strains in similar background (Big Blue® C57BL/6) were generated after backcrossing the $Ogg1^{-/-}$ mice with C57BL/6 mice (Stratagen/dark cycle. Mice were fed with standard diet and drinking water was provided *ad libitum*. The genotypes of the mice were routinely determined by conventional PCR-genotyping. The experiments were performed in conformity with the laws and regulations for animal experiments in Norway and were approved by the local officer of the Animal Board under the Ministry of Agriculture in Norway.

2.2.2 Experimental design

The *in vivo* experiment was performed at the animal facilities of the Norwegian Institute of Public Health at the Department of Chemicals and Radiation (MIKS) in 2010.

A total of 72 male mice (36 WT and 36 were KO mice), were randomly divided into groups of 6 mice per group.

There were three different treatment groups per genotype per time. The treatment groups were as follows: Ag20 (n=6), Ag200 (n=6), and vehicle control (n=6). Because of technical reasons, 2 of the mice (WT vehicle control, 1 week; and WT Ag200, 1 week) could not be included in the experiment.

Ag-particles were freshly prepared as described in section 2.1.2 each time and administered intravenously (i.v.) by the tail vein at a dose of 5 mg/kg bw. The control group received saline water containing PBS (10%) and BSA (10%).

Exposure day was sat as day 0. Mice were sacrificed by cervical dislocation 1 or 7 days post exposure.

	Genotype	Vehicle control	Ag20	Ag200
Day 1	WT	6	6	6
	KO	6	6	6
Day 7	WT	5	6	5
	KO	6	6	6

Table 2.2.1: Number of animals per treatment group. *Total number of mice in the experimental design was 72, but due to technical reasons, two of the mice could not be included in the study. The final number of animals therefore was 70.*

2.2.3 Harvesting of tissues

Tissues were harvested immediately after termination by cervical dislocation, and the harvested tissues were then immediately frozen on dry ice. From each mouse, the brain, liver, lung and testes were harvested, giving a total of four tissue samples per mouse, and a total of 288 samples were harvested. The tissues were stored at -80°C until use.

2.3 RNA isolation

2.3.1 Tissue homogenization

RNA is very easily degraded by a variety of Ribonucleases (RNases), and RNA degrading enzymes are present in the environment. Therefore, it is of high importance that all parts of the RNA isolation process to be done as quickly and efficiently as possible.

Quick and efficient tissue homogenization is an important factor in order to obtain a high quality RNA which can be used for downstream analysis such as qPCR assay. To establish a quick and robust homogenization protocol, we compared two homogenization methods: Ultra-Turrax (IKA-Werke, Germany) and Precellys (Bertin Technologies, France). After tissue homogenization, total RNA was isolated from the samples and RNA quantity and quality was determined as described in section 2.3.3.

The Ultra-Turrax® T8 disperser tool is designed for homogenization of biological tissue-samples by means of blades which rotate at high speeds. The sample is disrupted and homogenized by a combination of mechanical shearing and turbulence. This was the standard method for homogenization of tissue used in the lab. The Ultra Turrax was run for 45 sec per sample, with additional time added if there were still visible pieces of tissue in the lysate.

The Precellys®24 tissue homogenizer disrupts tissue by subjecting pre-filled lysis tubes with ceramic beads to high-speed multi-directional motion. The shaking movement of the Precellys disrupts the tissue by turbulence. The tissue sample, along with lysis solution, is added to a pre-filled lysing tube containing 50 pieces of 1.4 mm ceramic beads.

The frozen tissue was packed in small aluminium-foils and was kept on dry-ice. The tissue samples were fragmented using a pestle while still in wrapped with the aluminium-foils and approximately 45 mg tissue was transferred to the pre-filled tube containing lysis solution (500 µL) and quickly weighed. The lysis solution was adjusted by adding 250 µL lysis solution per 25 grams of extra tissue weight if the tissue weight exceeded 45 mg. In homogenization run using the Precellys, eight samples were homogenized by using the tissue disruption program. The settings used were 5000 rpm for 20 sec, repeated 2 times with a 5 second interval between the runs. Every part of the procedure was done as quickly as possible to prevent RNA degradation.

For homogenization with the Ultra-Turrax, samples were inserted into the tube with lysis solution and the UltraTurrax was immediately turned on. The sample was homogenized for 45 seconds, or until there was no visible tissue debris in the sample and one sample. In the latter case, time of homogenization was recorded. As with the Precellys, every part of the procedure was performed as quickly as possible to prevent RNA degradation.

The homogenized tissue lysates were stored at -80°C until use.

2.3.2 RNA isolation

Total RNA was extracted from the homogenized tissue lysates using the GenElute Mammalian Total RNA Miniprep Kit (Sigma-Aldrich, USA), according to manufacturer's instructions, with a few minor modifications.

RNA from liver, lung and testes of the animals sacrificed at day 7 was isolated prior to this work at the Department of Chemicals and Radiation following the same RNA isolation protocol as used in this work.

The RNA isolation procedure is a multi-step procedure of removing cellular debris, DNA and other contaminants (figure 2.3.1). The homogenized tissue lysate is filtered to remove cellular debris and remaining pieces of tissue, and after filtration, is mixed with ethanol to facilitate the binding of RNA to a special RNA binding column. Repeated filtration and washing with different wash buffers gradually removes non-RNA material, whereas RNA is bound to the binding column. In the final step, the RNA is eluted and available for quality control and downstream analysis. As in the homogenization step, all equipment, surfaces and gloves were washed with the RNase inhibitor RNase Away to create an RNase-free environment.

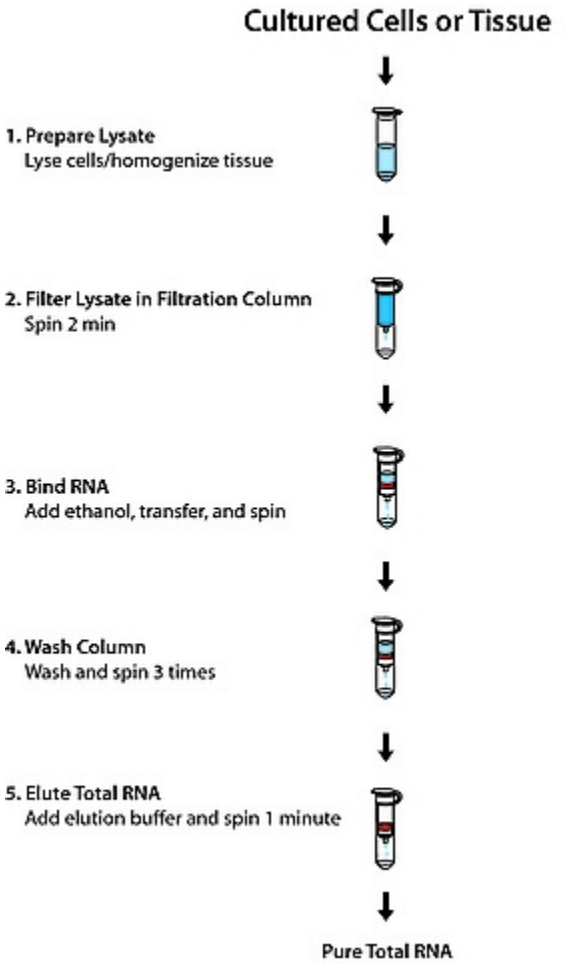

Figure 2.3.1: Procedure for isolation of RNA from tissue homogenate. *For further details, refer to the protocol in appendix A.2.*

2.3.3 Analysis of RNA quantity and quality

High quality RNA is a necessity for downstream analyses such as qPCR and microarray. The quantity and quality of RNA was therefore assessed before proceeding with downstream steps. The RNA quantity and purity of the samples were analysed using the NanoDrop1000

Spectrophotometer (NanoDrop Technologies, USA). The NanoDrop measures the sample's absorbance of light at different wavelengths, and uses this to determine the quality and purity of RNA. RNA and DNA absorb light at 260 nm, and the Nanodrop software estimates the concentration of nucleic acids according to the absorbance at 260 nm. Proteins and phenols absorb light at 280, and other contaminants such as carbohydrates and salts absorb light at 230 nm. By calculating the A260/A280- and A260/A230-ratios, the software gives an indication of the purity of the sample. A 260/280 ratio of around 1.8 for DNA and 2.0 for RNA indicates a pure sample and a 260/230 ratio below 2.0 indicates contaminants.

The samples were measured according to the manual of the NanoDrop1000 software (v. 3.8.1), as described in detail in appendix A.3.

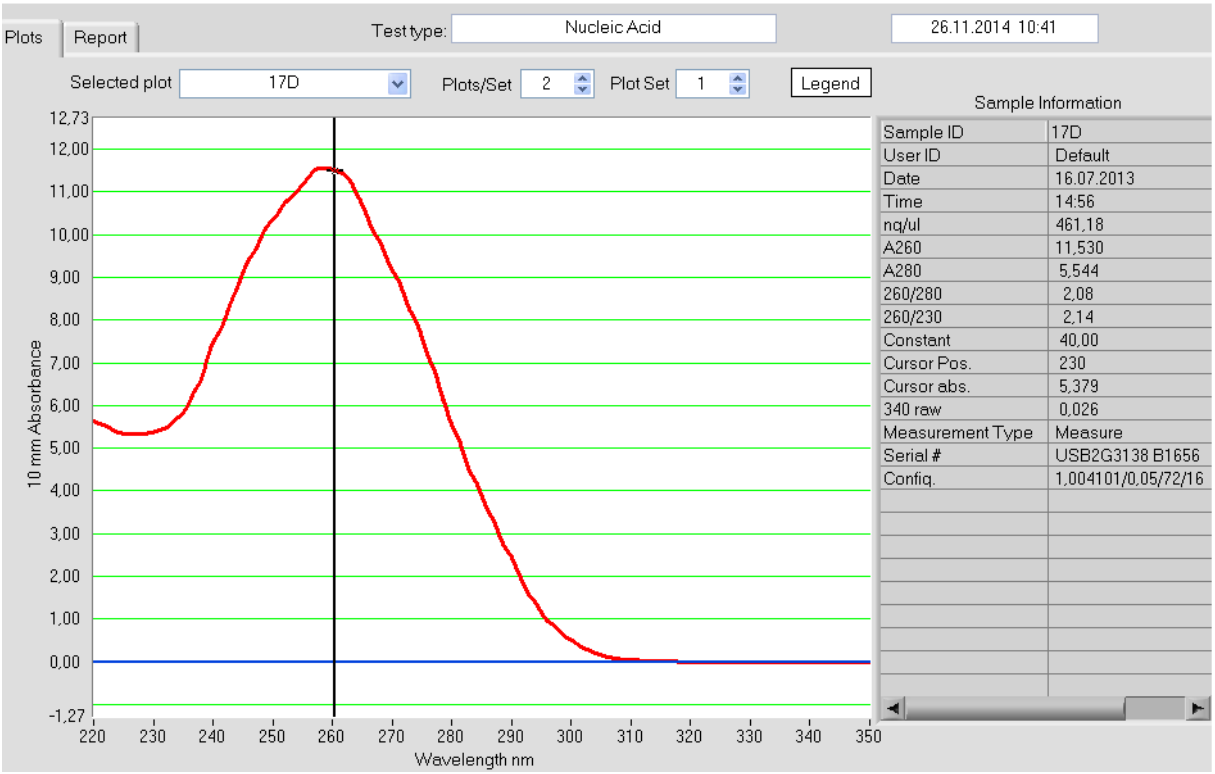

Figure 2.3.2: A typical nanodrop measurement for a RNA sample. *The absorbance curve peaks at 260 nm where RNA absorbs light, and there is just one peak (additional peaks would indicate the presence of contaminants). Run details like RNA yield, OD260/280- and OD260/230 ratios are given on the right. The figure is an adapted screenshot from the Nanodrop1000 software v.3.8.1.*

RNA quality is determined by two parameters: the purity measurement, as descried above, and the integrity of the RNA molecules. The RNA integrity of the samples was measured using the Agilent 2100 Bioanalyzer and the RNA 6000 Nano Assay kit (Agilent Technologies, USA). The Agilent 2100 Bioanalyzer is a chip-based capillary gel-electrophoresis, which allows for automated and objective classification of RNA integrity. This is done by assigning a degradation factor ranging from 1 to 10, with 1 being the most degraded and 10 being the most intact, to each of the RNA samples. In this way it is easy to compare the integrity of the samples.

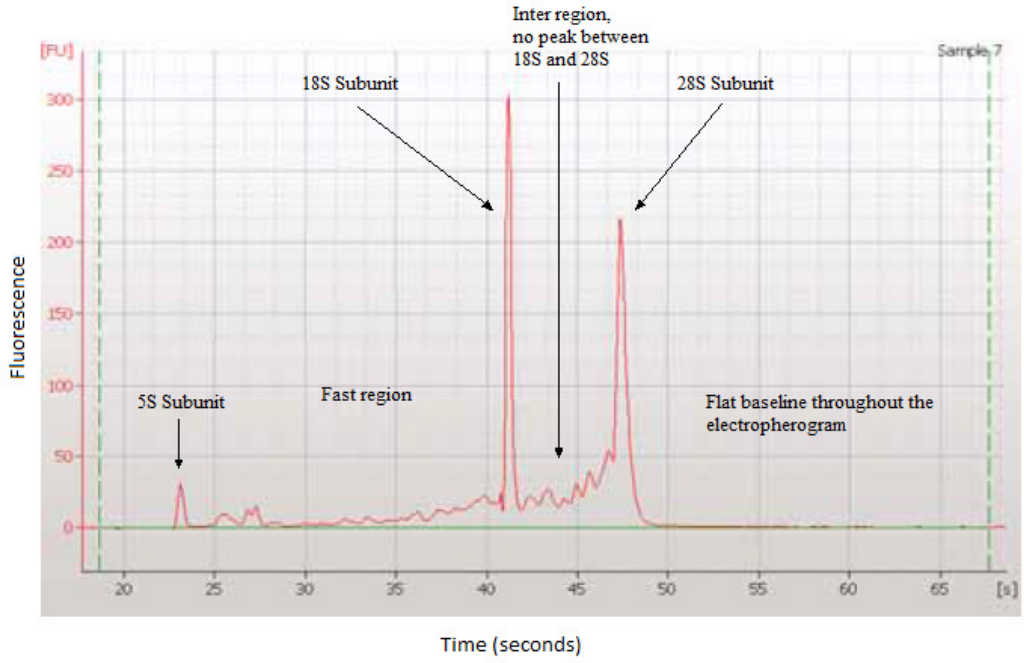

Figure 2.3.3: Agilent Bioanalyzer electropherogram showing the regions that are indicative of RNA quality. *The electropherogram is for intact RNA with RIN close to 10, and a ribosomal ratio (28S:18S) close to 1.9. The figure is adapted with modifications from (Schroeder et al., 2006).*

The Agilent 2100 Bioanalyzer uses gel-electrophoresis-chips from the RNA 6000 Nano assay kit. Preparation protocol for the reagents and chip are listed in A.4.

2.4 Gene expression analysis

The main objective of this thesis was to investigate whether exposure to Ag20 and Ag200 particles affect the expression of genes related to inflammation, oxidative stress, antioxidant defence, intercellular signalling or DNA damage repair. To achieve this objective, a panel of 22 genes involved in these pathways was investigated by qPCR assay.

2.4.1 cDNA synthesis by reverse transcription

RNA molecules cannot serve as templates for the real-time quantitative PCR assay (qPCR). Therefore, the isolated RNA has to be converted to complementary DNA (cDNA) by a reverse transcription (RT) reaction before the gene expressions of the samples can be measured.

This cDNA synthesis was performed using the High-Capacity cDNA Reverse Transcription Kit from Applied Biosystems (USA). The Multiscribe^{TM} Reverse Transcriptase enzyme supplied by the kit converts the RNA to cDNA in the presence of random primers, nucleotides (dNTP) and a magnesium containing buffer. The cDNA population produced from

the RT reaction should reflect the original mRNA population both in terms of transcript amount and complexity. A detailed protocol for cDNA synthesis is described in appendix A.5.

2.4.2 Quantitative Real time PCR (qPCR)

The modern qPCR enables quantification of the PCR products in "real time" during each PCR cycle. This real time quantification is based on monitoring the fluorescent signal emitted as it occurs during the amplification process. Sequence specific or non-specific fluorescent dyes may be used for this purpose.

In this assay, the non-specific fluorescent dye SYBR Green was used as part of the KAPA SYBR® FAST Universal 2X qPCR Master Mix (Kapa Biosystems, USA). The SYBR Green dye binds to the double stranded helix of DNA produced in the qPCR reaction, and quantification of the products is done by measuring the fluorescence after each PCR cycle. The time it takes for the fluorescence to reach a defined threshold level, the quantification cycle (Cq), and this is used as an estimate for the amount of cDNA for the specific gene in the original sample. Gene specific primers were designed using the online Universal Probe Library System (Roche Applied Systems, Oslo, Norway) and the primer sequences used are listed in appendix A.7.

cDNA from each sample was diluted 1:10 with double-distilled RNase/DNase free water and 5 µL of diluted cDNA sample was pipetted from the stock-plate into 384-well plates in quadruplicates using the Bravo Automated Liquid Handling Platform. This plate layout allowed us to measure the expression of two genes on all samples (two different genotypes, two different days and three different treatments) from one tissue in one run, greatly reducing errors due to run-to-run variation. All qPCR reactions were done in duplicate. A detailed protocol for the qPCR mastermix and settings is described in appendix A.6.

2.5 Statistical analysis

Statistical analyses were performed using the JMP software v. 11.1.1 and Microsoft Office Excel 2010, and p-values < 0.05 were accepted as statistically significant.

For the ROS generation experiments, the Shapiro-Wilk test was used to evaluate whether the data showed a normal distribution and the equality of variance was evaluated using the Levene test of homogeneity of variance. If the data were not normally distributed, the data were log-transformed before statistical analysis to obtain normally distributed data. One-way analysis of variance (ANOVA) was used to analyse the ROS generation experiments data.

Analysis of a possible dose-response relationship was done by a mixed model approach using the log-transformed fluorescence intensity as a fixed variable and the experiment date as a random variable to minimize the impact of run-to-run variation.

Statistical analysis of the RNA yield, purity and integrity for the optimization of the homogenization method was carried out by one-way ANOVA or by the non-parametric Mann-Whitney U test when the data were not normally distributed. Normal distribution was evaluated using the Shapiro-Wilk test. The RNA yield and purity in the main animal study was also analysed by one-way ANOVA followed by *post hoc* Dunnett's tests to allow for multiple comparisons, or by the non-parametric Kruskal Wallis test. ANOVA is thought to be a fairly robust method, so even if some of the underlying assumptions (normality and equal variances) are not fulfilled, it might still be used with some cautions.

The gene expression data were analysed using the comparative $2^{-\Delta\Delta Cq}$ method described by Livak and Schmittgen (2001). The quantification cycle (Cq) is the fractional cycle number at which the fluorescence exceeds a fixed threshold and this was recorded by the SDS v.1.3 software during each qPCR run. The raw Cq-values were exported to Microsoft Office Excel, and Cq-values radically different from other technical replicates were defined as outliers and removed. All Cq-values above 35 were considered beyond limit of detection and replaced with 35, as Cq-values that are above 35 are generally not reliable (Duale *et al.*, 2012, 2014). The Cq-values of the target genes were then normalized against the geometric average of four reference genes identified by the BestKeeper software Pfaffl, Tichopad, Prgomet, & Neuvians, 2004). In short the calculations of the $2^{-\Delta\Delta Cq}$ method were carried out as follows:

$\Delta Cq(\text{sample}) = Cq(\text{target gene}) - Cq(\text{reference gene})$

$\Delta\Delta Cq = \Delta Cq(\text{sample}) - Cq(\text{control}).$

$\text{Fold change} = 2^{-\Delta\Delta Cq}$

Where the $2^{-\Delta\Delta Cq}$ represents the fold change and the interpretation of data is as follows, if:

$2^{-\Delta\Delta Cq} = 1 \rightarrow$ No change in gene expression

$2^{-\Delta\Delta Cq} > 1 \rightarrow$ Induction/increase relative to untreated control

$2^{-\Delta\Delta Cq} < 1 \rightarrow$ Repression/decrease relative to untreated control

The distribution of the $2^{-\Delta\Delta Cq}$ values are asymmetric, due to the conversion of an exponential process (PCR amplification), therefore the range given in $2^{-\Delta\Delta Cq}$ are also asymmetric (Livak and Schmittgen, 2001). This makes it difficult to interpret $2^{-\Delta\Delta Cq}$ values. A value of 2 and 0.5 represent the same fold change in different directions. Therefore, the $2^{-\Delta\Delta Cq}$ value was subsequently log2-transformed in order to make the values symmetrical around zero. For further discussion of the need for normalization and selection of reference genes, refer to the discussion, section 4.2.3.

Statistical analysis of the gene expression data was done by using the one-way ANOVA followed by a *post hoc* Dunnett's test using the ΔCq-values to allow for multiple comparisons, i.e. comparison between treatment groups.

3 Results

3.1 Cell culture study

3.1.1 Measurements of ROS-generation after treatment with Ag20- or Ag200-particles in mouse embryonic fibroblast cells.

In this experiment, the main objective was to evaluate whether Ag20- or Ag200-particles could stimulate ROS generation in MEF cells *in vitro*. *Ogg1*$^{+/+}$ (WT) and *Ogg1*$^{-/-}$ (KO) MEF-cells were treated with different concentrations of Ag20- and Ag200-particles for 3, 6, and 24 hours (see materials and methods section 2.1.3), and ROS-generation was measured by monitoring the fluorescence intensity of the fluorescent dye DCFH-DA. Cells treated with different concentrations of hydrogen peroxide (H_2O_2) were used as positive control.

The experiments showed that there was a higher overall level of ROS-generation in KO cells than in the WT cells at most doses at most time points. Although the difference is not statistically significant at all measurement points and concentrations, the difference is clearly visible from the data shown in figure 3.1.1. There were no statistically significant differences in ROS-generation between the different time points, though ROS-generation seems to be at similar leves at 3 and 24 hours (figure 3.1.1A and 3.1.1C), but somewhat lower at 6 hours (figure 3.1.1B).

When differences caused by the different treatments were investigated, statistically significant increases in ROS generation was found at 24 hours after exposure in KO-cells treated with Ag20-concentrations of 20 µg/mL and higher and Ag200-concentrations of 100 µg/mL and higher. Though the ROS generation at 3 or 6 hours was not significantly increased compared with control for either genotype, a tendency of increased ROS was observed in the KO cells. The WT cells seem to be far less affected by the treatment than the KO cells, judging from the fluorescence levels.

When investigating the dose-response relationship of ROS-generation after exposure to Ag20- or Ag200-particles, a slight correlation was found. Though statistically significant, there was only a minor dose-dependent increase in ROS generation.

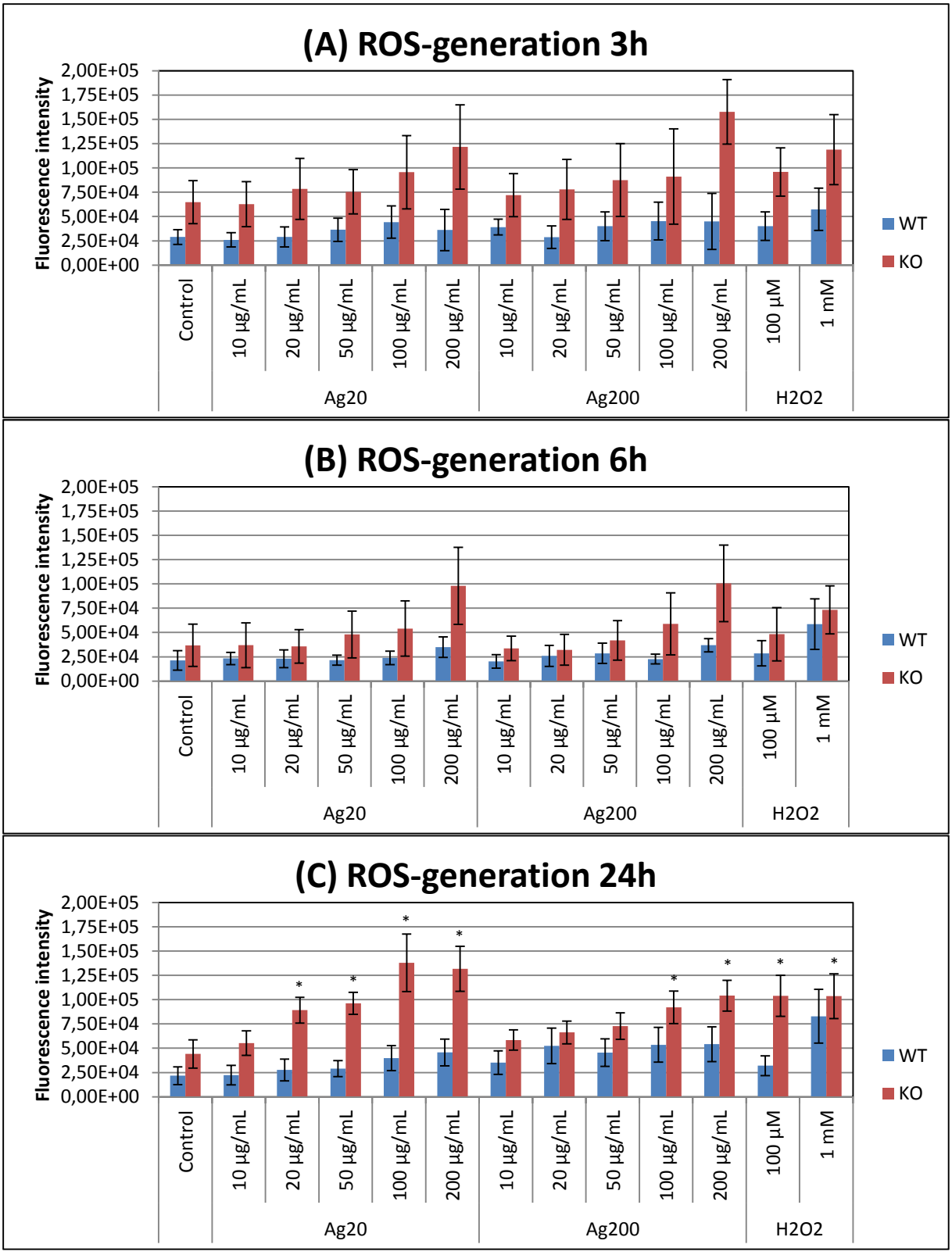

Figure 3.1.1: Generation of ROS at (A) 3 hours, (B) 6 hours and (C) 24 hours for wild type- and knock out-MEF-cells. *MEF WT cells and MEF KO cells were incubated with DCF-DA for 20 minutes, and ROS-generation was monitoring by measuring the fluorescence every three minutes for one hour following incubation, and the data presented are the mean of the final measurement-cycle, one hour after start of the measurement. The values are expressed as mean of four independent experiments with three technical replicates each ± SEM. *p < 0.05: Statistically significant versus control.*

3.1.2 Mitochondrial membrane potential assay after treatment with Ag20- or Ag200-particles in mouse embryonic fibroblast cells

The mitochondrial membrane potential (ΔΨm) is an important parameter of mitochondrial function, and may be used as an early apoptosis marker. In order to investigate the connection between ROS generation and apoptosis, the JC-1 mitochondrial membrane potential assay was performed after 24-hour exposure to Ag20- or Ag200-particles as described in section 2.1.2. 24 hour exposure to Ag-particles was chosen based on our ROS-measurements where we found the highest levels of ROS at this time point, as described in section 3.1.1.

The JC-1 fluorescent dye selectively enters the mitochondria and change colour depending on the mitochondrial membrane potential. In healthy cells with high mitochondrial membrane potential, the JC-1 dye forms complexes known as J-aggregates that emit a red fluorescence, whereas in unhealthy cells with low ΔΨm, the dye remains in its monomeric form, emitting green fluorescence. The ratio between the fluorescence intensity of the J-aggregates (red) to that of the JC-1 monomers (green) was used as an indicator of cell health according to the manufacturer's protocol, i.e. the lower the ratio, the more cells with a low ΔΨm, indicating compromised health.

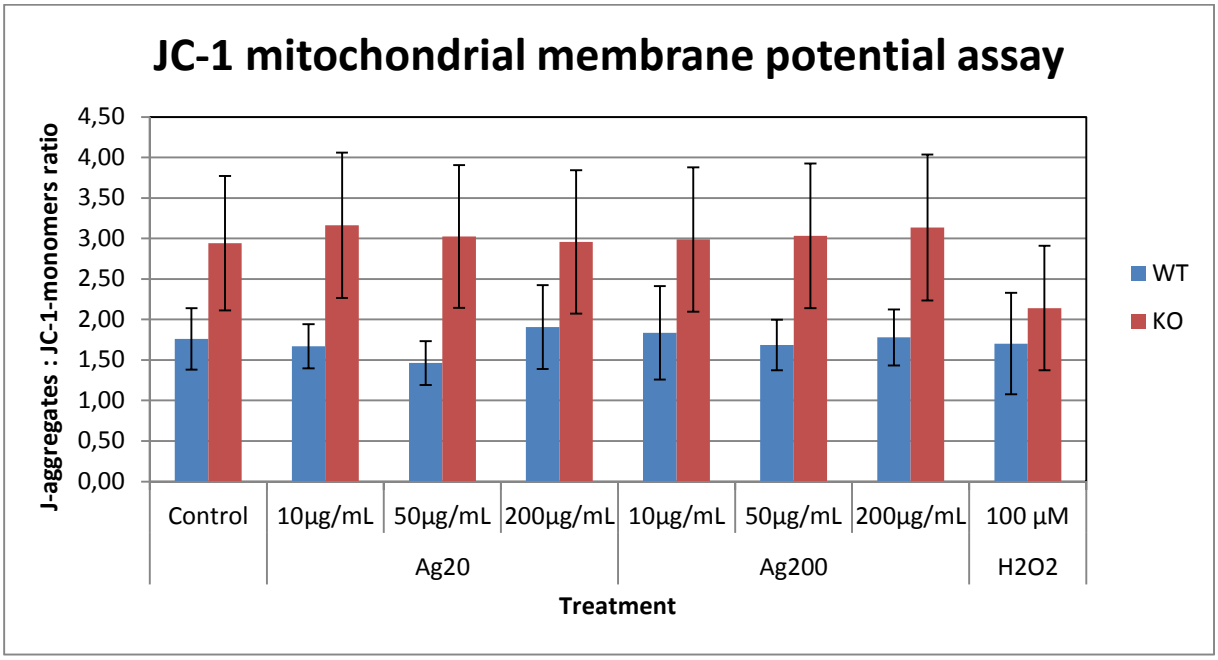

Figure 3.1.2: JC-1 mitochondrial membrane potential assay on MEF-cells treated with Ag20- or Ag200-particles for 24 hours. *J-aggregates are formed in cells with high mitochondrial membrane potential (ΔΨm), and JC-1 monomers are formed in cells with low ΔΨm, i.e. the lower the ratio, the lower average ΔΨm, and less healthy cells. Ratios are presented as mean of four independent experiments with three independent replicates each ± SEM.*

The JC-1 mitochondrial membrane potential assay showed no visible trends, other than somewhat lower aggregates to monomers-ratio, indicating less healthy cells, in the positive control group treated with 100 µM H_2O_2. As H_2O_2 was used as a positive control, significant difference from control was expected, and the reason for this lack of effect is unclear. It was noted that there was very large run-to-run variation in the response.

3.2 Animal study

Animal studies are expensive, time consuming and complex to conduct. It is therefore very important that the tissues obtained from such studies should be used as efficiently as possible. The more assays performed per experimental animal, the less *in vivo* experiments are needed. Biologic material obtained from *in vivo* studies should therefore be regarded as a limited and treasured resource, and should be used as efficiently as possible.

Another important aspect of efficient use of tissue samples in several assays and maybe in several different projects is the 3-Rs-principle, which should be met by all animal studies. The 3-R's approach is aimed at maximizing the animal welfare of experimental animals by replacing animal studies with non-animal methods whenever possible, refining the post-study analysis methodology to obtain the most information possible from the fewest animals possible, and refining the animal experiment to remove or minimize potential pain, suffering or distress in the experimental animals.

In this thesis, the main goal was to identify genes that are significantly differentially expressed in brain or testis samples from WT and KO treated with Ag20- or Ag200-particles *in vivo.*

3.2.1 Optimization of tissue-homogenization method

The main goal with optimizing the tissue-homogenization method was to obtain high quality and quantity RNA from as little tissue as possible. By using the samples in an efficient way, several assays can be performed from the same tissue samples. Prior to isolation of RNA from the animal study, a pilot study was performed where RNA was isolated from different tissues of two untreated mice to optimize the tissue homogenization method. In order to establish a robust tissue-homogenization method, two different methods were evaluated by isolating RNA from the tissues and comparing the quantity and quality of the RNA.

As shown in figure 3.2.1, The RNA yield (RNA µg/mg tissue) obtained from the two homogenization methods was similar for brain and lung samples, while a significantly higher RNA yield was obtained for UltraTurrax method in liver samples and a significantly higher yield was obtained for Precellys method in testis samples.

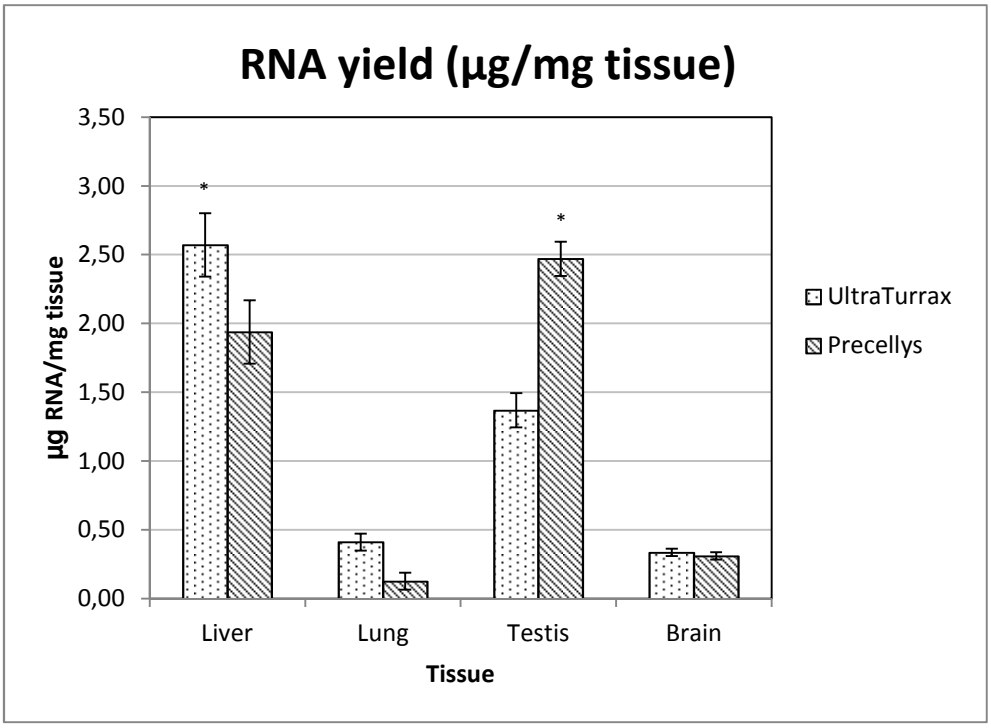

Figure 3.2.1: Comparison of RNA yield from different tissues using two different homogenization methods. *Sample sizes (n=number of technical replicates): Liver using UltraTurrax (n=10) and Precellys (n=12), lung UltraTurrax (n=6) and Precellys (n=4), Testis UltraTurrax (n=6) and Precellys (n=6), Brain UltraTurrax (n=8) and Precellys (n=8). RNA yield is presented as average ± SEM. *p < 0.05: Significant difference versus the other homogenization method.*

The RNA quality consists of RNA purity and integrity. The RNA purity is the absence of contaminants (such as proteins, carbohydrates, lipids and salts) and this was measured by spectrophotometry as described in materials and methods section 2.3.3.1. As shown in figure 3.2.2A, similar and comparable average OD 260/280 ratios were observed from both methods. An OD260/280-ratio between 1.9 and 2.1 indicates pure RNA and both methods gave an average OD260/280-ratio close to 2. The OD260/280 ratio is an estimate of the purity of the type of nucleic acid measured, as different bases absorb light at different wavelengths, DNA and RNA will have slightly different OD260/280-ratios.

However, the average OD 260/230-ratio, which gives an estimate of contaminants such as proteins and carbohydrates, was higher for the samples homogenized by Precellys method than those homogenized by UltraTurrax method, except for lung tissues (figure 3.2.2B).

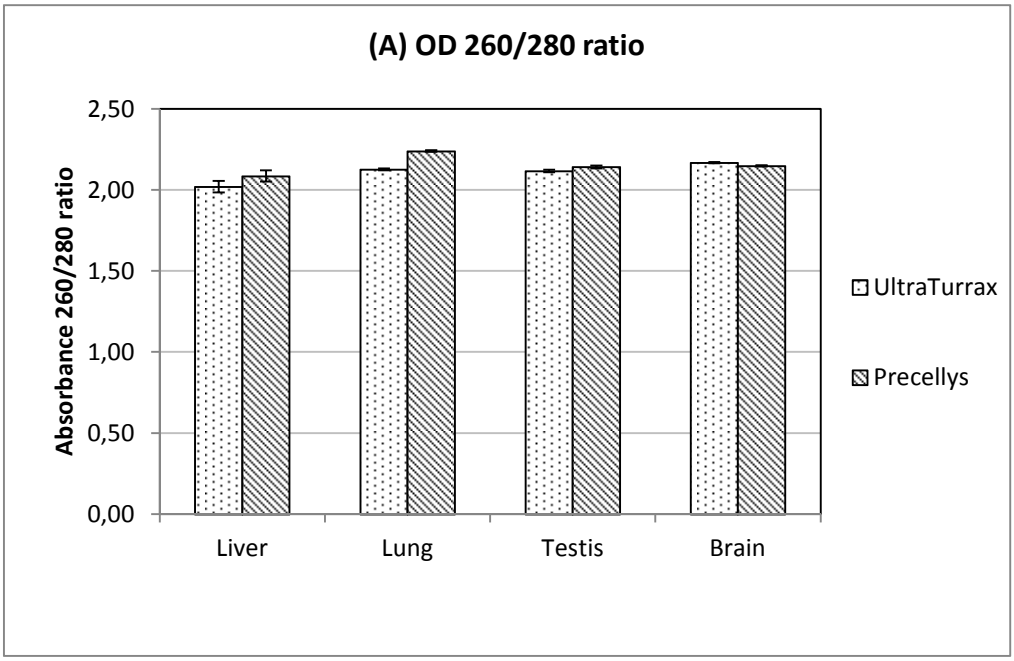

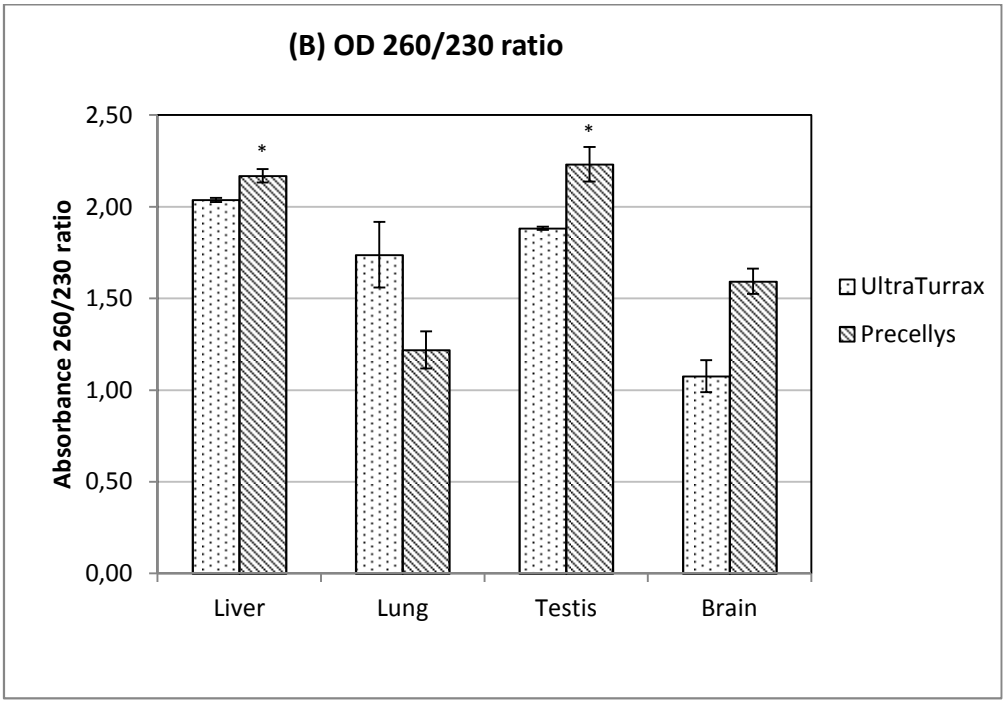

Figure 3.2.2: Comparison of RNA purity using two different homogenization methods. *(A) OD260/280 ratio of around 2.0 for RNA indicates a pure sample. (B) OD260/230 ratio below 2.0 indicates contaminants. Sample sizes (n=number of technical replicates): liver using UltraTurrax (n=10) and Precellys (n=12), lung UltraTurrax (n=6) and Precellys (n=4), testis UltraTurrax (n=6) and Precellys (n=6), Brain UltraTurrax (n=8) and Precellys (n=8). OD260/280-ratios are presented as mean ± SEM. *p < 0.05 Significant difference versus the other homogenization method.*

RNA integrity is another RNA quality parameter and together with RNA purity gives the overall RNA quality. The integrity of the RNA samples homogenized using the two methods was measured with the Agilent 2100 bioanalyzer (see materials and methods section 2.3.3.2), and the RNA integrity numbers (RIN) were calculated using the Agilent 2100 Expert Software. The software assigns all measured samples a RIN value ranging from 1 to 10, with

RIN=1 being the most degraded RNA and RIN=10 being the most intact one. As shown in figure 3.2.3, the RIN values observed were similar for both methods in all tissues but liver, where it was statistically significantly higher for UltraTurrax.

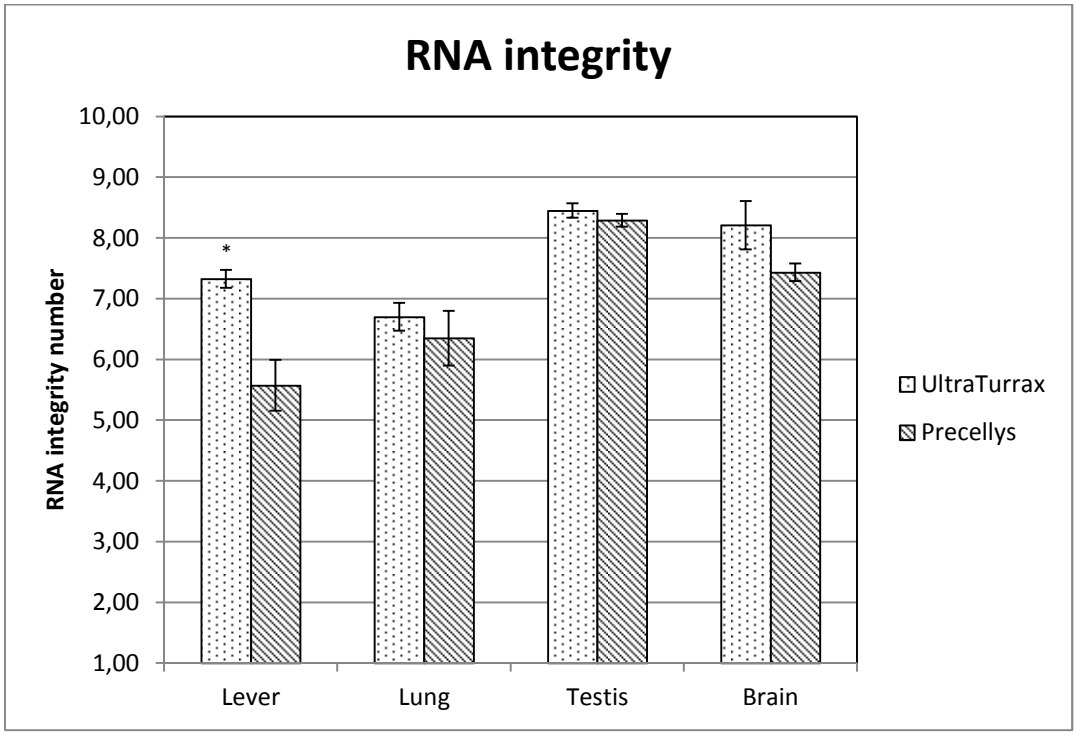

Figure 3.2.3: Comparison of integrity of RNA from different tissues using two different homogenization methods. *RNA integrity is given as a number between 1 and 10, where 1 is the most degraded RNA profile and 10 is the most intact (see materials and methods section 2.3.3.2). Sample sizes (n=number of technical replicates): liver using UltraTurrax (n=10) and Precellys (n=12), lung UltraTurrax (n=6) and Precellys (n=4), testis UltraTurrax (n=6) and Precellys (n=6), Brain UltraTurrax (n=8) and Precellys (n=8). RIN-numbers are presented as average ± SEM.*

Overall, based on these data, high-quality RNA could be extracted from both homogenization methods. Even though there are some statistically significant differences between the two methods, all measurements were within acceptable range for good quality RNA.

From these results, the UltraTurrax homogenization method was selected for the RNA-isolation procedure for the animal study samples, mainly because the UltraTurrax was the cheapest method with low operating cost. The choice of homogenization method is further discussed in section 4.2.1.

All samples, i.e., liver, lung, brain and testis tissues (n=70 samples/tissue, i.e. a total of 280) from the animal study were homogenized using the UltraTurrax method, and then total RNA was extracted from these samples. The RNA quality control was done by spectrophotometry to assess the quantity and purity of the isolated RNA and the results are presented in appendix D.2.

There were differences in RNA yield between the different tissues, and this was expected, as cells produce different amounts of mRNA according to function. E.g. the liver has a high level of metabolism and therefore is rich in RNA, whereas the more stable conditions in the brain requires a lower level of RNA. The isolation of RNA from lung is generally viewed as difficult, as the lung tissue is very thin, and therefore is prone to thawing and subsequent RNA-degradation during the RNA-isolation procedure. The average OD 260/280 and OD 260/230-ratio was comparable between the samples (appendix D.2) and the ratios were within acceptable range.

As RNA cannot be used as template in the qPCR reaction, the RNA was copied into cDNA by reverse transcription PCR (see materials and methods, section 2.4.1). The cDNA yield and purity was measured by spectrophotometry as previously described by measuring the OD260/280 and OD260/230 ratios, and all the samples met the criteria for high quality cDNA. There were no statistically differences in either of the parameters between genotypes, time or treatments. Only cDNA samples from testis and brain were used further in the qPCR assay, because it was not possible to analyse all the samples due to time limitations. The samples from liver and lung will be analysed by qPCR at the Department in the future.

3.2.2. Gene expression analysis in brain and testis of WT and KO mice treated with Ag20- or Ag200-particles

An investigation of how Ag particle treatments modulated the expression of some selected genes involved in inflammation, intercellular signalling, antioxidant defence, oxidative stress and DNA damage repair pathways was conducted using the qPCR assay. Samples from vehicle treated mice were used as control samples; hence, all other samples were compared against the control samples, and the results are shown in figures 3.2.4 – 3.2.9.

To minimize variation due to technical factors, the data from the qPCR analysis were normalized against a set of reference genes. We found that four reference genes met our requirements of stability, and these genes are shown in figures D.1 – D.2 in appendix D.

We did not observe significant genotype differences in gene expression, except for the inflammation-related gene *Tnf-α*. Though the difference in expression of this gene was statistically significant, the difference was small. When we sorted genotype differences by tissue, we observed significant differences in expression for more genes, particularly in antioxidant-related genes in testis and some antioxidant-related genes in brain. There were statistically significant differences in expression between the two tissues for all the genes.

Overall, the effect of the treatments on the gene expression was moderate, with only a few genes being close to a ±2-fold difference relative to control.

3.2.2.1 Effects of Ag-particles on genes involved in inflammation and intercellular signalling:

Due to the interconnection of inflammation and oxidative stress, the expression of genes involved in inflammation pathways was investigated. The qPCR data are presented in figure 3.2.4 for the cytokine-related genes, and in figure 3.2.5 for genes involved in mediating inflammation responses through intracellular signalling.

We observed a statistically significant up-regulation of the *Il-1β* gene in brains of Ag20-exposed KO-mice sacrificed at day 1 (figure 3.2.4A). The *Il-1β* gene encodes for the Interleukin beta protein, which is a proinflammatory cytokine produced by activated macrophages, as well as neutrophils, epithelial- and endothelial cells. There were minor changes in the expression of some of the other cytokine-related genes, but in brain none of these were statistically significant.

In the testes, there was a statistically significant reduction in the expression of the gene *Tnf-α* in KO mice exposed to Ag20-particles and sacrificed at day 1 (figure 3.2.4B). The *Tnf-α* gene encodes for the cytokine Tumour necrosis factor alpha, which is mainly produced by activated macrophages of the immune system to mediate inflammatory response. There was also observed a statistically significant, though minor, increase in the expression of *Il-1α* in WT mice treated with Ag200 and sacrificed at day 1.

For the genes involved in intercellular communication and mediation of inflammatory response, there was observed some changes in gene expression between the treatments (figure 3.2.5). There was a statistically significant increase in the expression of the *Cd47*-gene in the brains of KO-mice treated with Ag20-particles. The expression of *Cd200* was found to be significantly induced, and expression of *Cd200r1* significantly reduced in the brains of WT-mice treated with both Ag-particles. Though neither are significantly different from control, there seems to be opposite regulation of the *Cd200r1*-gene in WT and KO-mice, with decreased expression in brains of WT mice at day 1 following both Ag-particle treatments, and an increase of similar magnitude at the same time and with the same treatments in KO-mice.

In summary, both particle types appear to affect the expression of genes involved in inflammation and intercellular signalling, primarily at day 1 following exposure.

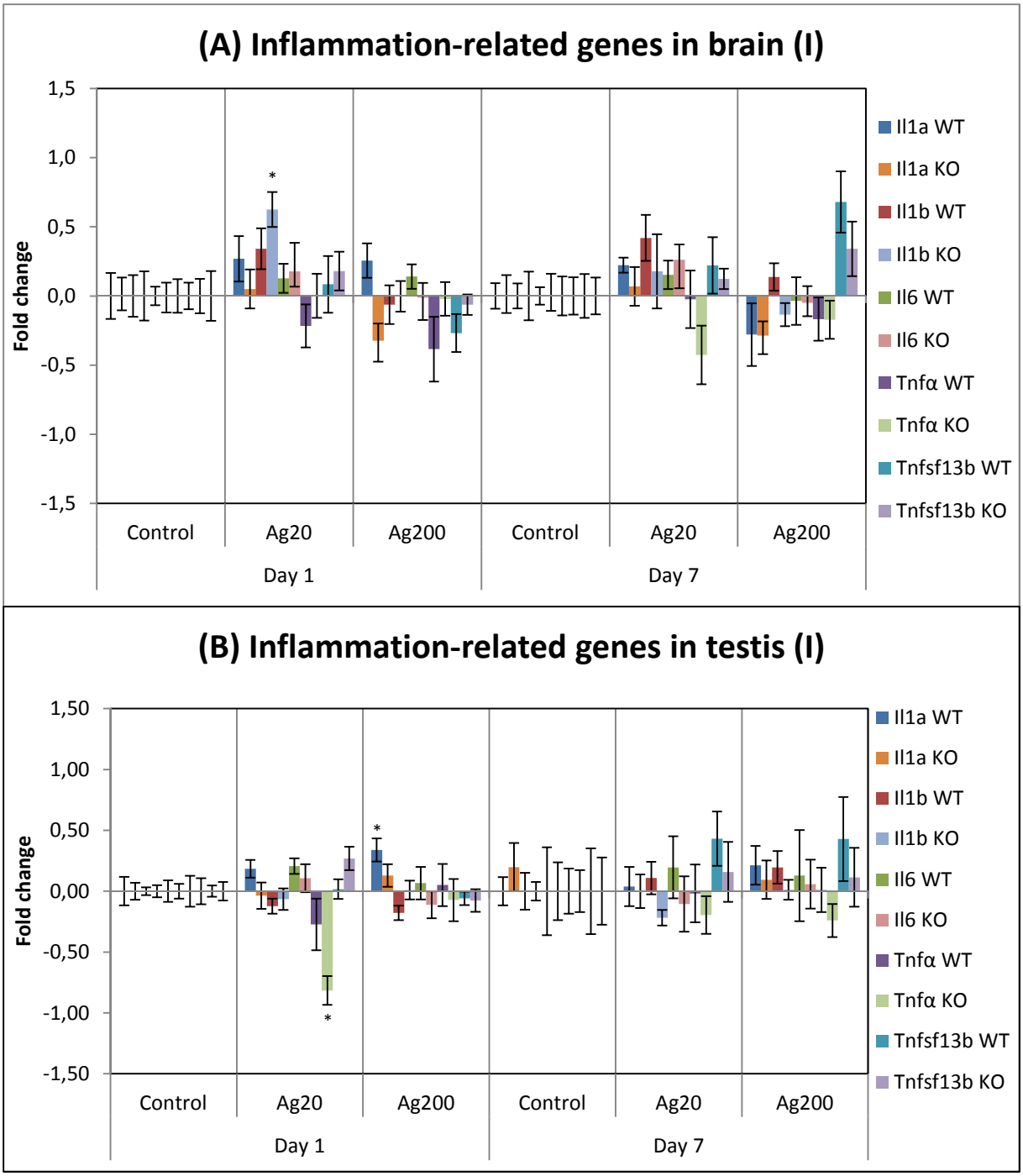

Figure 3.2.4: Gene expression of inflammation-related genes in brain (A) and testis (B). *Treatment groups are WT day 1 control (n=6), Ag20 (n=6), Ag200 (n=6); WT day 7 control (n=5), Ag20 (n=6), Ag200 (n=5);KO day 1 control (n=6), Ag20 (n=6), Ag200 (n=6); KO day 7 control (n=5), Ag20 (n=6), Ag200 (n=5). n=number of experimental animals. Values are presented as fold change in* $2^{-\Delta\Delta Cq}$*-value ± SEM. *p < 0.05: Statistically significant versus control. **p < 0.01: Statistically significant versus control*

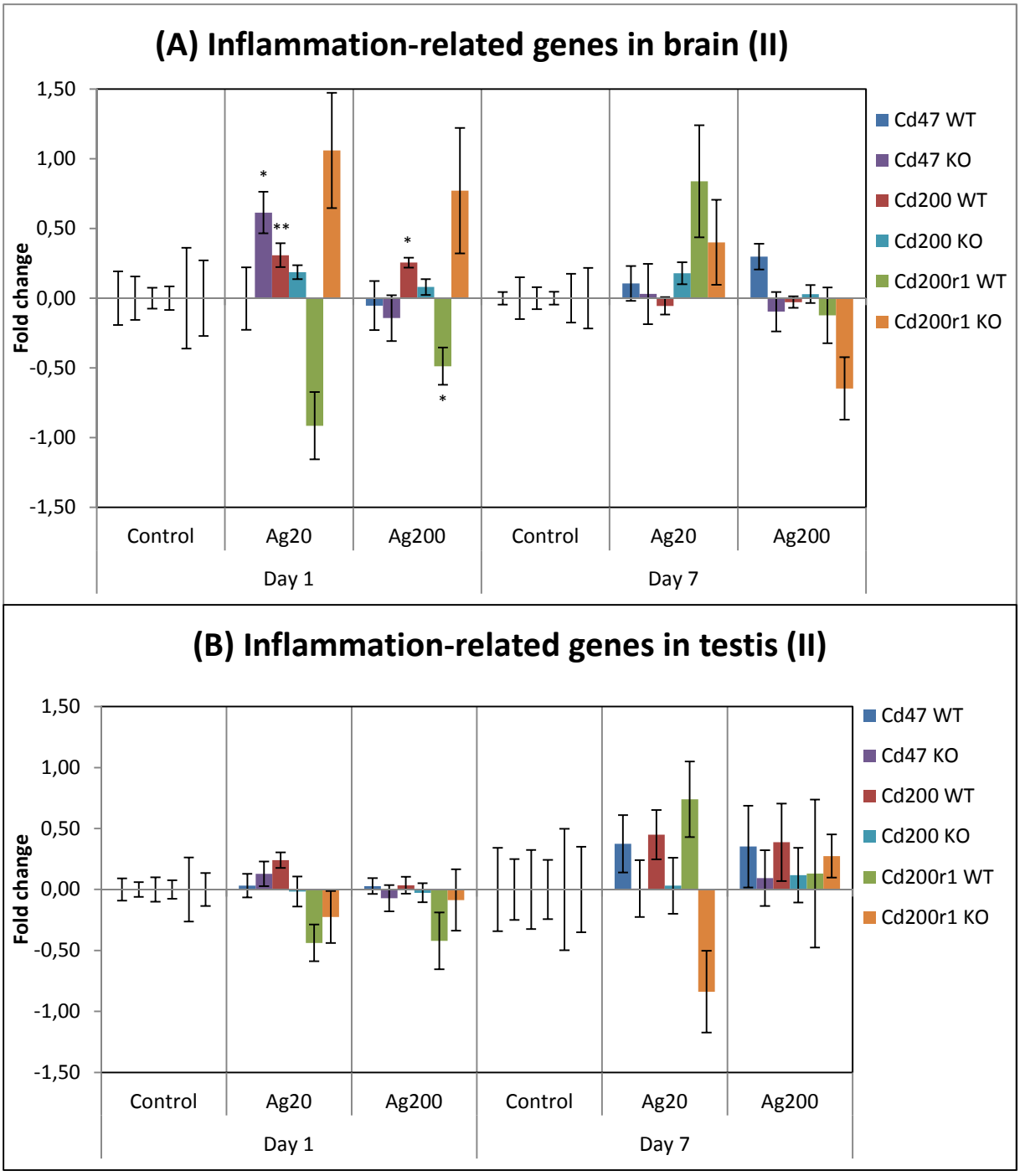

Figure 3.2.5: Gene expression of intercellular signalling-related genes in brain (A) and testis (B). *Treatment groups are WT day 1 control (n=6), Ag20 (n=6), Ag200 (n=6); WT day 7 control (n=5), Ag20 (n=6), Ag200 (n=5);KO day 1 control (n=6), Ag20 (n=6), Ag200 (n=6); KO day 7 control (n=5), Ag20 (n=6), Ag200 (n=5). n=number of experimental animals. Values are presented as fold change in $2^{-\Delta\Delta Cq}$-value ± SEM. *p < 0.05: Statistically significant versus control. **p < 0.01: Statistically significant versus control*

3.2.2.2 Effects of Ag-particles on genes related to oxidative stress and antioxidant-defence:

As the main objective of this thesis was to evaluate oxidative stress as a possible mechanism for Ag-particle toxicity, a panel of genes involved in induction of oxidative stress and in antioxidant defence pathways were investigated. The qPCR data for the antioxidant defence pathway-genes are presented in figure 3.2.6 and 3.2.7, and the data for the NADPH oxidase genes, who are involved in ROS formation of immune cells, are presented in figure 3.2.8.

In brain, it was observed statistically significant, though small, up-regulation of *Sod1* in both genotypes at day 1 following exposure to Ag20-particles. There seems to be a slight up-regulation of the genes *Sod3* and Cat in the brains of both genotypes at day 1 following exposure to Ag20-particles.At day 7, *Sod3* and *Cat* were statistically significantly up-regulated in both genotypes after treatment with Ag200-particles. *Sod3* encodes for the superoxide dismutase enzyme, which is responsible for the detoxification of superoxide radicals into hydrogen peroxide, and the *Cat*-gene encodes for the catalase-enzyme which is responsible for the further decomposition of H_2O_2 into water and oxygen (see the introduction chapter, section 1.3.2 and figure 1.3.1). It should be noted that although statistically significant, the expressions of all antioxidant related genes in figure 3.2.6A are small, with less than 1-fold increase relative to control. It was further observed that expression of *Gpx2* was significantly increased at day 7 in the brains of WT mice treated with Ag20, and that expression of *Nrf2* was significantly decreased at day 1 in KO mice treated with Ag200 (figure 3.2.7A).

In testes, we observed fewer significant responses to the treatment, than we did in brain. Expression of *Gpx2* was significantly reduced at day 7 in the testes of KO mice exposed to Ag20-particles (figure 3.2.7B). Other than that, there are few notable changes in the expression of antioxidant-related genes in testis. As with the gene expression in brain, the differences in expression are generally low, especially for the genes presented in figure 3.2.6.

Our study investigated the potential changes in the expression of genes involved in the NADPH oxidase complex, as this complex is known to produce ROS as a part of the immune response towards pathogens (Sankarapandi, *et al.*, 1998). In the brains of KO-mice, we observed statistically significant up-regulation of all three of the investigated genes at day 1 following treatment with Ag20-particles. At day 7, the expressions of these genes in KO are at similar levels as that of the control. Though not statistically significant, there seems to be a slight increase of the expression of all the investigated genes in WT at day 7 following exposure to both particle types. We also noted a rather large variance in the data for WT brain at day 7.

We did not observe statistically significant changes in the expression of NADPH oxidase related genes in testis. There are some possibly interesting trends showing a slightly increased expression of *Nox4* and *Noxo1* in WT after exposure to both particle types, similar to what we see in brain, but there is also large variation in the data, as seen by the standard error of the mean (figure 3.2.8).

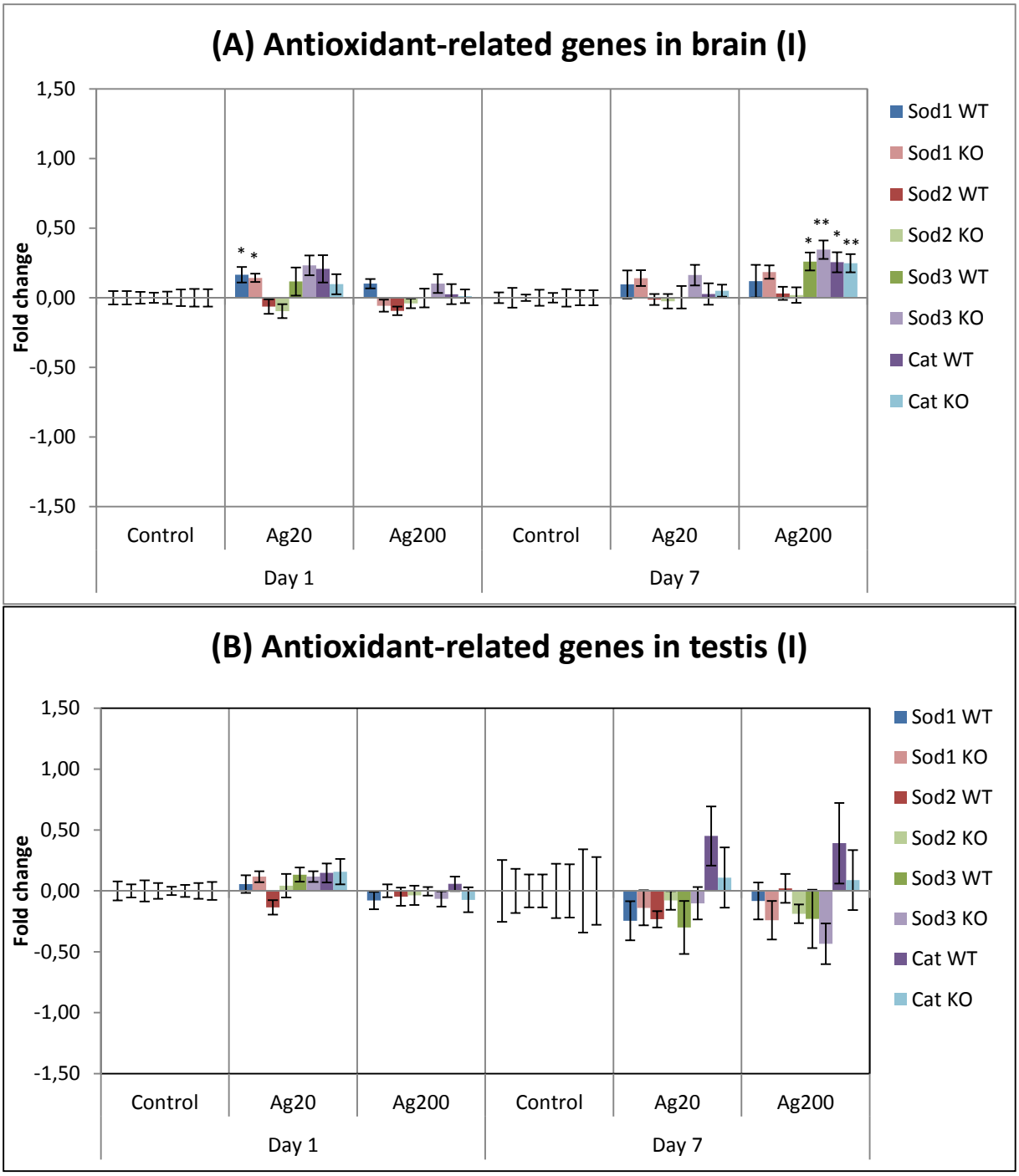

Figure 3.2.6: Gene expression of antioxidant-related genes (I) in brain (A) and testis (B). *Treatment groups are WT day 1 control (n=6), Ag20 (n=6), Ag200 (n=6); WT day 7 control (n=5), Ag20 (n=6), Ag200 (n=5);KO day 1 control (n=6), Ag20 (n=6), Ag200 (n=6); KO day 7 control (n=5), Ag20 (n=6), Ag200 (n=5). n=number of experimental animals. Values are presented as fold change in $2^{-\Delta\Delta Cq}$-value ± SEM. *p < 0.05: Statistically significant versus control. **p < 0.01: Statistically significant versus control*

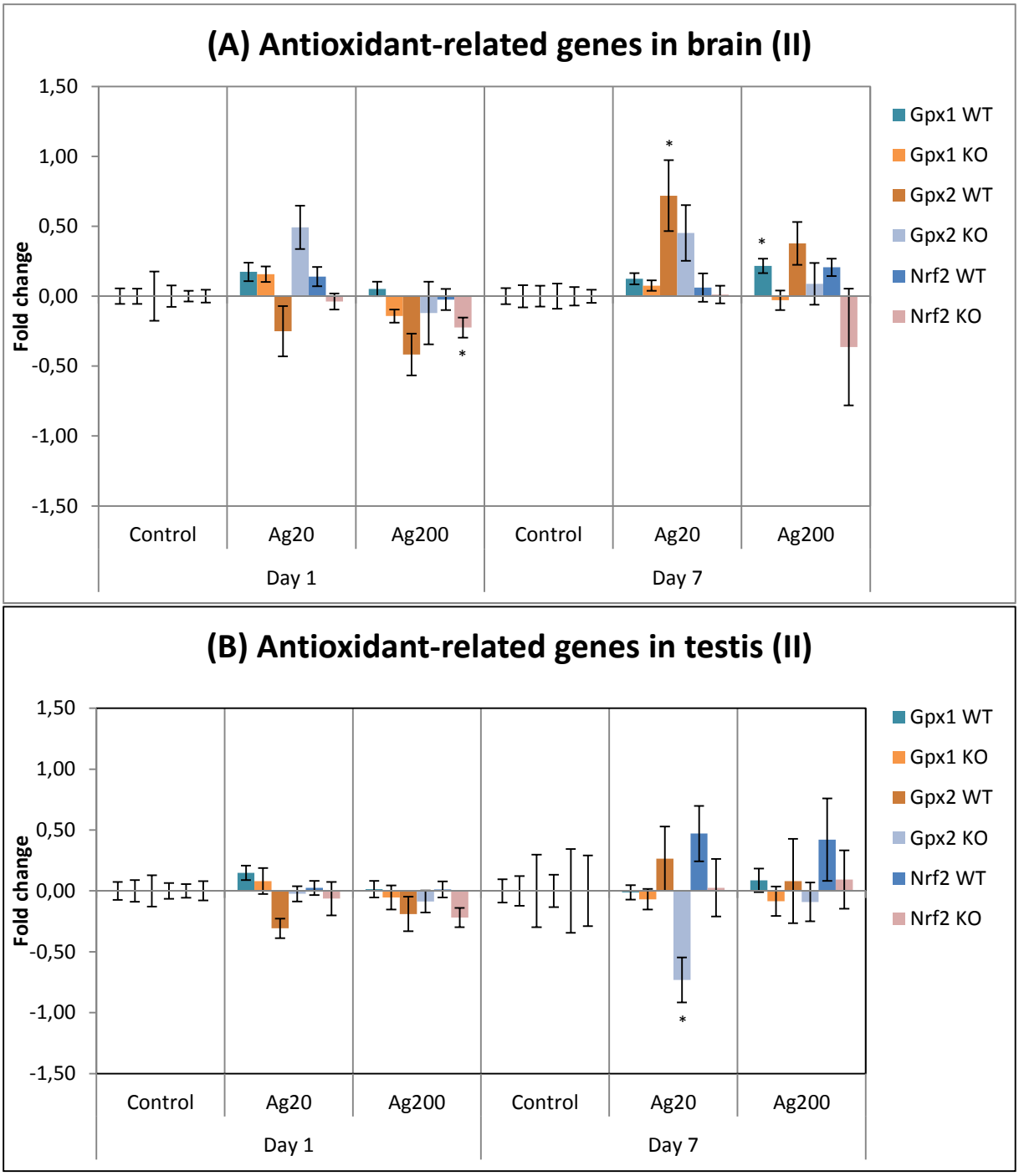

Figure 3.2.7: Gene expression of antioxidant-related genes (II) in brain (A) and testis (B). *Treatment groups are WT day 1 control (n=6), Ag20 (n=6), Ag200 (n=6); WT day 7 control (n=5), Ag20 (n=6), Ag200 (n=5);KO day 1 control (n=6), Ag20 (n=6), Ag200 (n=6); KO day 7 control (n=5), Ag20 (n=6), Ag200 (n=5). n=number of experimental animals. Values are presented as fold change in* $2^{-\Delta\Delta Cq}$*-value ± SEM. *p < 0.05: Statistically significant versus control. **p < 0.01: Statistically significant versus control*

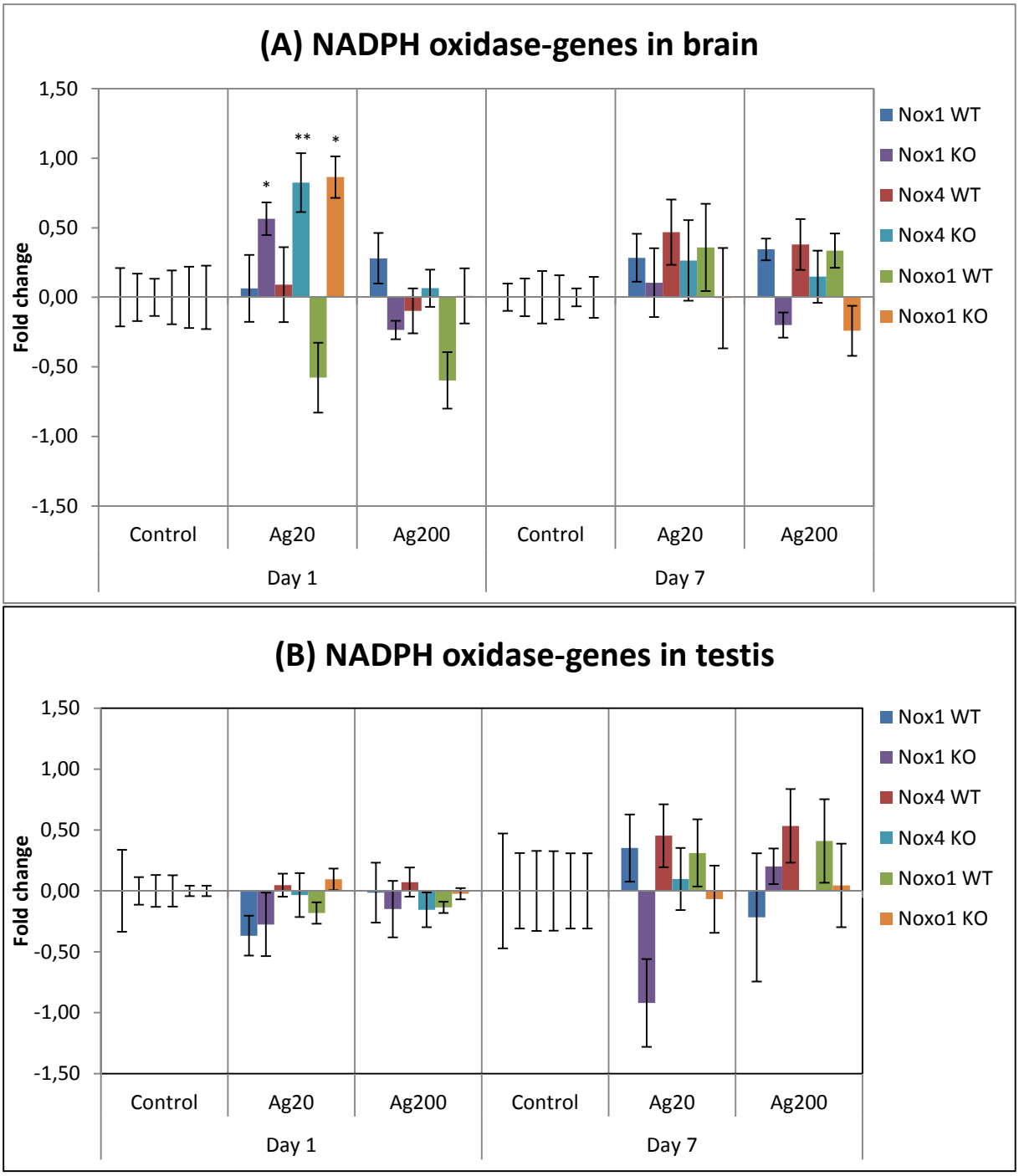

Figure 3.2.8: Gene expression of oxidative stress-related genes in brain (A) and testis (B). *Treatment groups are WT day 1 control (n=6), Ag20 (n=6), Ag200 (n=6); WT day 7 control (n=5), Ag20 (n=6), Ag200 (n=5);KO day 1 control (n=6), Ag20 (n=6), Ag200 (n=6); KO day 7 control (n=5), Ag20 (n=6), Ag200 (n=5). n=number of experimental animals. Values are presented as fold change in* $2^{-\Delta\Delta Cq}$*-value ± SEM. *Statistically significant versus control ($p < 0.05$). **Statistically significant versus control ($p < 0.01$)*

3.2.2.3 Effects of Ag-particles on genes related to DNA repair:

ROS generation is linked to a range of cellular damage, including damage to the DNA. Previous studies have showed that Ag-particles cause DNA strand breaks, and it is possible that this damage occurs as a result of oxidative DNA damage. We investigated the expression of a panel of four genes involved in the DNA damage repair pathway, all involved in the removal of the 8-OxoG lesion, and the results are shown in figure 3.2.9.

Our experiment showed a significantly decreased expression of *Neil2* at day 1 in the brains of KO mice exposed to either types of Ag-particles. The decreased expression of *Neil2* after treatment with Ag200 was, however, low, and therefore should be interpreted with caution. We also observed statistically significant decrease in the expression of *Apex1* in brains of WT mice exposed to Ag200, though the difference in expression relative to control was low for this gene as well

In the testis of exposed animals, we observed no statistically significant differences in expression of DNA damage repair related genes in response to any of the treatments. The genes *Neil1*, *Neil2* and *Neil3* might be slightly induced in WT mice at day 7, but the results are not statistically significant, and the variation in the data is large.

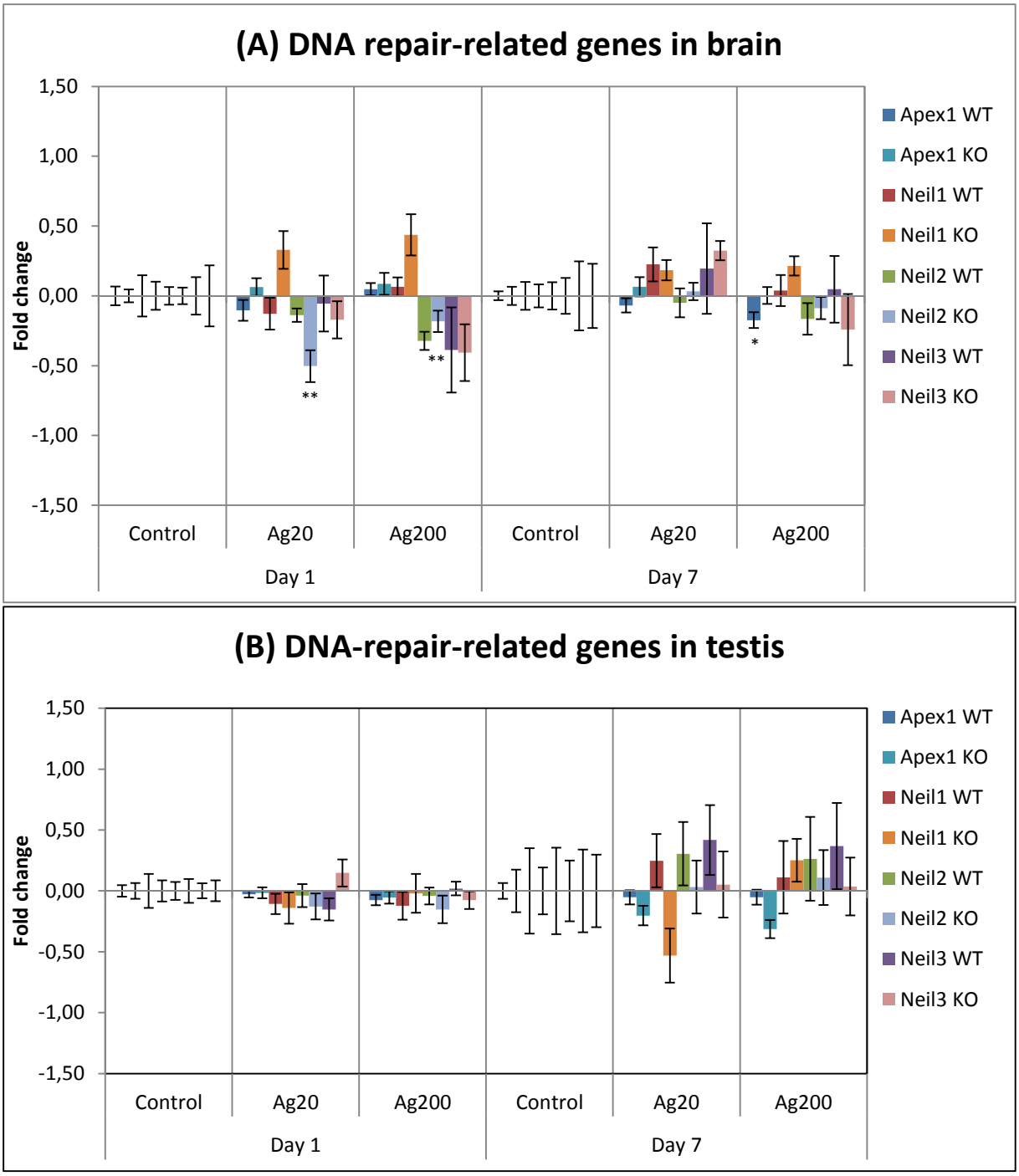

Figure 3.2.9: Gene expression of DNA repair-related genes in brain (A) and testis (B). *Treatment groups are WT day 1 control (n=6), Ag20 (n=6), Ag200 (n=6); WT day 7 control (n=5), Ag20 (n=6), Ag200 (n=5);KO day 1 control (n=6), Ag20 (n=6), Ag200 (n=6); KO day 7 control (n=5), Ag20 (n=6), Ag200 (n=5). n=number of experimental animals. Values are presented as fold change in $2^{-\Delta\Delta Cq}$-value ± SEM. *p < 0.05: Statistically significant versus control. **p < 0.01: Statistically significant versus control*

4 Discussion

ROS are present in all cells and are produced by mitochondria and in cytoplasmic oxidation processes. ROS may be harmful to the organism, but on the other hand, they also act as messengers in a variety of cellular processes. Under environmental stress the cell will increase ROS generation, and this increase can pose a threat to cells by causing peroxidation of lipids, oxidation of proteins, and damage to nucleic acids, enzyme inhibition and cell death (Sharma *et al.*, 2012). Unrepaired oxidative damage may eventually cause adverse health effects like cancer in humans. There are several reports on the Ag-particle-mediated ROS generation (Foldbjerg, *et al.*, 2011; Lee, *et al.*, 2014; Li *et al.*, 2003), and the mitochondria have been found to be a sensitive target for Ag particle toxicity (Hussain, *et al.*, 2005; Piao, *et al.*, 2011).

The induction of ROS generation and possible effects of the mitochondrial membrane was investigated following *in vitro* exposure to Ag-particles in MEF cells. Most toxicity data of Ag-particles are *in vitro* data, and *in vivo* data are still scarce. This thesis builds on a previous mice experiment in our lab, where oxidative stress in testis, liver and lung after Ag-particle exposure was investigated (Asare, *et al.*, 2014). In order to get a deeper understanding of Ag-particles induction of oxidative stress, we examined the expression levels of a panel of 22 selected genes involved in the processes of oxidative stress, antioxidant defence, intercellular signalling, inflammation and DNA damage repair in tissues from brain and testis by qPCR assay. This experiment was correlated with a mechanistic *in vitro* experiment.

4.1 Cell culture study

In vitro systems cannot exactly replicate the complex interactions that happen in an intact organism *in vivo*, but they can provide important mechanistic information about the effect of a compound on biological systems. *In vitro* studies are valuable as mechanistic support for *in vivo* studies.

The MEF cell lines (wild type- ($Ogg1^{+/+}$) and knockout- ($Ogg1^{-/-}$)) used in this study were isolated from mouse embryos, and then the cells were immortalized. Immortalized MEF cells are commonly used in toxicological studies (e.g. Ahamed, *et al.*, 2008; Lee, *et al.*, 2014). As MEF cell lines can be generated from genetically manipulated mouse embryos, these cell lines can be a powerful tool to investigate molecular mechanisms for toxicity. As we wanted to investigate the effects of impaired repair of oxidative DNA damage on Ag-particle induced ROS generation, MEF cells were ideal. However, there are some issues when extrapolating findings from *in vitro* cell line experiments to humans. Particularly when the cells are immortalized using viral transformation and they were established from other species, and the findings must thus be interpreted with caution. MEF cells were selected to resemble the KO mice used in the animal study. In this way, it would be easier to relate our findings *in vitro* cell culture study with the *in vivo* data.

Nanoparticles are known to interfere with most of toxicity assays in *in vitro*, making the interpretation of the results difficult (Kroll *et al.*, 2012; Ong *et al.*, 2014). Sabatini *et al.*

(2007) showed that silver NPs interacted directly with fluorescent dyes and quenched their signals, presumably by binding to their surface. Ong, *et al.* (2014), examined the interference of four different nanoparticles on six different *in vitro* toxicity assays, and found that each nanoparticle interfered with at least one of these assays. Even though there are no reports on the interference of Ag-particles on the performance of the exact assays used in this thesis, it is reasonable to assume that Ag-particles may interfere with these assays.

4.1.1 Measurements of ROS-generation in MEF-cells

The investigation of ROS-generation in the MEF (WT and KO) cell lines after treatment with Ag20- and Ag200-particles using the fluorescent probe DCFH-DA, showed that a statistically significantly higher level of ROS-generation in the KO cells with all the different treatment groups, including the control group, compared with the effects observed in the WT-cells following the treatments (figure 3.1.1). The reason for the higher ROS level in the KO-cells upon the treatments is unclear. One explanation can be that the lack of the *Ogg1* gene may lead to high background level of ROS. Bacsi *et al.* (2007) and co-workers have reported that an increased background level of ROS in a subset of the MEF KO cell lines compared with WT cells, and as the MEF cells they used are established by the same procedure as the cells used in our experiment (Klungland *et al.*, 1999), it is likely that our MEF cells retain similar characteristics.

Although the KO MEF cells showed an increased background level of ROS, there is still a clear Ag-particles mediated dose-dependent increase in the ROS levels. Our results are in agreement with previous studies of Ag-particles and ROS generation *in vitro* (Bartlomiejczyk *et al.*, 2013). Foldbjerg, *et al.* (2011) observed significantly increased levels of ROS 24 hours after the treatment of the human alveolar cell line, A549, with 78 nm AgNPs at concentrations ranging from 2.5 to 15 µg/mL.

Lee, *et al.* (2014) studied ROS-generation in the NIH 3T3 mouse embryonic fibroblast cell-line after exposure to Ag-particles also using the DCFH-DA-assay, and found that ROS levels were significantly increased after 3 and 6 hours following exposure to 15 mg/ml AgNPs. Piao, *et al.* (2011) found that AgNPs induce increased ROS-generation at 0.5, 1, 3, 6 and 12 hours after exposure of Human Chang liver cells to concentrations of 4 µg/mL. In light of these results, we would have expected significant increases in ROS generation at 3 and 6 hours as well as at 24 hours.

We observed a high inter-run variation in our results, and this may to some degree have masked our results, and could have been avoided by using some form of inter run control (IRC). In addition, the DCFH-DA-assay is known to be interfered with by NPs, especially at higher concentrations. Kroll, *et al.* (2012) investigated the effect of 24 different engineered nanoparticles on the DCF-assay, and found that all nanoparticle types interfered with the assay by reducing detection of DCF fluorescence at concentrations of 32 µg/ml and above. This is therefore a possible explanation of the lack of significant increases in ROS generation.

4.1.2. Mitochondrial membrane potential assay

The possible effects on the mitochondrial membrane potential of WT and KO MEF cells after 24 hours of Ag-particle exposure (figure 3.1.2) showed no clear response to any of the treatments, except a slight decrease in the positive controls treated with H_2O_2.

As previously noted, nanoparticle interference has been shown in many *in vitro* toxicity assays, and it is a possible explanation for the lack of clear response in our study. As the kit protocol did not include immediate removal of the particles before centrifuging the plate, it is likely that most of the particles were still in the plate at the time of measurement. Even with interference of Ag-particles, this cannot explain the lack of responses in the positive control group treated with H_2O_2. The reason for this is still unknown and due to the high cost of the kits used and the time-frame of my thesis, the experiment was not repeated. The only other studies that to our knowledge have reported using the JC-1 assay after treatment with Ag-particles have only used the JC-1 assay for confocal imaging (Stensberg *et al.*, 2014), or have failed to report their results from their flow-cytometric fluorescence assessment (Piao, *et al.*, 2011).

4.2 Animal study

4.2.1 Optimal homogenization method

High quality RNA is a prerequisite for gene expression profiling studies (e.g. qPCR or microarray), and obtaining good quality RNA was one of the main goals of this thesis. Two tissue homogenization methods performance were evaluated in regards to RNA yield, purity and integrity (figures 3.2.1 – 3.2.3). From this method comparison, a high quality RNA with sufficient RNA amount was obtained from both homogenization methods. However, the UltraTurrax method was selected due to slightly better results in the RNA integrity test, as well as it being the most cost- and time-efficient method of the two. In addition, UltraTurrax was the method was used for isolation of the RNA samples from liver, lung and testes of mice sacrificed at day 7 of the experiment, which was performed prior to this thesis.

4.2.2 Gene expression analysis by qPCR assay

In this thesis, the transcriptional response of a panel of 22 genes based on their role in oxidative stress, antioxidant defence, intercellular signalling, inflammation and DNA damage repair, following exposure of WT and KO mice with Ag-particles was evaluated by qPCR assay. Samples from vehicle treated mice were used as control samples; hence, all other samples were compared to the control samples. There are few studies examining the effects of

exposure to Ag-particles on gene expression pattern of mice, and the data available in the literature for direct comparison is scarce. It is therefore difficult to discuss the findings.

Nevertheless, a number of variables must be controlled and reduced to minimal levels in order to obtain a reliable and reproducible gene expression results. These variables include, the amount of starting material, enzyme efficiencies, tissue differences, sample handling and individual differences, which all may affect the qPCR assay, and hence may lead to misinterpretation of the results. It is therefore very important to remove pre- or post-analytical systematic biases caused by technical rather than biological sources from the qPCR data. The effects of this "noise" can be removed from the data using good normalization strategies, while still maintaining the ability to detect significantly differentially expressed genes. There are several ways to remove technical biases and using reference genes are considered a gold standard for normalization of qPCR data. A good reference gene should have a constant level of expression independent of experimental treatments. The stability of a total of six potential reference genes selected based on literature (Huggett *et al.*, 2005) and previous experience in our lab were evaluated. The expression level of four of the six examined reference genes was relatively stable across both treatment and tissue groups and the results are presented in appendix D (figure D.1 and D.2). The geometrical average of the four reference genes were used to normalize the qPCR data employing the comparative ΔΔCq-method (Livak and Schmittgen, 2001) and it is a recommended normalization strategy (Vandesompele *et al.*, 2002).

We did not observe significant genotype differences in gene expression, except for the inflammation-related gene *Tnf-α*. Though the difference in gene expression was statistically significant, the difference was small. When we took both genotype and tissue into consideration, we observed significant differences in expression for more genes, particularly in antioxidant-genes in testis and some antioxidant-genes in brain. There were, as expected, significant differences in expression between the two tissues for all the genes.

In general, the gene expression analysis showed only a limited to moderate response to the treatments; only the transcript levels of a few of genes were close to the ±2-fold change, with no genotype- specific pattern. Notably the gene expression in testis showed limited response for all treatments (figures. 3.2.4B – 3.2.9B).

4.2.2.1 Effects on genes involved in inflammation and intercellular signalling

One of the greatest concerns in Ag-particle induced toxicity is oxidative stress as previously described in the introduction (section 1.3). Inflammation is closely linked to oxidative stress, and hence is an important mechanism to address in this thesis. It has been shown that pro-inflammatory cytokines enhance expression and activation of NADPH oxidases (Nox) that result in free radicals generation and oxidative stress (Mander, *et al.*, 2006; Mo, *et al.*, 2009). Based on *in vitro* studies inflammation is a suggested mechanism of silver nanoparticles toxicity (Bartlomiejczyk, *et al.*, 2013). However, there have only been a few *in vivo* studies investigating inflammation in relation to Ag-particle exposure.

The Ag-particles gave some effects on the inflammation-related genes, however, the magnitude of the expression levels were not high. *Il-1β* was statistically significantly up-regulated in KO brain following exposure to AgNPs. In testis, *Tnf-α* was significantly down-regulated in the KO mice following exposure to nanoparticles, whereas *Il-1α* was up-regulated in WT after exposure to Ag200-particles. However, the increase of *Il-1α* is so small it should be regarded as on the borderline of significance and it's biological significance should be interpreted with caution. Previous experiments in our lab showed that Ag-particles induced apoptosis and necrosis time- and dose-dependently in primary testicular cells form WT and KO (*Ogg1*$^{-/-}$) C56BL6 mice, and in human embryo tumour cell line NT2 (Asare, *et al.*, 2012). Necrotic cells could stimulate to inflammation which could be enhanced by proinflammatory cytokines. Whether necrosis occurs *in vivo* as well *in vitro* after Ag-particle exposure is difficult to predict.

The genes *Cd47*, *Cd200* and *Cd200r1* (figure 3.2.5) all encode for proteins with important functions in intercellular signalling and inflammation, and we found all of these genes to be modulated by exposure to Ag-particles.

Cd47 was significantly induced in the brains of KO mice at day 1 in the group treated with Ag20-particles. *Cd47* modulates cell motility, leukocyte adhesion and migration, phagocytosis, and activation of platelets (Brown and Frazier, 2001; Parkos *et al.*, 1996), and has been shown to trigger cell death in a wide range of cell types, including activated T-cells, monocytes and dendritic cells (Johansson *et al.*, 2004). Xing *et al.* (2009) observed that activation of *Cd47* elevated levels of active caspase 3, a protease central in apoptosis, and increased the generation of reactive oxygen species (ROS) in a time-dependent manner. Our results may suggest that *Cd47* is involved in the toxicity of Ag-particles. To our knowledge, there have been no other studies investigating the expression of *Cd47* after treatment with Ag-particles, and this makes our findings difficult to interpret.

A moderate increase in the expression of *Cd200* was observed in the brains of WT mice at day 1 with both Ag-particles. *Cd200* (in earlier studies referred to as OX2) is expressed in a wide variety of cell types including neurons and endothelial cells in the central nervous system (CNS) (Wright *et al.*, 2001), whereas it's receptor, *Cd200r1*, is predominantly restricted to cells of myeloid origin, such as macrophages and microglia (Wright *et al.*, 2003). Binding of the *Cd200* ligand to the *Cd200* and *Cd200r1* receptor present on the surface of myeloid cells, have been shown to limit inflammation by decreasing macrophage activity (Hoek *et al.*, 2000; Walker and Lue, 2013). The expression of the *Cd200r1* receptor seems to be genotype dependent, with down-regulation in WT cells and up-regulation in KO cells at day 1 following exposure to both particle types. The increased expression of *Cd200* suggests activation of this anti-inflammatory system. However, as the regulation of the receptor and its ligand will vary during the course of the inflammatory response, the information from just one time point is difficult to interpret.

4.2.2.3 Effects on genes related to oxidative stress and antioxidant-defence

Generation of ROS and induction of oxidative stress has long been the primary hypothesis of Ag-particle toxicity (Bartlomiejczyk, *et al.*, 2013; Foldbjerg, *et al.*, 2011), but only a few studies have investigated this *in vivo*. Rahman *et al.* (2009) investigated the expression of a large panel of genes related to oxidative stress in mouse brains 24 hours after a single intraperitoneal injection with Ag-particles of 25 nm. This study has however been criticized for using doses that are all excessively high (100, 500 and 1000 mg/kg bw), and may therefore lack relevance to human exposure (Johnston, *et al.*, 2010).

In this thesis, we observed that Ag-particles affected the expression of several genes linked to oxidative stress and antioxidant defence, primarily in brain. Of particular interest is the increased expressions of the antioxidant enzyme genes *Sod1*, *Sod3*, Cat which were visible in the brains of both genotypes at day 1 following exposure to Ag20 particles, and at day 7 following exposure to Ag200 particles in both genotypes (figure 3.2.6A),. These results should be interpreted with a great deal of caution, as the differences from control, although statistically significant, are small. However, the results are still interesting, as the pattern is spanning several genes, and occurs in brains from both genotypes. To our knowledge, this is the first time Ag-particle mediated changes in the gene expression of brain have been shown to occur at moderate doses. A possible explanation for the response to Ag20-particles at day 1 and to Ag200-particles at day 7 may be the decreased rate of excretion of the larger particles as shown by Dziendzikowska, *et al.* (2012).

Another interesting cluster of gene responses is the increased expression of NADPH oxidase-genes at day 1 in KO-mice exposed to Ag20-particles (see fig. 3.2.8). NADPH oxidases are found in neutrophil granulocytes of the immune system, where they generate superoxide to combat pathogens. An increase in the expression of these genes may suggest that immune cells target the AgNPs as pathogens and attempts to destroy by generating ROS. This induction of NADPH oxidases and antioxidant-related genes in brain is in agreement with previous studies of the role of NADPH oxidases in damage caused by ultrafine particles (Mo, *et al.*, 2009). This indicates that ROS generated by the NADPH oxidase complex as a response to Ag-particles may be a possible mechanism of toxicity.

The gene expression of the testes seems to be less affected by the Ag particle treatment, with no statistically significant effects on genes related to oxidative stress and antioxidant defence, other than a reduced expression of *Gpx2* at day 7 in KO mice exposed to Ag20-particles. There is also possibly a slight increase in the expression of NADPH oxidase complex-related genes at day 7 following exposure to both Ag20 and Ag200 in the WT mice. The reason for the reduced effects of Ag-particles on the gene expression in testis as opposed to brain is unclear.

4.2.2.4 Effects on genes involved in DNA damage repair

Approximately 240,000 spontaneous DNA lesions occur daily in each mammalian cell (Billen, 1990). Environmental stress, such as exposure to Ag-particles, may add to the burden, and may also introduce more complex damages that might lead to an overload of the repair mechanisms. Unrepaired DNA damage may result in cell death, and more importantly can cause mutagenesis and carcinogenesis, and it is therefore crucial for the cell to be able to repair DNA efficiently. In this work we examined expression of important genes in the BER repair pathway *Apex1*, *Neil1*, *Neil2* and *Neil3*. BER is the major pathway to repair single strand breaks and remove base lesions and are initiated by a DNA glycosylase (e.g. *Ogg1*) which recognize and excises the damaged base (e.g. 8-oxoG) (Krokan, *et al.*, 2000). As the *Ogg1* enzyme is important for the primary mechanism for removal of oxidative DNA lesions, we expected an increase in the expression of the examined DNA damage repair related genes in the KO mice.

Our results show only a limited effect of Ag-particle exposure on the expression of genes related to DNA damage repair in both brain and testis. We observed a significantly decreased expression of the *Neil2* gene, which is thought to be one possible back-up mechanism for repair of 8-OxoG-lesions (Katafuchi, *et al.*, 2004), at day 1 in brains of KO-mice. We also observed a slight induction of *Neil1* in brains of KO mice at day 1. In testis, we found no statistically significant effects on expression of DNA damage repair-related genes.

Previous studies in our lab have shown that exposure to Ag-particles cause DNA strand breaks both *in vitro* (Asare, *et al.*, 2012) and *in vivo* (Asare, *et al.*, 2014), and an increased expression of DNA damage repair associated genes would therefore be expected, especially in the KO mice. A possible explanation for the lack of induction of the alternative DNA damage repair pathways is that the pathways studied are supplemented by other mechanisms. Nucleotide excision repair (NER) has been suggested to be another backup mechanism for the DNA damage repair normally conducted by BER (Lin and Sancar, 1989; Sunesen *et al.*, 2002).

4.2.3: Relevance of findings in a regulatory- and human health perspective

Even if ROS generation is a suggested mechanism of Ag-particle toxicity, studies have examined ROS generation caused by Ag-particles *in vivo*. Generation of ROS and induction of oxidative stress is associated with pathogenic mechanisms of a long list of diseases, including atherosclerosis, neurodegenerative diseases such as Alzheimer's and Parkinson's disease, cancer, inflammatory diseases, diabetes mellitus, as well as infertility and aging (Agarwal *et al.*, 2014; Durackova, 2010; Mittal *et al.*, 2014).

This thesis has focused mainly on the possible effects of Ag-particle exposure on gene expression in brain and testis, as both neurodegenerative diseases and male infertility are associated with oxidative stress, and as such, Ag-particle exposure may contribute to this. In particular, concern has been voiced over the possible neurotoxic effects of Ag-particles

(Sharma and Sharma, 2012), where some studies have suggested that exposure to Ag-particles may directly induce learning- and memory deficits in rats (Liu, *et al.*, 2012). The ability of Ag-particles to trigger oxidative stress and inflammation in the CNS have also been suggested to increase the risk of developing neurodegenerative diseases such as Parkinson's disease (Lucchini *et al.*, 2012; Myhre, *et al.*, 2013). However, further research into the mechanisms of Ag-particle toxicity is required to establish this link.

Male fertility problems affects about 7.5 % of all couples trying to conceive, and oxidative stress is noted as one of several mediators of male infertility (Agarwal, *et al.*, 2014). In addition, it has been shown that Ag-particles directly affect both spermatogonia and Leydig cells of the testis (Ema, *et al.*, 2010; Garcia *et al.*, 2014). The genotoxic abilities of Ag-particles should also be of concern for reproductive toxicity, as in addition to possible mutagenesis or carcinogenesis, mutations in germ cells may be passed on causing dysfunctions in the next generation (Skinner, 2014). Concern regarding the increasing use of Ag-particles is therefore well-founded, and risk assessment strategies are needed.

As there are relatively few well-conducted *in vivo* experiments suitable for risk assessment of Ag-particles, more *in vivo* data in this area is needed. Mechanistic studies as presented in this thesis are used as support for mode of action of compounds in risk assessment. This needs to be backed up by more functional assays. In this thesis we investigated changes in gene expression following exposure to Ag-particles *in vivo*, and our findings would benefit from further analysis of protein expression (e.g. Western blotting) to investigate the effects at a physiologic level. Our findings contribute with novel mechanistic understanding of Ag-particle toxicity *in vivo*.

4.3 Conclusions

In this thesis, we have found that Ag-particles induce generation of reactive oxygen species *in vitro*. We were not able to determine whether Ag-particle exposure affects the mitochondrial membrane potential, possibly due to interference from the particles themselves on the assay. Our observations of increased ROS generation *in vitro* are supported by the gene expression results, which showed significant, but moderate, changes in the expression levels of genes related to oxidative stress and antioxidant defence. In particular, the small increase in expression of antioxidant enzyme-genes and the up-regulation of the ROS producing NADPH oxidase genes, and the *Cd47* gene in brains of KO mice are interesting.

Overall, the gene expression result shows some effects upon Ag-particle exposure, however, the changes in the expression level were moderate. Further, our results indicate that ROS generation and induction of oxidative stress, possibly through the NADPH oxidase or the *Cd47* pathways, is a plausible mechanism of Ag-particle toxicity. Long-term animal studies may be needed to get more insight in Ag-particles ability to induce chronic inflammation.

4.4 Future work

An immediate follow-up of this study should analyse the cDNA from liver and lung by qPCR assay and investigate changes in the gene expression. An alternative assay for apoptosis such as PI/Hoechst or the Annexin V assay could be used to investigate at which concentrations the Ag-particles used in this study causes cell death in MEF cells. Along with an investigation of the gene expression of MEF cells exposed to similar concentrations of Ag-particles that we have shown to cause ROS generation results from these studies would be a good way to relate the *in vitro* results to the effects on gene expression seen *in vivo*. Supporting the gene expression data with data on protein expression using Western blotting may be performed to link the changes in gene expression to a physiologic response.

Further insight in how nanoparticles interfere with common *in vitro* toxicity assays is vital for future studies of the mechanisms of nanoparticle toxicity.

5 References

Agarwal, A., Virk, G., Ong, C., and du Plessis, S. S. (2014). Effect of oxidative stress on male reproduction. *The world journal of men's health* **32**(1), 1-17

Ahamed, M., Karns, M., Goodson, M., Rowe, J., Hussain, S. M., Schlager, J. J., and Hong, Y. (2008). DNA damage response to different surface chemistry of silver nanoparticles in mammalian cells. *Toxicology and applied pharmacology* **233**(3), 404-10

Arora, S., Jain, J., Rajwade, J. M., and Paknikar, K. M. (2009). Interactions of silver nanoparticles with primary mouse fibroblasts and liver cells. *Toxicology and applied pharmacology* **236**(3), 310-8

Asare, N., Instanes, C., Sandberg, W. J., Refsnes, M., Schwarze, P., Kruszewski, M., and Brunborg, G. (2012). Cytotoxic and genotoxic effects of silver nanoparticles in testicular cells. *Toxicology* **291**(1-3), 65-72

Asare, N., Slagsvold, H., Lindeman, B., Olsen, A., Gromadzka-Ostrowska, J., Meczynska-Wielgosz, S., Kruszewski, M., Brunborg, G., and Instanes, C. (2014). Genotoxicity and gene expression modulation of silver and titanium dioxide nanoparticles in mice. Manuscript submitted for publication.

AshaRani, P. V., Hande, M. P., and Valiyaveettil, S. (2009). Anti-proliferative activity of silver nanoparticles. *BMC cell biology* **10**, 65

Babior, B. M. (2004). NADPH oxidase. *Current opinion in immunology* **16**(1), 42-7

Bacsi, A., Chodaczek, G., Hazra, T. K., Konkel, D., and Boldogh, I. (2007). Increased ROS generation in subsets of OGG1 knockout fibroblast cells. *Mechanisms of ageing and development* **128**(11-12), 637-49

Bart, J., Groen, H. J., van der Graaf, W. T., Hollema, H., Hendrikse, N. H., Vaalburg, W., Sleijfer, D. T., and de Vries, E. G. (2002). An oncological view on the blood-testis barrier. *The Lancet. Oncology* **3**(6), 357-63

Bartlomiejczyk, T., Lankoff, A., Kruszewski, M., and Szumiel, I. (2013). Silver nanoparticles -- allies or adversaries? *Annals of agricultural and environmental medicine : AAEM* **20**(1), 48-54

Bianca, V. D., Dusi, S., Bianchini, E., Dal Pra, I., and Rossi, F. (1999). beta-amyloid activates the O-2 forming NADPH oxidase in microglia, monocytes, and neutrophils. A possible inflammatory mechanism of neuronal damage in Alzheimer's disease. *The Journal of biological chemistry* **274**(22), 15493-9

Bihari, P., Vippola, M., Schultes, S., Praetner, M., Khandoga, A. G., Reichel, C. A., Coester, C., Tuomi, T., Rehberg, M., and Krombach, F. (2008). Optimized dispersion of nanoparticles for biological *in vitro* and *in vivo* studies. *Particle and fibre toxicology* **5**, 14

Billen, D. (1990). Spontaneous DNA damage and its significance for the "negligible dose" controversy in radiation protection. *Radiation research* **124**(2), 242-5

Boisen, K. A., Main, K. M., Rajpert-De Meyts, E., and Skakkebaek, N. E. (2001). Are male reproductive disorders a common entity? The testicular dysgenesis syndrome. *Annals of the New York Academy of Sciences* **948**, 90-9

Brown, E. J., and Frazier, W. A. (2001). Integrin-associated protein (CD47) and its ligands. *Trends in cell biology* **11**(3), 130-135

Cardozo-Pelaez, F., Sanchez-Contreras, M., and Nevin, A. B. (2012). Ogg1 null mice exhibit age-associated loss of the nigrostriatal pathway and increased sensitivity to MPTP. *Neurochemistry international* **61**(5), 721-30

Casarett, L., Doull, J., and Klaassen, C. (2008). *Casarett and Doull's toxicology : The Basic Science of Poisons*. McGraw-Hill.

Cheng, K. C., Cahill, D. S., Kasai, H., Nishimura, S., and Loeb, L. A. (1992). 8-Hydroxyguanine, an abundant form of oxidative DNA damage, causes G----T and A----C substitutions. *The Journal of biological chemistry* **267**(1), 166-72

Durackova, Z. (2010). Some current insights into oxidative stress. *Physiological research / Academia Scientiarum Bohemoslovaca* **59**(4), 459-69

Dziendzikowska, K., Gromadzka-Ostrowska, J., Lankoff, A., Oczkowski, M., Krawczynska, A., Chwastowska, J., Sadowska-Bratek, M., Chajduk, E., Wojewodzka, M., Dusinska, M., and Kruszewski, M. (2012). Time-dependent biodistribution and excretion of silver nanoparticles in male Wistar rats. *Journal of applied toxicology : JAT* **32**(11), 920-8

Edwards-Jones, V. (2009). The benefits of silver in hygiene, personal care and healthcare. *Letters in applied microbiology* **49**(2), 147-52

Ema, M., Kobayashi, N., Naya, M., Hanai, S., and Nakanishi, J. (2010). Reproductive and developmental toxicity studies of manufactured nanomaterials. *Reproductive toxicology (Elmsford, N.Y.)* **30**(3), 343-52

Foldbjerg, R., Dang, D. A., and Autrup, H. (2011). Cytotoxicity and genotoxicity of silver nanoparticles in the human lung cancer cell line, A549. *Archives of toxicology* **85**(7), 743-50

Foldbjerg, R., Irving, E. S., Hayashi, Y., Sutherland, D. S., Thorsen, K., Autrup, H., and Beer, C. (2012). Global gene expression profiling of human lung epithelial cells after exposure to nanosilver. *Toxicological sciences : an official journal of the Society of Toxicology* **130**(1), 145-57

Gaiser, B. K., Hirn, S., Kermanizadeh, A., Kanase, N., Fytianos, K., Wenk, A., Haberl, N., Brunelli, A., Kreyling, W. G., and Stone, V. (2013). Effects of silver nanoparticles on the liver and hepatocytes *in vitro*. *Toxicological sciences : an official journal of the Society of Toxicology* **131**(2), 537-47

Garcia-Reyero, N., Kennedy, A. J., Escalon, B. L., Habib, T., Laird, J. G., Rawat, A., Wiseman, S., Hecker, M., Denslow, N., Steevens, J. A., and Perkins, E. J. (2014). Differential effects and potential adverse outcomes of ionic silver and silver nanoparticles *in vivo* and *in vitro*. *Environmental science & technology* **48**(8), 4546-55

Garcia, T. X., Costa, G. M., Franca, L. R., and Hofmann, M. C. (2014). Sub-acute intravenous administration of silver nanoparticles in male mice alters Leydig cell function and testosterone levels. *Reproductive toxicology (Elmsford, N.Y.)* **45**, 59-70

Green, D. R., and Reed, J. C. (1998). Mitochondria and apoptosis. *Science (New York, N.Y.)* **281**(5381), 1309-12

Gromadzka-Ostrowska, J., Dziendzikowska, K., Lankoff, A., Dobrzynska, M., Instanes, C., Brunborg, G., Gajowik, A., Radzikowska, J., Wojewodzka, M., and Kruszewski, M. (2012). Silver nanoparticles effects on epididymal sperm in rats. *Toxicology letters* **214**(3), 251-258

Higuchi, R., Dollinger, G., Walsh, P. S., and Griffith, R. (1992). Simultaneous amplification and detection of specific DNA sequences. *Bio/technology (Nature Publishing Company)* **10**(4), 413-7

Hoek, R. M., Ruuls, S. R., Murphy, C. A., Wright, G. J., Goddard, R., Zurawski, S. M., Blom, B., Homola, M. E., Streit, W. J., Brown, M. H., Barclay, A. N., and Sedgwick, J. D. (2000). Down-regulation of the macrophage lineage through interaction with OX2 (CD200). *Science (New York, N.Y.)* **290**(5497), 1768-71

Huggett, J., Dheda, K., Bustin, S., and Zumla, A. (2005). Real-time RT-PCR normalisation; strategies and considerations. *Genes and immunity* **6**(4), 279-84

Hussain, S. M., Hess, K. L., Gearhart, J. M., Geiss, K. T., and Schlager, J. J. (2005). *In vitro* toxicity of nanoparticles in BRL 3A rat liver cells. *Toxicology in vitro : an international journal published in association with BIBRA* **19**(7), 975-83

Johansson, U., Higginbottom, K., and Londei, M. (2004). CD47 ligation induces a rapid caspase-independent apoptosis-like cell death in human monocytes and dendritic cells. *Scandinavian journal of immunology* **59**(1), 40-9

Johnston, H. J., Hutchison, G., Christensen, F. M., Peters, S., Hankin, S., and Stone, V. (2010). A review of the *in vivo* and *in vitro* toxicity of silver and gold particulates: particle attributes and biological mechanisms responsible for the observed toxicity. *Critical reviews in toxicology* **40**(4), 328-46

Katafuchi, A., Matsubara, M., Terato, H., Iwai, S., Hanaoka, F., and Ide, H. (2004). Damage specificity of human DNA glycosylases for oxidative pyrimidine lesions. *Nucleic acids symposium series (2004)*(48), 175-6

Kim, Y. S., Kim, J. S., Cho, H. S., Rha, D. S., Kim, J. M., Park, J. D., Choi, B. S., Lim, R., Chang, H. K., Chung, Y. H., Kwon, I. H., Jeong, J., Han, B. S., and Yu, I. J. (2008). Twenty-eight-day oral toxicity, genotoxicity, and gender-related tissue distribution of silver nanoparticles in Sprague-Dawley rats. *Inhalation toxicology* **20**(6), 575-83

Kim, Y. S., Song, M. Y., Park, J. D., Song, K. S., Ryu, H. R., Chung, Y. H., Chang, H. K., Lee, J. H., Oh, K. H., Kelman, B. J., Hwang, I. K., and Yu, I. J. (2010). Subchronic oral toxicity of silver nanoparticles. *Particle and fibre toxicology* **7**, 20

Klungland, A., Rosewell, I., Hollenbach, S., Larsen, E., Daly, G., Epe, B., Seeberg, E., Lindahl, T., and Barnes, D. E. (1999). Accumulation of premutagenic DNA lesions in mice defective in removal of oxidative base damage. *Proceedings of the National Academy of Sciences of the United States of America* **96**(23), 13300-5

Korani, M., Rezayat, S. M., Gilani, K., Arbabi Bidgoli, S., and Adeli, S. (2011). Acute and subchronic dermal toxicity of nanosilver in guinea pig. *International journal of nanomedicine* **6**, 855-62

Krokan, H. E., Nilsen, H., Skorpen, F., Otterlei, M., and Slupphaug, G. (2000). Base excision repair of DNA in mammalian cells. *FEBS letters* **476**(1), 73-77

Kroll, A., Pillukat, M. H., Hahn, D., and Schnekenburger, J. (2012). Interference of engineered nanoparticles with *in vitro* toxicity assays. *Archives of toxicology* **86**(7), 1123-36

Kruszewski, M., Brzoska, K., Brunborg, G., Asare, N., Dobrzynska, M., Dusinská, M., Fjellsbø, L. M., Georgantzopoulou, A., Gromadzka-Ostrowska, J., Gutleb, A. C., Lankoff, A., Magdolenová, Z., Pran, E. R., Rinna, A., Instanes, C., Sandberg, W. J., Schwarze, P., Stepkowski, T., Wojewódzka, M., and Refsnes, M. (2011). Toxicity of Silver Nanomaterials in Higher Eukaryotes. *Advances in Molecular Toxicology* **5**, 179 - 218

Kumari, A., and Yadav, S. K. (2011). Cellular interactions of therapeutically delivered nanoparticles. *Expert opinion on drug delivery* **8**(2), 141-51

Lankoff, A., Sandberg, W. J., Wegierek-Ciuk, A., Lisowska, H., Refsnes, M., Sartowska, B., Schwarze, P. E., Meczynska-Wielgosz, S., Wojewodzka, M., and Kruszewski, M. (2012). The effect of agglomeration state of silver and titanium dioxide nanoparticles on cellular response of HepG2, A549 and THP-1 cells. *Toxicology letters* **208**(3), 197-213

Lee, Y. H., Cheng, F. Y., Chiu, H. W., Tsai, J. C., Fang, C. Y., Chen, C. W., and Wang, Y. J. (2014). Cytotoxicity, oxidative stress, apoptosis and the autophagic effects of silver nanoparticles in mouse embryonic fibroblasts. *Biomaterials* **35**(16), 4706-15

Li, N., Sioutas, C., Cho, A., Schmitz, D., Misra, C., Sempf, J., Wang, M., Oberley, T., Froines, J., and Nel, A. (2003). Ultrafine particulate pollutants induce oxidative stress and mitochondrial damage. *Environmental health perspectives* **111**(4), 455-60

Lin, J. J., and Sancar, A. (1989). A new mechanism for repairing oxidative damage to DNA: (A)BC excinuclease removes AP sites and thymine glycols from DNA. *Biochemistry* **28**(20), 7979-84

Lin, Z., Monteiro-Riviere, N. A., and Riviere, J. E. (2014). Pharmacokinetics of metallic nanoparticles. *Wiley interdisciplinary reviews. Nanomedicine and nanobiotechnology*

Liu, P., Huang, Z., and Gu, N. (2013). Exposure to silver nanoparticles does not affect cognitive outcome or hippocampal neurogenesis in adult mice. *Ecotoxicology and Environmental Safety* **87**(0), 124-130

Liu, Y., Guan, W., Ren, G., and Yang, Z. (2012). The possible mechanism of silver nanoparticle impact on hippocampal synaptic plasticity and spatial cognition in rats. *Toxicology letters* **209**(3), 227-31

Livak, K. J., and Schmittgen, T. D. (2001). Analysis of relative gene expression data using real-time quantitative PCR and the 2(-Delta Delta C(T)) Method. *Methods (San Diego, Calif.)* **25**(4), 402-8

Lubick, N. (2008). Nanosilver toxicity: ions, nanoparticles—or both? *Environmental science & technology* **42**(23), 8617-8617

Lucchini, R. G., Dorman, D. C., Elder, A., and Veronesi, B. (2012). Neurological impacts from inhalation of pollutants and the nose-brain connection. *Neurotoxicology* **33**(4), 838-41

Malboeuf, C. M., Isaacs, S. J., Tran, N. H., and Kim, B. (2001). Thermal effects on reverse transcription: improvement of accuracy and processivity in cDNA synthesis. *BioTechniques* **30**(5), 1074-8, 1080, 1082, passim

Mander, P. K., Jekabsone, A., and Brown, G. C. (2006). Microglia proliferation is regulated by hydrogen peroxide from NADPH oxidase. *Journal of immunology (Baltimore, Md. : 1950)* **176**(2), 1046-52

Marklund, S. L. (1984). Extracellular superoxide dismutase and other superoxide dismutase isoenzymes in tissues from nine mammalian species. *The Biochemical journal* **222**(3), 649-55

Marklund, S. L., Westman, N. G., Lundgren, E., and Roos, G. (1982). Copper- and zinc-containing superoxide dismutase, manganese-containing superoxide dismutase, catalase, and glutathione peroxidase in normal and neoplastic human cell lines and normal human tissues. *Cancer research* **42**(5), 1955-61

McAuliffe, M. E., and Perry, M. J. (2007). Are nanoparticles potential male reproductive toxicants? A literature review. *Nanotoxicology* **1**(3), 204-210

Mittal, M., Siddiqui, M. R., Tran, K., Reddy, S. P., and Malik, A. B. (2014). Reactive oxygen species in inflammation and tissue injury. *Antioxidants & redox signaling* **20**(7), 1126-67

Mo, Y., Wan, R., Chien, S., Tollerud, D. J., and Zhang, Q. (2009). Activation of endothelial cells after exposure to ambient ultrafine particles: the role of NADPH oxidase. *Toxicology and applied pharmacology* **236**(2), 183-93

Muhlfeld, C., Rothen-Rutishauser, B., Blank, F., Vanhecke, D., Ochs, M., and Gehr, P. (2008). Interactions of nanoparticles with pulmonary structures and cellular responses. *American journal of physiology. Lung cellular and molecular physiology* **294**(5), L817-29

Mullis;, K. B., Erlich;, H. A., Arnheim;, N., Horn;, G. T., Saiki;, R. K., and Scharf, S. J. (1987). Process for amplifying, detecting, and/or-cloning nucleic acid sequences. In (Vol. 4,683,195. Cetus Corporation, Emeryville, Calif., United States.

Myhre, O., Andersen, J. M., Aarnes, H., and Fonnum, F. (2003). Evaluation of the probes 2′,7′-dichlorofluorescin diacetate, luminol, and lucigenin as indicators of reactive species formation. *Biochemical Pharmacology* **65**(10), 1575-1582

Myhre, O., Utkilen, H., Duale, N., Brunborg, G., and Hofer, T. (2013). Metal dyshomeostasis and inflammation in Alzheimer's and Parkinson's diseases: possible impact of environmental exposures. *Oxidative medicine and cellular longevity* **2013**, 726954

Nel, A., Xia, T., Madler, L., and Li, N. (2006). Toxic potential of materials at the nanolevel. *Science (New York, N.Y.)* **311**(5761), 622-7

Nishanth, R. P., Jyotsna, R. G., Schlager, J. J., Hussain, S. M., and Reddanna, P. (2011). Inflammatory responses of RAW 264.7 macrophages upon exposure to nanoparticles: Role of ROS-NFκB signaling pathway. *Nanotoxicology* **5**(4), 502-516

Oberdorster, G., Maynard, A., Donaldson, K., Castranova, V., Fitzpatrick, J., Ausman, K., Carter, J., Karn, B., Kreyling, W., Lai, D., Olin, S., Monteiro-Riviere, N., Warheit, D., and Yang, H. (2005a). Principles for characterizing the potential human health effects from exposure to nanomaterials: elements of a screening strategy. *Particle and fibre toxicology* **2**, 8

Oberdorster, G., Oberdorster, E., and Oberdorster, J. (2005b). Nanotoxicology: an emerging discipline evolving from studies of ultrafine particles. *Environmental health perspectives* **113**(7), 823-39

Oberdorster, G., Sharp, Z., Atudorei, V., Elder, A., Gelein, R., Kreyling, W., and Cox, C. (2004). Translocation of inhaled ultrafine particles to the brain. *Inhalation toxicology* **16**(6-7), 437-45

Olsen, A.-K., Lindeman, B., Wiger, R., Duale, N., and Brunborg, G. (2005). How do male germ cells handle DNA damage? *Toxicology and applied pharmacology* **207**(2, Supplement), 521-531

Olsen, A. K., Bjortuft, H., Wiger, R., Holme, J., Seeberg, E., Bjoras, M., and Brunborg, G. (2001). Highly efficient base excision repair (BER) in human and rat male germ cells. *Nucleic acids research* **29**(8), 1781-90

Olsen, A. K., Duale, N., Bjoras, M., Larsen, C. T., Wiger, R., Holme, J. A., Seeberg, E. C., and Brunborg, G. (2003). Limited repair of 8-hydroxy-7,8-dihydroguanine residues in human testicular cells. *Nucleic acids research* **31**(4), 1351-63

Ong, K. J., MacCormack, T. J., Clark, R. J., Ede, J. D., Ortega, V. A., Felix, L. C., Dang, M. K., Ma, G., Fenniri, H., Veinot, J. G., and Goss, G. G. (2014). Widespread nanoparticle-assay interference: implications for nanotoxicity testing. *PloS one* **9**(3), e90650

Park, E. J., Bae, E., Yi, J., Kim, Y., Choi, K., Lee, S. H., Yoon, J., Lee, B. C., and Park, K. (2010). Repeated-dose toxicity and inflammatory responses in mice by oral administration of silver nanoparticles. *Environmental toxicology and pharmacology* **30**(2), 162-8

Park, K. (2013). Toxicokinetic differences and toxicities of silver nanoparticles and silver ions in rats after single oral administration. *Journal of toxicology and environmental health. Part A* **76**(22), 1246-60

Park, K., Park, E. J., Chun, I. K., Choi, K., Lee, S. H., Yoon, J., and Lee, B. C. (2011). Bioavailability and toxicokinetics of citrate-coated silver nanoparticles in rats. *Archives of pharmacal research* **34**(1), 153-8

Parkos, C. A., Colgan, S. P., Liang, T. W., Nusrat, A., Bacarra, A. E., Carnes, D. K., and Madara, J. L. (1996). CD47 mediates post-adhesive events required for neutrophil migration across polarized intestinal epithelia. *The Journal of cell biology* **132**(3), 437-50

Petit, P. X., Lecoeur, H., Zorn, E., Dauguet, C., Mignotte, B., and Gougeon, M. L. (1995). Alterations in mitochondrial structure and function are early events of dexamethasone-induced thymocyte apoptosis. *The Journal of cell biology* **130**(1), 157-67

Piao, M. J., Kang, K. A., Lee, I. K., Kim, H. S., Kim, S., Choi, J. Y., Choi, J., and Hyun, J. W. (2011). Silver nanoparticles induce oxidative cell damage in human liver cells through inhibition of reduced glutathione and induction of mitochondria-involved apoptosis. *Toxicology letters* **201**(1), 92-100

Powers, C. M., Badireddy, A. R., Ryde, I. T., Seidler, F. J., and Slotkin, T. A. (2011). Silver nanoparticles compromise neurodevelopment in PC12 cells: critical contributions of silver ion, particle size, coating, and composition. *Environmental health perspectives* **119**(1), 37-44

Rahman, M. F., Wang, J., Patterson, T. A., Saini, U. T., Robinson, B. L., Newport, G. D., Murdock, R. C., Schlager, J. J., Hussain, S. M., and Ali, S. F. (2009). Expression of genes related to oxidative stress in the mouse brain after exposure to silver-25 nanoparticles. *Toxicology letters* **187**(1), 15-21

Rejeski, D., and Lekas, D. (2008). Nanotechnology field observations: scouting the new industrial west. *Journal of Cleaner Production* **16**(8–9), 1014-1017

Rim, K. T., Song, S. W., and Kim, H. Y. (2013). Oxidative DNA damage from nanoparticle exposure and its application to workers' health: a literature review. *Safety and health at work* **4**(4), 177-86

Sabatini, C. A., Pereira, R. V., and Gehlen, M. H. (2007). Fluorescence modulation of acridine and coumarin dyes by silver nanoparticles. *Journal of fluorescence* **17**(4), 377-82

Sankarapandi, S., Zweier, J. L., Mukherjee, G., Quinn, M. T., and Huso, D. L. (1998). Measurement and characterization of superoxide generation in microglial cells: evidence for an NADPH oxidase-dependent pathway. *Archives of biochemistry and biophysics* **353**(2), 312-21

Schleh, C., Holzwarth, U., Hirn, S., Wenk, A., Simonelli, F., Schaffler, M., Moller, W., Gibson, N., and Kreyling, W. G. (2013). Biodistribution of inhaled gold nanoparticles in mice and the influence of surfactant protein D. *Journal of aerosol medicine and pulmonary drug delivery* **26**(1), 24-30

Schroeder, A., Mueller, O., Stocker, S., Salowsky, R., Leiber, M., Gassmann, M., Lightfoot, S., Menzel, W., Granzow, M., and Ragg, T. (2006). The RIN: an RNA integrity number for assigning integrity values to RNA measurements. *BMC molecular biology* **7**, 3

Seeberg, E., Eide, L., and Bjoras, M. (1995). The base excision repair pathway. *Trends in biochemical sciences* **20**(10), 391-7

Sharma, H. S., Hussain, S., Schlager, J., Ali, S. F., and Sharma, A. (2010). Influence of nanoparticles on blood-brain barrier permeability and brain edema formation in rats. *Acta neurochirurgica. Supplement* **106**, 359-64

Sharma, H. S., and Sharma, A. (2012). Neurotoxicity of engineered nanoparticles from metals. *CNS & neurological disorders drug targets* **11**(1), 65-80

Sharma, P., Jha, A. B., Dubey, R. S., and Pessarakli, M. (2012). Reactive oxygen species, oxidative damage, and antioxidative defense mechanism in plants under stressful conditions. *Journal of Botany* **2012**

Silverthorn, D. U., Ober, W. C., Garrison, C. W., Silverthorn, A. C., and Johnson, B. R. (2009). *Human physiology: an integrated approach*. Pearson/Benjamin Cummings.

Skinner, M. K. (2014). Environmental stress and epigenetic transgenerational inheritance. *BMC medicine* **12**(1), 153

Soumya, R. S., and Hela, P. G. (2013). Nano silver based targeted drug delivery for treatment of cancer. *Der Pharmacia Lettre* **5**(4), 189-197

Stensberg, M. C., Madangopal, R., Yale, G., Wei, Q., Ochoa-Acuna, H., Wei, A., McLamore, E. S., Rickus, J., Porterfield, D. M., and Sepulveda, M. S. (2014). Silver nanoparticle-specific mitotoxicity in Daphnia magna. *Nanotoxicology* **8**(8), 833-42

Stevens, J. L., Liu, H., Halleck, M., Bowes, R. C., Chen, Q. M., and van de Water, B. (2000). Linking gene expression to mechanisms of toxicity. *Toxicology letters* **112-113**, 479-86

Sunesen, M., Stevnsner, T., Brosh, R. M., Jr., Dianov, G. L., and Bohr, V. A. (2002). Global genome repair of 8-oxoG in hamster cells requires a functional CSB gene product. *Oncogene* **21**(22), 3571-8

Surendiran, A., Sandhiya, S., Pradhan, S. C., and Adithan, C. (2009). Novel applications of nanotechnology in medicine. *The Indian journal of medical research* **130**(6), 689-701

Tiwari, D. K., Jin, T., and Behari, J. (2011). Dose-dependent in-vivo toxicity assessment of silver nanoparticle in Wistar rats. *Toxicology mechanisms and methods* **21**(1), 13-24

Trickler, W. J., Lantz, S. M., Murdock, R. C., Schrand, A. M., Robinson, B. L., Newport, G. D., Schlager, J. J., Oldenburg, S. J., Paule, M. G., Slikker, W., Jr., Hussain, S. M., and Ali, S. F. (2010). Silver nanoparticle

induced blood-brain barrier inflammation and increased permeability in primary rat brain microvessel endothelial cells. *Toxicological sciences : an official journal of the Society of Toxicology* **118**(1), 160-70

Vandesompele, J., De Preter, K., Pattyn, F., Poppe, B., Van Roy, N., De Paepe, A., and Speleman, F. (2002). Accurate normalization of real-time quantitative RT-PCR data by geometric averaging of multiple internal control genes. *Genome biology* **3**(7), Research0034

Vlachou, E., Chipp, E., Shale, E., Wilson, Y. T., Papini, R., and Moiemen, N. S. (2007). The safety of nanocrystalline silver dressings on burns: a study of systemic silver absorption. *Burns : journal of the International Society for Burn Injuries* **33**(8), 979-85

Walker, D. G., and Lue, L. F. (2013). Understanding the neurobiology of CD200 and the CD200 receptor: a therapeutic target for controlling inflammation in human brains? *Future neurology* **8**(3)

Wijnhoven, S. W. P., Peijnenburg, W. J. G. M., Herberts, C. A., Hagens, W. I., Oomen, A. G., Heugens, E. H. W., Roszek, B., Bisschops, J., Gosens, I., Van de Meent, D., Dekkers, S., de Jong, W. H., Van Zijverden, M., Sips, A. J. A. M., and Geertsma, R. E. (2009). Nano-silver - a review of available data and knowledge gaps in human and environmental risk assessment. *Nanotoxicology* **3**(2), 109-138

Wong, K. K., Cheung, S. O., Huang, L., Niu, J., Tao, C., Ho, C. M., Che, C. M., and Tam, P. K. (2009). Further evidence of the anti-inflammatory effects of silver nanoparticles. *ChemMedChem* **4**(7), 1129-35

Wright, G. J., Cherwinski, H., Foster-Cuevas, M., Brooke, G., Puklavec, M. J., Bigler, M., Song, Y., Jenmalm, M., Gorman, D., McClanahan, T., Liu, M. R., Brown, M. H., Sedgwick, J. D., Phillips, J. H., and Barclay, A. N. (2003). Characterization of the CD200 receptor family in mice and humans and their interactions with CD200. *Journal of immunology (Baltimore, Md. : 1950)* **171**(6), 3034-46

Wright, G. J., Jones, M., Puklavec, M. J., Brown, M. H., and Barclay, A. N. (2001). The unusual distribution of the neuronal/lymphoid cell surface CD200 (OX2) glycoprotein is conserved in humans. *Immunology* **102**(2), 173-9

Xing, C., Lee, S., Kim, W. J., Jin, G., Yang, Y. G., Ji, X., Wang, X., and Lo, E. H. (2009). Role of oxidative stress and caspase 3 in CD47-mediated neuronal cell death. *Journal of neurochemistry* **108**(2), 430-6

Xu, J. (2005). Preparation, culture, and immortalization of mouse embryonic fibroblasts. *Current protocols in molecular biology / edited by Frederick M. Ausubel ... [et al.]* **Chapter 28**, Unit 28.1

Zhang, Y. J., Pan, H. Y., and Gao, S. J. (2001). Reverse transcription slippage over the mRNA secondary structure of the LIP1 gene. *BioTechniques* **31**(6), 1286-1290

Appendix A: Detailed protocols

A.1 Cell maintenance

A.1.1 Passaging

After seeding, the cells enter a lag period followed by a period of exponential growth. When seeding approximately 1 million cells/75 cm^2 for the KO cells and 500 000 cells/75 cm^2 for the WT cells, the MEF cultures reached a confluence of approximately 80% three to four days after seeding.

Procedure

All work where the cell flask was open was done under sterile conditions under laminar flow. All equipment used was sterilized with 70 % ethanol before entering the laminar flow bench.

a) Trypsin (0.05 % trypsin, 0.1 mM etylenediaminetetraacetic acid (EDTA)), phosphate buffered saline without calcium and magnesium (PBS) and growth medium was preheated to 37 °C in the cell cultivator.

b) The growth medium (15 mL) in the culture flasks was removed and the cells washed gently twice with 15 mL of PBS to remove remains of growth medium, as foetal calf serum in the medium inhibits trypsin.

c) 2 mL of trypsin was added to the cells, whereof 1 mL was instantly removed. The cells were incubated with the remaining 1 mL of trypsin at 37 °C for 3 min.

d) After incubation, the cells were inspected under microscope to verify that the trypsination was successful. This can be visually seen by observing rounding of the cells.

e) The cells were unfastened from the bottom of the flaks by gently tapping the sides of the flask.

f) The trypsin was inactivated and the cells harvested by flushing the bottom of the flask with 4 mL of growth medium. The process was repeated with another 5 mL of medium to ensure that all cells were harvested. The harvested cells were stored on ice until seeding.

g) Cells were counted using a Bürker-chamber.

h) After counting, the cells were resuspended in the growth medium and 1 mL of the cell suspension was added to a 75 cm^2 flask along with 14 mL of growth medium.

A.1.2 Cell counting

Cell concentration (number of cells/mL) was determined by counting in a Bürker-chamber. 100 µL cell suspension was mixed with 100 µL Trypan blue. Trypan blue is a dye that does

not traverse membranes of healthy cells. As the dye passes the membranes of dead or damaged cells, these will appear with a distinctive blue colour under a microscope.

A Bürker counting chamber is a thick glass microscope slide with a rectangular indentation that creates a chamber. The chamber holds 10 µL, and an imprinted grid on the chamber surface allows for an easy counting of cells in this volume:

The grid is divided into 9 large squares, and each square is bounded by a triple set of lines. The centre line of these is the edge of the counting area, and all living and dead cells within the central lines of a large square were counted, also those which touched the lower and left border, but not those which touch the lower and left borders. 5 out of the 9 squares were counted.

A.1.3 Thawing of cells

a) The cells were defrosted under running water for approximately 2 min, after which cell line and passage number was noted.

b) The cells were transferred to a 15 mL tube containing 13 mL growth medium, preheated to 37 °C. This tube was centrifuged at 200 x g at 8 °C for 5 min.

c) The supernatant was discarded, and the cells were resuspended in 15 mL of preheated growth medium. The cell suspension was seeded in a 75 cm^2 cell culture flask.

A.2 RNA isolation

Procedure

a) The lysate was filtered through a filtration column to remove cellular debris, pieces of insufficiently homogenized tissue and shear DNA. The lysate was centrifuged at 14100 g for 15 sec. As the column has a capacity of 700 uL, the process was repeated if the lysate volume was greater.

b) Binding of RNA to the binding column was facilitated by adding 500 uL of 70 % ethanol to the filtered lysate.

c) Lysate/ethanol-mix was pipetted into binding columns and centrifuged at 14100 g (max speed) for 15 sec, and the flow-through liquid discarded. The procedure was repeated until all the lysate had been spun through the binding column.

d) 500 uL of wash solution 1 was added to the binding column and spun at 14100 g for 15 sec. After this step the binding column was transferred to a fresh 2 mL tube.

e) 500 uL of wash solution 2 was added to the binding column and spun at 14100 g for 15 sec. The process was then repeated for a third column wash. After the second wash, the columns were centrifuged for 2 min at maximum speed to dry the columns of ethanol. This drying-step is given as an optional step in the procedure following the kit.

f) The binding column was then transferred to a fresh 2 mL tube and 50 uL of Elution solution was pipetted directly onto the filter, covering the entire filter area. The samples were centrifuged at maximum speed for 1 minute.

A.3 Nanodrop spectrophotometer

a) The system was initiated with a sample of 1.5 µl distilled water.

b) "RNA-40" was chosen for RNA samples and "other-39" for cDNA samples.

c) A blank measurement was conducted using 1.5 µl elution solution from the GenElute Mammalian Total RNA Miniprep Kit for RNA and RNase-free water for cDNA.

d) 1.5 µl of the sample was pipetted onto the pedestal.

e) The system measured the absorbance of the sample giving the concentration in ng/µl, as well as A260/280- and A260/230-ratios.

f) The retention system was cleaned with a distilled water sample.

A.4 Protocol for the RNA Nano 6000 Assay for RIN determination

The RNA 6000 gel was prepared according to the manufacturer's instructions:

a) The reagents were allowed to equilibrate to room temperature for 30 minutes before use, after which 550µL of RNA 6000 Nano gel matrix was spun down through a spin filter at 1500 g for 10 minutes.

b) The filtered gel was divided in aliquots of 65 µL and stored at 4 °C.

The gel-dye mix was then prepared:

a) Room-tempered dye concentrate was vortexed for 10 seconds and spun down, after which 1 µl of the RNA 6000 Nano dye concentrate was added to a 65 µL aliquot of RNA 6000 Nano gel.

b) The gel-dye mix was thoroughly vortexed and stored at 4 °C in the dark, to be used within one day.

c) The gel-dye mix was spun down for 10 minutes at room temperature at 13000 g.

The gel-dye mix was loaded onto a RNA Nano chip:

a) 9.0 µL of gel-dye mix was added to the bottom of well marked G

b) The gel-dye mix was pressurized using the syringe supplied with the kit. After 30 seconds of pressurizing, the plunger was released.

c) 9.0 µL of the gel-dye mix was added to the two top-left wells of the chip.

After loading the gel-dye mix, the samples were added to the chip:

a) An aliquot of the supplied ladder was thawed on ice, and 1 µL was added to the well marked with a ladder-symbol.

b) The RNA-samples were heat denatured at 70°C for 2 minutes before loading them on the chip.1 µL of each sample was pipetted into each of the 12 sample wells.

c) The chip was then vortexed using the IKA vortex mixer at 2400 rpm for 60 seconds.

d) The prepared chip was inserted in the Agilent 2100 bioanalyzer and the run was started within 5 minutes.

A.5 Protocol for cDNA synthesis

Protocol:

a) Isolated RNA was thawed on ice, transferred to 96-well reaction plates and diluted with ddH2O to give a concentration of 100 ng/µL in all of the samples. In samples where there were insufficient RNA to obtain this concentration, the samples were diluted 1:1 with ddH_2O in order to prevent buffers etc. used in RNA-isolation to interfere with cDNA synthesis. The remaining RNA was stored at -80°C.

Component	**Volume per reaction (µL)**
10X RT Buffer	2,0
25X dNTP Mix	0,8
10X RT Random Primers	2,0
MultiScribe™ Reverse Transcriptase	1,0
Nuclease-free H_2O	4,2
Total volume per reaction	10,0

Table A.5.1: RT-PCR Mastermix.

b) After dilution, 10 µL of each sample was transferred to another 96-well reaction plate. The plate containing the stock of diluted RNA was stored at -80°C

c) The reverse transcription master mix was prepared as described in the kit (table A.5.1). All the components were allowed to thaw at 4°C before use

d) 10 µL RT master mix was added to each well with diluted RNA. The plate was subsequently sealed with adhesive cover and centrifuged for 1 minute at 400 G.

	Step 1	**Step 2**	**Step 3**	**Step 4**
Temperature	25 °C	37 °C	85 °C	4 °C
Time	10 min	120 min	5 min	∞

Table A.5.2: RT-PCR program.

e) The cDNA synthesis was done using the Eppendorf Mastercycler Gradient (Eppendorf, Germany) at the conditions listed in table 2.

f) Quantity and purity of synthesized cDNA was measured using the Nanodrop 1000 Spectrophotometer as described in appendix A section A.3.

g) cDNA was stored at -20°C until use.

A.6 Protocol for qPCR

Preparation of mastermix was done by thawing the components listed in table A.6.1 on ice, and mixing them thoroughly. A separate mastermix was prepared for every gene investigated in the qPCR (two for each run). One mastermix was pipetted into the first column of a 96 well PCR plate, and another mastermix in the second column. The plate was sealed with adhesive film and centrifuged at 800 g and 4 °C for 1 minute. 7 µL prepared mastermix was then pipetted into each well on a 384 well plate containing diluted cDNA by the Bravo Automated Liquid Handling Platform.

Component	**Volume per reaction (µL)**
KAPA SYBR FAST Universal qPCR mastermix	5.0
Primer Forward	1.0
Primer Reverse	1.0

Table A.6.1: qPCR Mastermix

The qPCR was run using the BioRad CFX384 Touch real-time PCR detection system with the settings listed in table A.6.2.

Step	**Temperature**	**Time (minutes:seconds)**
1	95 °C	3:00
2	95 °C	0:03
3	60 °C	0:20
Plate read	-	-
4	72 °C	0:30
5 GO TO step 2, 39 more times	-	-
6 Melt curve	65 °C to 95 °C. Increment 0.5 °C	0:05
Plate read	-	-

Table A.6.2: Run protocol for qPCR using the KAPA SYBR FAST qPCR mastermix. *Program was run on the CFX384 Touch real-time PCR detection system.*

A.7 Target genes and primer sequences

Gene symbol	Gene name	Primer sequence forward	Primer sequence forward
Il-1α	Interleukin 1 alpha	CCACCAGCACAACTCTGAGATA	CCCAATAACCCTGTCAATTTCTT
Il-1β	Interleukin 1 beta	TTGGTTAAATGACCTGCAACA	GAGCGCTCACGAACAGTTG
Il-6	Interleukin 6	TGATGGATGCTACCAAACTGG	TTCATGTACTCCAGGTAGCTATGG
Tnf-α	Tumor necrosis factor alpha	CTGTAGCCCACGTCGTAGC	TTGAGATCCATGCCGTTG
Tnfsf13b	Tumor necrosis factor ligand superfamily member 13b	CGCCGACTATACGAAAAGGA	CCTGTTTGCCTCACCACTATT
Sod1	Superoxide dismutase 1 (soluble)	CAGGACCTCATTTTAATCCTCA	TGCCCAGGTCTCCAACAT
Sod2	Superoxide dismutase 2 (mitochondrial)	GACCCATTGCAAGGAACAA	GTAGTAAGCGTGCTCCCACAC
Sod3	Superoxide dismutase 3 (extracellular)	GGGGAGGCAACTCAGAGG	TGGCTGAGGTTCTCTGCAC
Cat	Catalase	GGAGCAGGTGCTTTTGGATACT	TCAGCTGAGCCTGACTCTCC
Gpx1	Glutathione peroxidase 1	TTCGGACACCAGGAGAATGG	TAAAGAGCGGGTGAGCCTTC
Gpx2	Glutathione peroxidase 2	GTTCTCGGCTTCCCTTGC	TTCAGGATCTCCTCGTTCTGA
Nrf2	Nuclear factor (erythroid-derived 2)-like 2	CATGATGGACTTGGAGTTGC	CCTCCAAAGGATGTCAATCAA
Apex1	Apurinic/apyrimidinic endonuclease 1	CGGGGAAGAACCCAAGTC	TCCTTCTCGGTTTTCTTTGC
Neil1	Nei endonuclease VIII-like 1 (E.coli)	TCGTAGACATCCGTCGCTTT	TGTCTGATAGGTTCCGAAGTACG
Neil2	Nei endonuclease VIII-like 2 (E.coli)	CCAGAGCAAAGAAAGCTAACAAA	ACCACCACTAAAATGGAGTACCA
Neil3	Nei endonuclease VIII-like 3 (E.coli)	GTGGTCTTCATCCGGCTGTT	ATCCTGCTTTACAGCACCTG
Cd47	Cluster of differentiation 47	CTGACCAAGGATCAGCCTGT	CATTTGGAGAAAACCACGAAA
Cd200	Cluster of differentiation 200	CTCTCCACCTACAGCCTGATTT	CTGGGTCACCACTTCCACTT
Cd200r1	Cluster of differentiation 200 receptor 1	AAGAATCAAACAACACAGAACAA CA	CTGTACAGACACTGTAGTGTTCACTTG
Nox1	NADPH oxidase 1	ACCACTGGCTCTCAGTTTTGT	GCCAAGGCAGTCCCAAGAA
Nox4	NADPH oxidase 4	CCCTAAACGTTCTACTTTTCTGGA	TGCTCTGCTTAAACACAATCCT
Noxo1	NADPH oxidase organizer 1	TTCAGGCAGCTCCAGAAGAC	TGTCAGCAATGGAGCATCAG

Table A.7: Target genes for qPCR with symbols, names and primer sequences.

Appendix B: Solutions and media

B.1 Cell culture medium

- 500 mL Dulbecco's Modified Eagle's Medium, with 4.5 g/L Glucose, without L-Glutamine.
- 55 mL (10%) Foetal Calf Serum
- 5.5 mL (1%) Penicillin-Streptomycin
- 5.5 mL (1%) L-Glutamine (200 mM)

Appendix C: Products and producers

Product	Producer	Country
2100 Bioanalyzer	Agilent Technologies	USA
96-well PCR Plate Non-skirted	4titude	UK
Absolutt alkohol prima (100 % (absolute) ethanol)	Kementyl Norge	Norway
BioWhittaker® Dulbecco's Modified Eagle's Medium, with 4.5 g/L Glucose, without L-Glutamine	Lonza	Belgium
BioWhittaker® L-Glutamine 200mM	Lonza	Belgium
BioWhittaker® PEN-STREP (penicillin-streptomycin)	Lonza	Belgium
BioWhittaker® Trypan Blue 0.4%	Lonza	Belgium
BioWhittaker® Trypsin EDTA	Lonza	Belgium
Bovine Serum Albumin, Fraction V	Sigma-Aldrich	USA
Bravo Automated Liquid Handling Platform	Agilent Technologies	USA
Centrifuge tubes 15 mL	Corning	USA
	TPP	Switzerland
Centrifuge tubes 50 mL	Corning	USA
	Greiner Bio-One	Austria
Corning flasks (25 cm^2, 75 cm^2, 162 cm^2)	Corning	USA
Costar Assay Plate 96 well Black with clear flat bottom	Corning	USA
CFX384 Touch real-time PCR detection system	Bio-Rad	USA
DCF-DA	Sigma-Aldrich	USA
Distilled water (dH_2O)	Locally produced, NIPH	Norway

Eppendorf Mastercycler Gradient	Eppendorf	Germany
Eppendorf tubes 1.5 mL	VWR	USA
GenElute Mammalian Total RNA Miniprep Kit	Sigma-Aldrich	USA
Hard shell PCR plate 384 well	Bio-Rad	USA
High-Capacity cDNA Reverse Transcription Kit	Applied Biosystems	USA
Hydrogen Peroxide 30%	Merck KGaA	Germany
JC-1 Mitochondrial Membrane Potential Assay Kit	Cayman Chemical	USA
KAPA SYBR FAST qPCR Kit	Kapa Biosystems	USA
Microtubes 1.5 mL EasiFit Black	Treff	Switzerland
Nanodrop 1000	Nanodrop Technologies	USA
Phosphate buffered saline (PBS)	Locally produced, NIPH	Norway
Precellys 24 tissue homogenizer	Bertin Technologies	France
RNA 6000 Nano Assay Kit	Agilent technologies	USA
RNase Away	Molecular BioProducts	USA
Silver particles (Ag20 and Ag200)	Plasmachem	Germany
UltraTurrax	IKA-Werke	Germany

Appendix D: Additional results

D.1 Reference gene stability

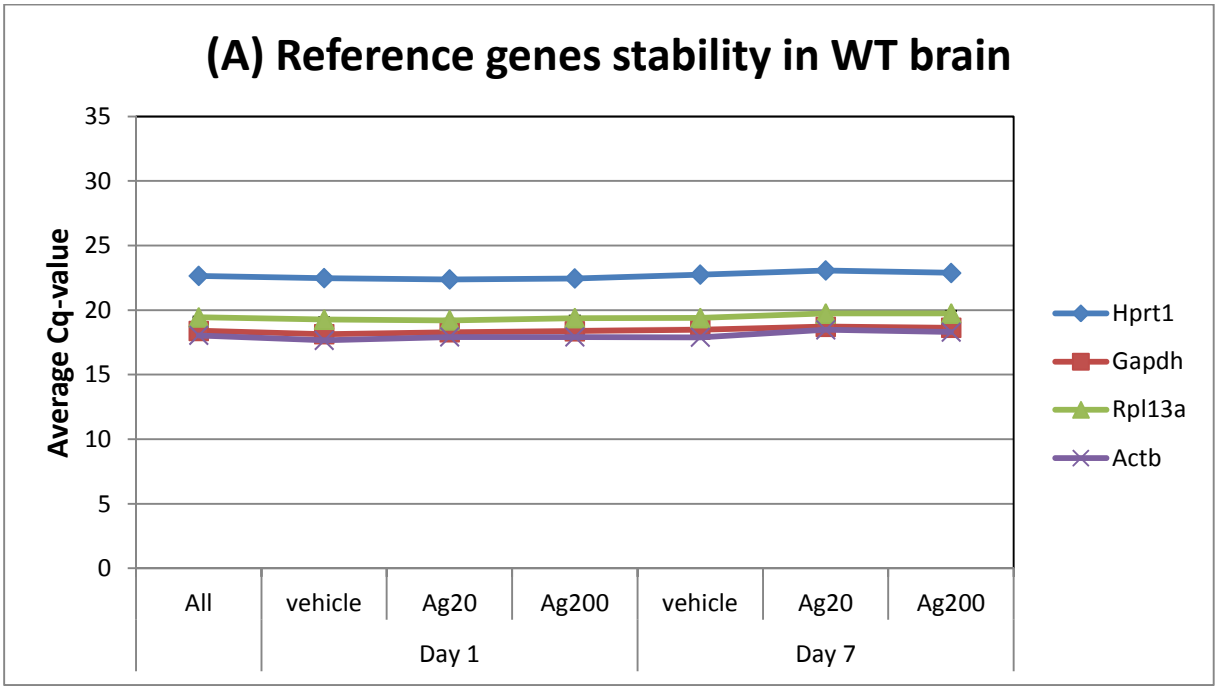

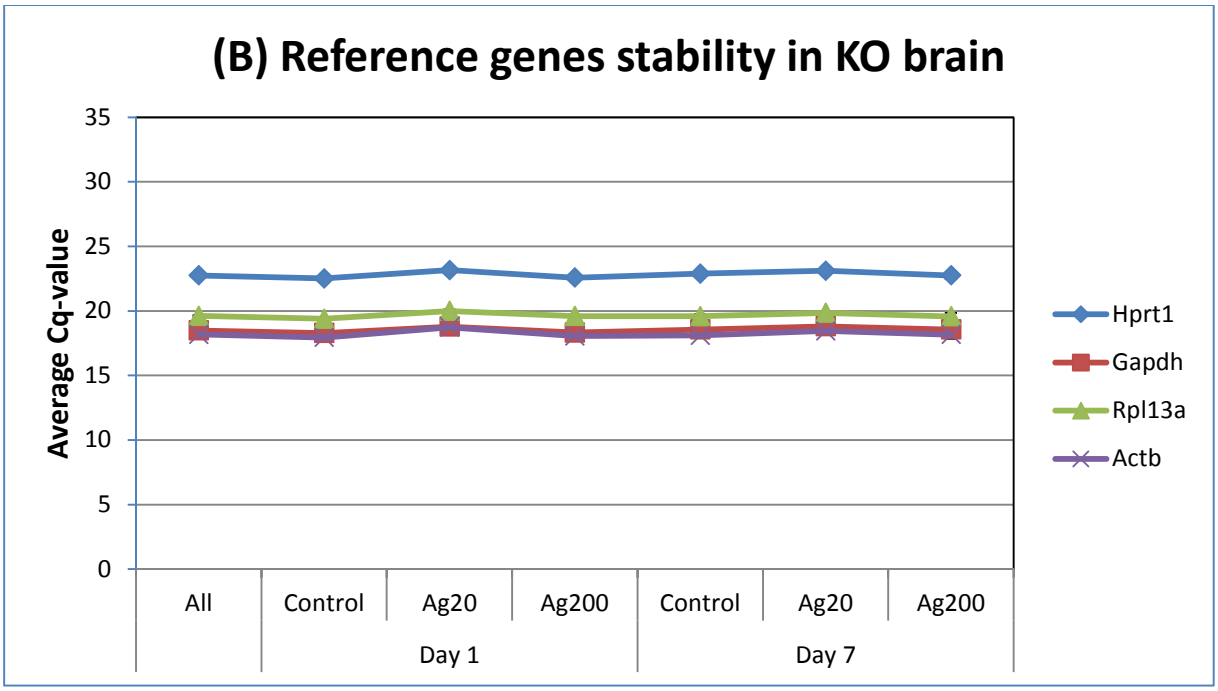

Figure D.1: Stability of reference genes in WT (A) and KO (B) brain. (A) WT *Treatment groups are day 1 control (n=6), Ag20 (n=6), Ag200 (n=6); day 7 control (n=5), Ag20 (n=6), Ag200 (n=5); (B) KO treatment groups are day 1 control (n=6), Ag20 (n=6), Ag200 (n=6); day 7 control (n=5), Ag20 (n=6), Ag200 (n=5). Values are presented as average raw Cq-value of treatment groups ± SEM.*

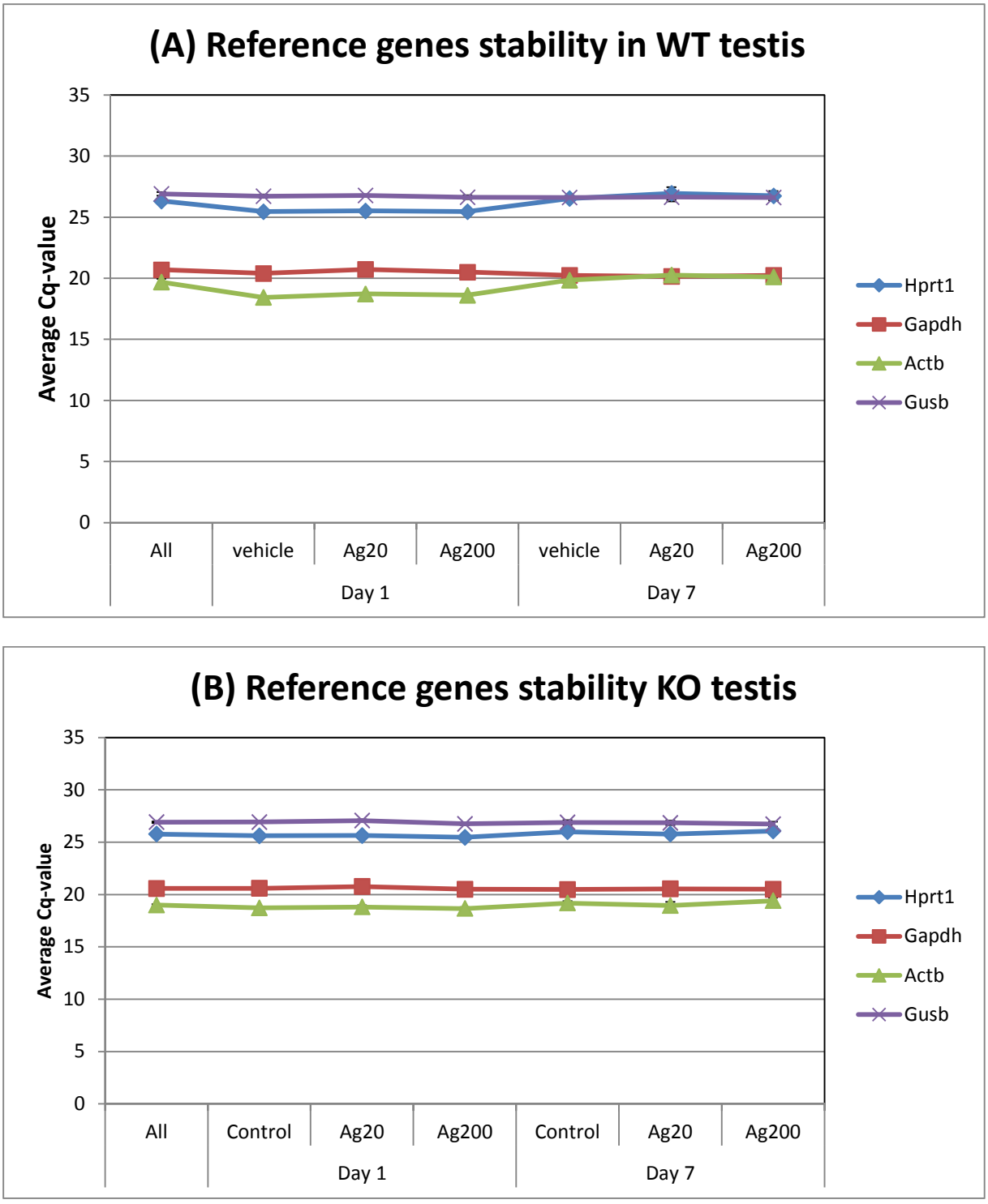

Figure D.2: Stability of reference genes in WT (A) and KO (B) testis. (A) WT *Treatment groups are day 1 control (n=6), Ag20 (n=6), Ag200 (n=6); day 7 control (n=5), Ag20 (n=6), Ag200 (n=5); (B) KO treatment groups are day 1 control (n=6), Ag20 (n=6), Ag200 (n=6); day 7 control (n=5), Ag20 (n=6), Ag200 (n=5). Values are presented as average raw Cq-value of treatment groups ± SEM.*

D.2: RNA quantity and quality in relation to genotype, time and treatment.

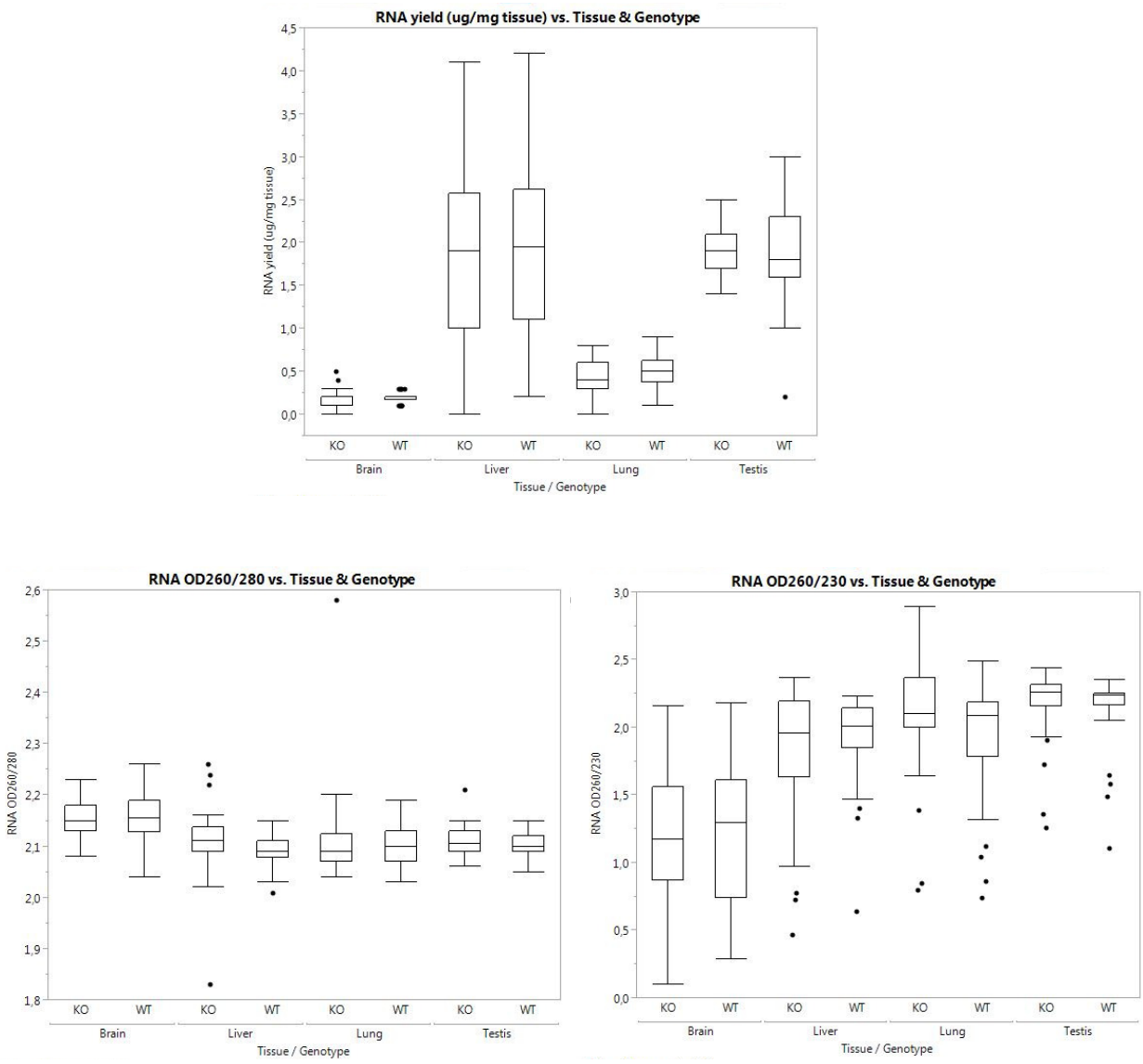

Figure D.2.1: RNA quality and purity in relation to genotype. *(A) RNA yield µg RNA/mg tissue, (B) OD260/280, (C) OD260/230. Sample sizes are brain KO n=36, brain WT n=34; liver KO n=36, liver WT n=34; lung KO n=36, brain WT n=34; testis KO n=36, brain WT n=34. n=number of animals.*

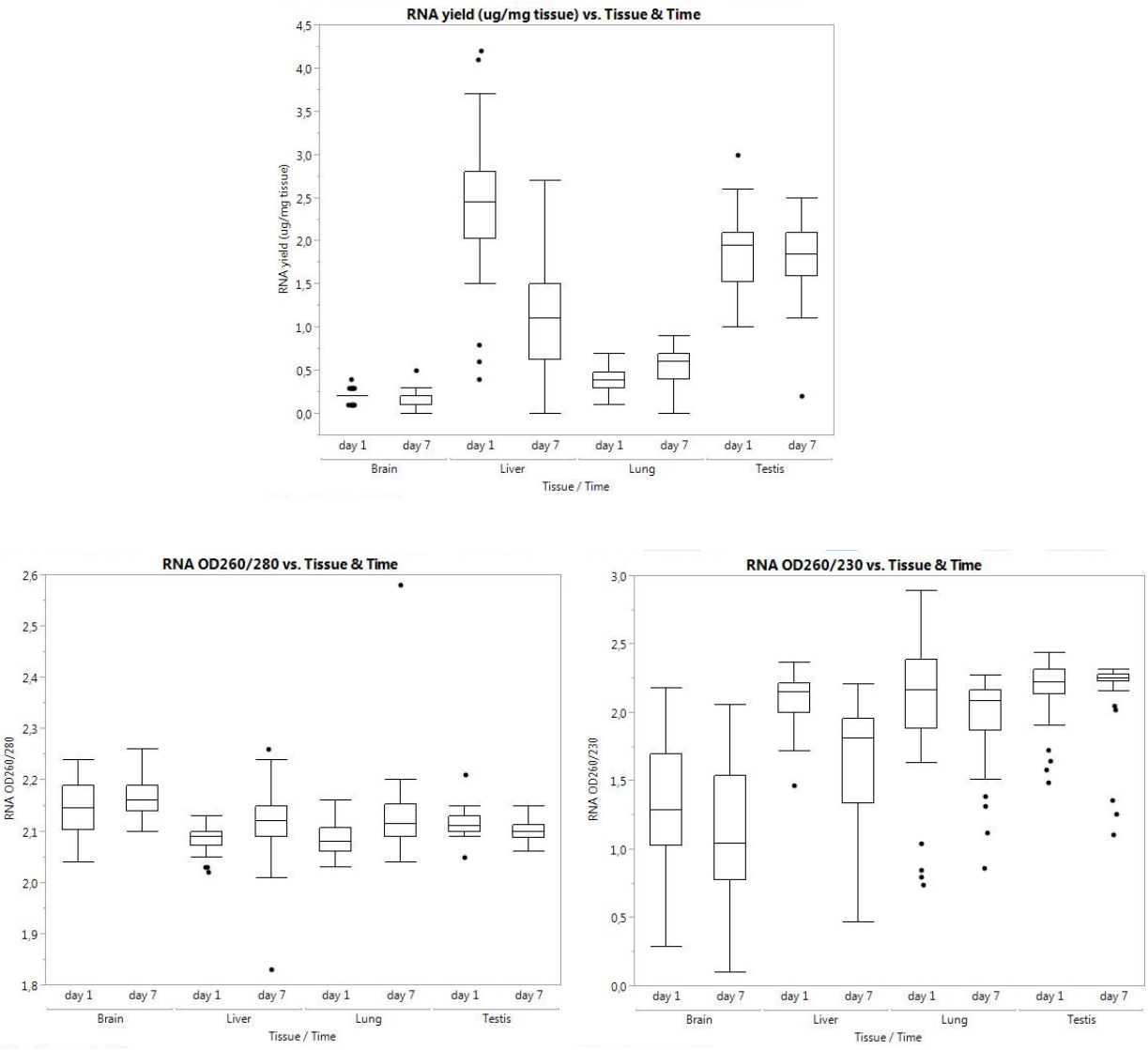

Figure D.2.2: RNA quality and purity in relation to time (experiment day). *(A) RNA yield µg RNA/mg tissue, (B) OD260/280, (C) OD260/230. Sample sizes are brain day1 n=36, brain day7 n=34; liver day1 n=36, brain day7 n=34; lung day1 n=36, brain day7 n=34; testis day1 n=36, brain day7 n=34; n=number of animals.*

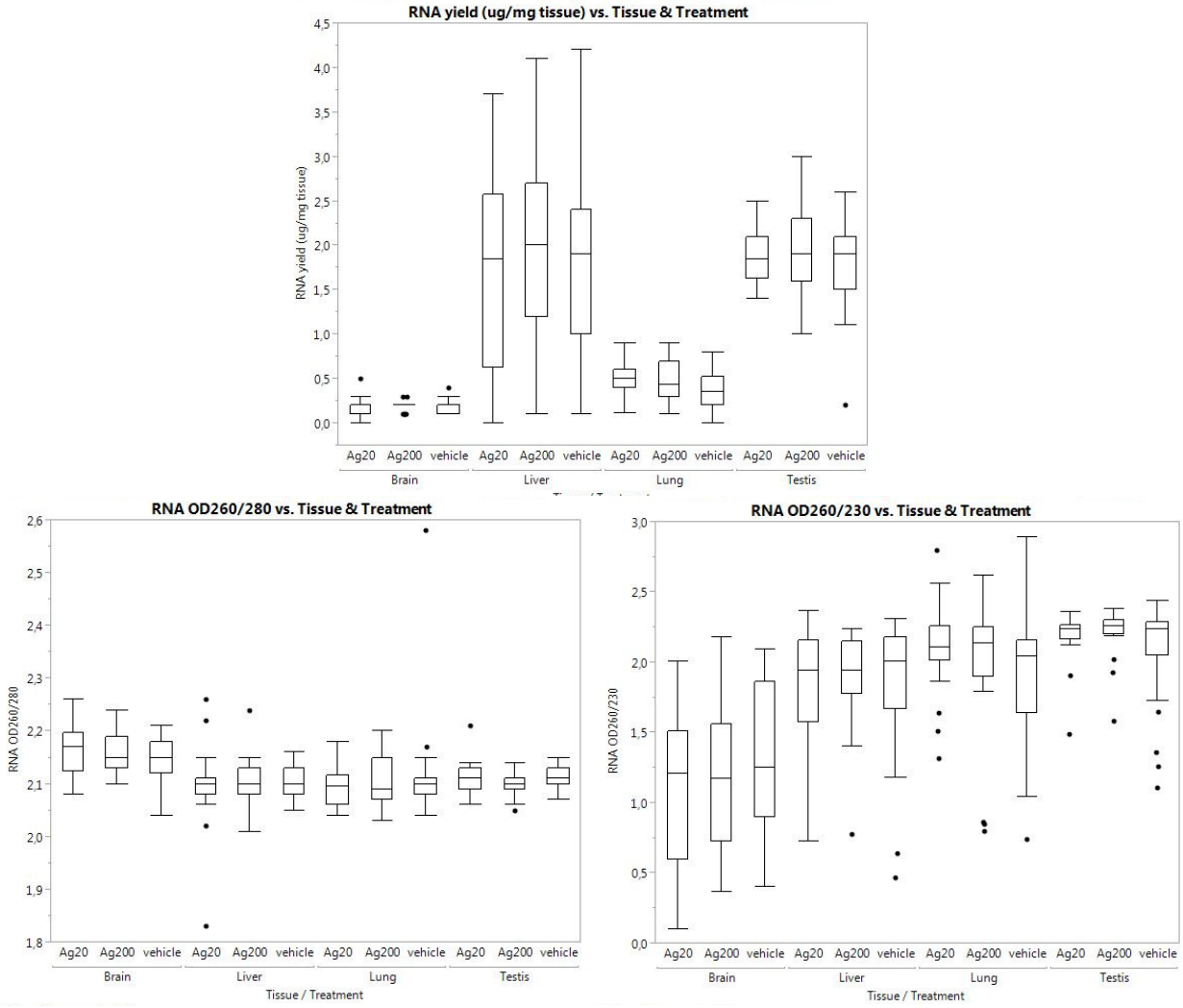

Figure D.2.3: RNA quality and purity in relation to treatment. *(A) RNA yield µg RNA/mg tissue, (B) OD260/280, (C) OD260/230. Vehicle represents the control group. Sample sizes are brain Ag20 n=24, brain Ag200 n=23, brain vehicle (control) n=23; liverAg20 n=24, liver Ag200 n=23, liver vehicle (control) n=23; lung Ag20 n=24, lung Ag200 n=23, lung vehicle (control) n=23; testis Ag20 n=24, testis Ag200 n=23, testis vehicle (control) n=23. n= number of animals.*